AD-A161 049 A COMPARISON OF SIX VERTICAL DISCRETIZATION SCHEMES(U) 1/2
NAVAL POSTGRADUATE SCHOOL MONTEREY CA M S JORDAN
SEP 85

UNCLASSIFIED F/G 12/1 NL

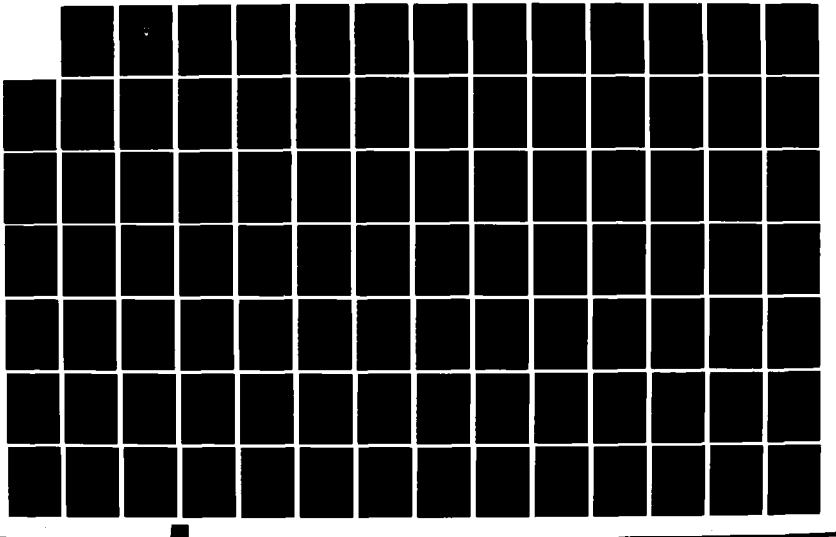

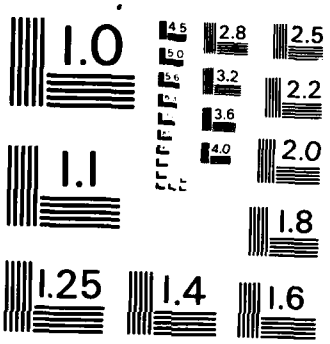

(2)

NAVAL POSTGRADUATE SCHOOL
Monterey, California

THESIS

A COMPARISON OF SIX VERTICAL DISCRETIZATION SCHEMES

by

Mary S. Jordan

September 1985

Thesis Advisor: Roger T. Williams

Approved for public release; distribution is unlimited

UNCLASSIFIED

SECURITY CLASSIFICATION OF THIS PAGE (When Data Entered)

REPORT DOCUMENTATION PAGE	READ INSTRUCTIONS BEFORE COMPLETING FORM
1. REPORT NUMBER	2. GOVT ACCESSION NO. AD-A161 049 / 3. RECIPIENT'S CATALOG NUMBER
4. TITLE (and Subtitle) A Comparison of Six Vertical Discretization Schemes	5. TYPE OF REPORT & PERIOD COVERED Master's Thesis September 1985
	6. PERFORMING ORG. REPORT NUMBER
7. AUTHOR(s) Mary S. Jordan	8. CONTRACT OR GRANT NUMBER(s)
9. PERFORMING ORGANIZATION NAME AND ADDRESS Naval Postgraduate School Monterey, California 93943-5100	10. PROGRAM ELEMENT, PROJECT, TASK AREA & WORK UNIT NUMBERS
11. CONTROLLING OFFICE NAME AND ADDRESS Naval Postgraduate School Monterey, California 93943-5100	12. REPORT DATE September 1985
	13. NUMBER OF PAGES 174
14. MONITORING AGENCY NAME & ADDRESS(if different from Controlling Office)	15. SECURITY CLASS. (of this report) Unclassified
	15a. DECLASSIFICATION/ DOWNGRADING SCHEDULE

16. DISTRIBUTION STATEMENT (of this Report)

Approved for public release; distribution is unlimited

17. DISTRIBUTION STATEMENT (of the abstract entered in Block 20, if different from Report)

18. SUPPLEMENTARY NOTES

19. KEY WORDS (Continue on reverse side if necessary and identify by block number)

Numerical Weather Prediction
Finite Elements
Finite Differences
Baroclinic Instability

20. ABSTRACT (Continue on reverse side if necessary and identify by block number)

Six vertical discretization schemes are compared for a linear, baroclinic, vorticity-divergence equation model. Variables are defined for two staggered and one unstaggered grids. A finite difference and a Galerkin finite element approximation are formulated for each of the three grids. The models are tested in three experiments. The largest difference between the grids occurs in the mid-atmosphere diabatic heat source experiment and

DD FORM 1 JAN 73 1473 EDITION OF 1 NOV 65 IS OBSOLETE

S N 0102-LF-014-6601

UNCLASSIFIED

SECURITY CLASSIFICATION OF THIS PAGE (When Data Entered)

#20 - ABSTRACT - CONTINUED

the unstaggered grid provides the best results. For the staggered grids, the results of the finite element models are not more accurate than the corresponding finite difference results. Oscillations occur in the temperature profiles near the surface for both staggered finite element models.

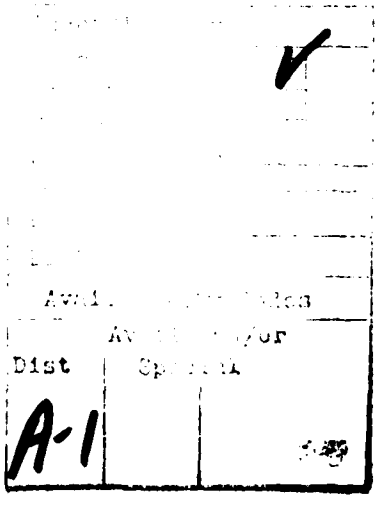

Approved for public release; distribution is unlimited.

A Comparison of Six Vertical Discretization Schemes

by

Mary S. Jordan
Captain, United States Air Force
B.S., University of Notre Dame, 1978
B.S., The Pennsylvania State University, 1979

Submitted in partial fulfillment of the
requirements for the degree of

MASTER OF SCIENCE IN METEOROLOGY

from the

NAVAL POSTGRADUATE SCHOOL
September 1985

Author: Mary S. Jordan
Mary S. Jordan

Approved by: Roger T. Williams
Roger T. Williams, Thesis Advisor

Mary Alice Rennick
Mary Alice Rennick, Second Reader

R. J. Renard by R. K. Elsberry
Robert J. Renard, Chairman,
Department of Meteorology

John Dyer
John Dyer,
Dean of Science and Engineering

ABSTRACT

Six vertical discretization schemes are compared for a linear, baroclinic, vorticity-divergence equation model. Variables are defined for two staggered and one unstaggered grids. A finite difference and a Galerkin finite element approximation are formulated for each of the three grids. The models are tested in three experiments. The largest difference between the grids occurs in the mid-atmosphere diabatic heat source experiment and the unstaggered grid provides the best results. For the staggered grids, the results of the finite element models are not more accurate than the corresponding finite difference results. Oscillations occur in the temperature profiles near the surface for both staggered finite element models.

TABLE OF CONTENTS

LIST OF FIGURES

I. INTRODUCTION

The finite elements method (FEM) has been used in several atmospheric prediction models (Staniforth and Mitchell, 1977; Williams and Schoenstadt, 1980, Béland, et al., 1983). The FEM is a special case of the Galerkin procedure in which the dependent variables are approximated by a finite sum of spatially varying basis functions with time dependent coefficients. The FEM basis functions are low order polynomials which are zero except in a localized region. The Galerkin procedure produces a set of coupled ordinary differential equations which are solved by using finite differences in time (Haltiner and Williams, 1980).

FEM models are potentially more accurate than finite difference method (FDM) models. Winninghoff (1968), Arakawa and Lamb (1977), and Schoenstadt (1980) have demonstrated the advantages of spatial staggering of predictive variables in finite difference approximations of shallow water equations. The results of Williams and Schoenstadt (1980) indicated that FEM models should either use staggered nodal points in the momentum equations or unstaggered nodal points in the vorticity-divergence equations.

The purpose of this research is to compare six linear, baroclinic, vorticity-divergence equation models. A finite difference and a finite element model are written for each of

the three vertical grids depicted in Figure 1. Grid A, which was originally developed by Lorenz (1960) for energy conservation, is a widely used grid for finite difference models. However, Tokioka (1978) has shown that this grid has a computational mode in the temperature field, and Arakawa (1984) has found a false small scale baroclinic instability with this grid. Tokioka (1978) also found that grid C has computational modes in all fields. Béland, et al., (1983), analyzed the finite element formulation for grid C and found noise generated by certain forms of friction. Grid B was introduced by Charney and Phillips (1953) for a finite difference quasi-geostrophic model. Tokioka's (1978) analysis has shown that this grid has no computational modes. It is hoped that the finite element formulation for this grid will have high accuracy without the problems the other grids have had with computational modes.

Each of the models used in this thesis are derived from the governing equations described in Chapter II. The models are one-wave spectral in the horizontal and have a fixed lid at the top of the atmosphere. Diabatic heating and mountain topography can be included in each model experiment.

The results of three experiments with analytic initial conditions will be examined. As described in Chapter III, the experiments are 1) an initial perturbation in the meridional flow, 2) flow over mountains, and 3) flow with a mid-atmosphere diabatic heat source. Each experiment will be presented with

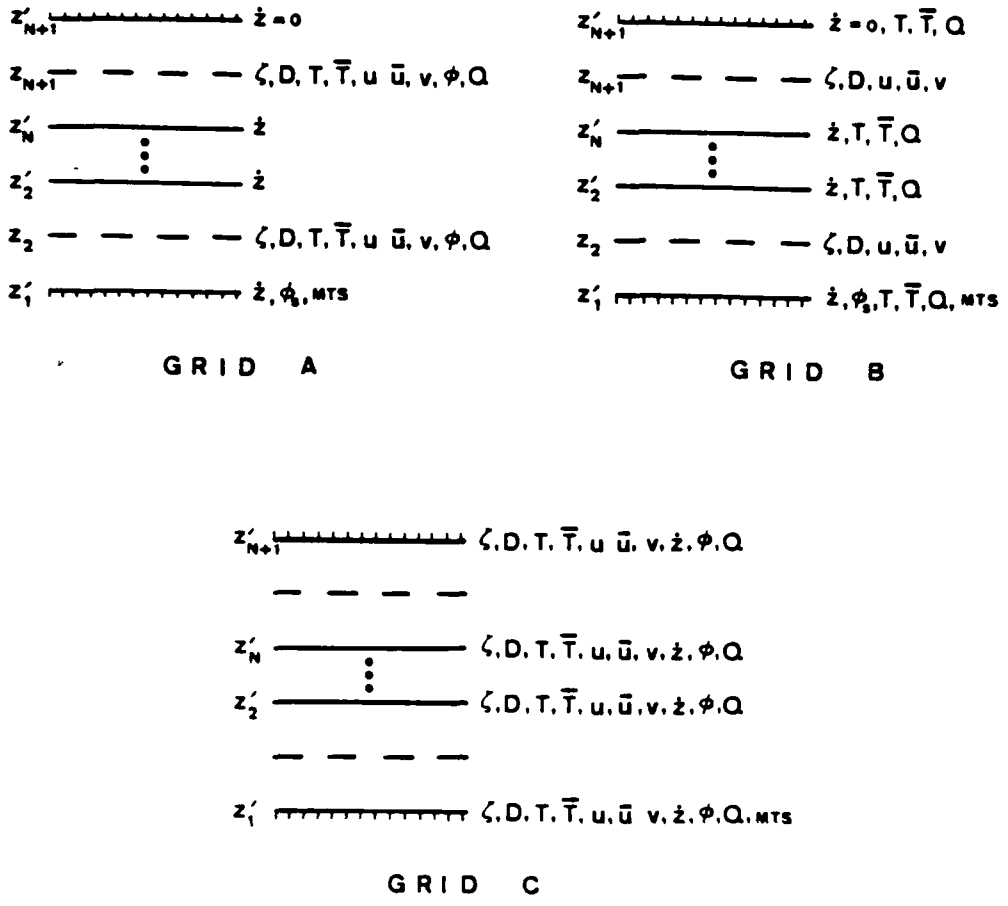

Figure 1. Three vertical grids to be compared for N-layer models. Perturbation variables are defined at either unstaggered levels (solid lines at height Z') or staggered levels (dashed lines at height Z). ζ is vorticity, D is divergence, T is potential temperature, $\bar{T}$ is basic state potential temperature, ϕ is geopotential, ϕ_s is surface geopotential, u is east-west velocity, $\bar{u}$ is basic state east-west velocity, v is north-south velocity, $\dot{z}$ is vertical velocity, Q is dibatic heating, and MTS is forced vertical velocity.

six and sixty vertical layers. The results of the 60-layer models will show if the models are converging to the same solution. For each model, comparison of the six and 60-layer results indicate how well the lower resolution model approximates the convergent solution. The purpose of these experiments is to identify any problem areas in the models and to demonstrate the general characteristics of each model.

II. MODEL DESCRIPTIONS

A. MODEL FEATURES

The six numerical models are developed with several features which make the models easy to modify for a wide range of experiments. The depth of the atmosphere, number of levels and the depth of each layer are variable in each model. Diabatic heating and forced vertical velocity due to mountain topography are included in the governing equations. The user can prescribe heating or forced vertical velocity functions, or run the model with these terms defined as zero. The models are written in modular structure using FORTRAN '77. There is parallel construction between models. The subroutines used in one model are very similar to those used in the other five models. The models run very quickly on an IBM-3033 mainframe. A 96-hour forecast for a 12-layer FEM uses less than five seconds of computer processing time.

B. GOVERNING EQUATIONS

Each model approximates the same set of governing equations. The vorticity (2-1), divergence (2-2), surface geopotential (2-3) equations and the first law of thermodynamics (2-4) are the prognostic equations for the forecast variables vorticity, divergence, surface geopotential and potential temperature. The surface geopotential equation is the lower boundary condition on the vertical velocity. The vertical

coordinate $Z = -\ln(p/p_0)$ is used, but the non-Boussinesq terms involving e^{-Z} are replaced by one. The prognostic equations in the coordinates x,y,Z,t are

$$\frac{d\zeta}{dt} + (\zeta+f)D + \beta v + \frac{\partial \dot{Z}}{\partial x}\frac{\partial v}{\partial x} - \frac{\partial \dot{Z}}{\partial y}\frac{\partial u}{\partial y} = 0 , \tag{2-1}$$

$$\frac{dD}{dt} + \left(\frac{\partial u}{\partial x}\right)^2 + \left(\frac{\partial v}{\partial y}\right)^2 + 2\frac{\partial u}{\partial y}\frac{\partial v}{\partial x} + \frac{\partial \dot{Z}}{\partial x}\frac{\partial u}{\partial Z} + \frac{\partial \dot{Z}}{\partial y}\frac{\partial v}{\partial Z} + \beta u - f\zeta + \nabla^2\phi = 0 , \tag{2-2}$$

$$\frac{d\phi_s}{dt} = MTS , \tag{2-3}$$

$$\frac{dT}{dt} = Q . \tag{2-4}$$

Here,

ζ is the vertical component of vorticity, $\zeta = \frac{\partial v}{\partial x} - \frac{\partial u}{\partial y}$,

D is the horizontal divergence, $D = \frac{\partial u}{\partial x} + \frac{\partial v}{\partial y}$,

ϕ is the geopotential, $\phi = gZ$,

ϕ_s is the surface geopotential,

T is the potential temperature,

u is the x-component of velocity,

v is the y-component of velocity,

$\dot{Z}$ is the vertical velocity,

Q is the diabatic heating per unit time per unit mass,

MTS is the forced vertical velocity due to flow over mountain topography, discussed in Chapter III,

f is the Coriolis parameter,

β is $\frac{df}{dy}$,

$\frac{d}{dt} = \frac{\partial}{\partial t} + u \frac{\partial}{\partial x} + v \frac{\partial}{\partial y} + \dot{Z} \frac{\partial}{\partial Z}$,

∇^2 is the horizontal Laplacian operator.

The prognostic equations are linearized by expanding the variables into the following mean state and perturbations:

$$u(x,Z,t) = \bar{u}(Z) + u'(x,Z,t) , \tag{2-5}$$

$$v(x,Z,t) = v'(x,Z,t) , \tag{2-6}$$

$$\dot{Z}(x,Z,t) = \dot{Z}'(x,Z,t) , \tag{2-7}$$

$$T(x,y,Z,t) = \bar{T}(y,Z) + T'(x,Z,t) , \tag{2-8}$$

$$\phi(x,y,Z,t) = \bar{\phi}(y,Z) + \phi'(x,Z,t) , \tag{2-9}$$

$$\phi_s(x,y,t) = \bar{\phi}_s(y) + \phi_s'(x,t) \tag{2-10}$$

$$\zeta(x,Z,t) = \zeta'(x,Z,t) , \tag{2-11}$$

$$D(x,Z,t) = D'(x,Z,t) , \tag{2-12}$$

$$Q(x,Z,t) = Q'(x,Z,t) , \tag{2-13}$$

$$MTS(x,t) = MTS'(x,t) . \tag{2-14}$$

The vorticity and divergence in this system are $\zeta = \frac{\partial v'}{\partial x}$, $D = \frac{\partial u'}{\partial x}$. The linearized forecast equations are

$$\frac{\partial \zeta'}{\partial t} = -fD' - \bar{u}\frac{\partial \zeta'}{\partial x} - \beta v' , \tag{2-15}$$

$$\frac{\partial D'}{\partial t} = f\zeta' - \bar{u}\frac{\partial D'}{\partial x} - \beta u' - \frac{\partial \dot{z}}{\partial x}\frac{d\bar{u}}{dz} - \frac{\partial^2 \phi'}{\partial x^2} , \tag{2-16}$$

$$\frac{\partial T'}{\partial t} = -\bar{u}\frac{\partial T'}{\partial x} - v'\frac{\partial \bar{T}}{\partial y} - \dot{z}\frac{\partial \bar{T}}{\partial z} + Q' , \tag{2-17}$$

$$\frac{\partial \phi_s'}{\partial t} = -\bar{u}\frac{\partial \phi_s'}{\partial x} - v'\frac{\partial \bar{\phi}_s}{\partial y} - R\bar{T}\dot{z} + MTS' , \tag{2-18}$$

where R is the gas constant for air.

The diagnostic variables, u', v', $\dot{z}'$, ϕ', are calculated from the forecast variables using the definitions of divergence, vorticity, the hydrostatic equation and the continuity equation. The relations are

$$\frac{\partial u'}{\partial x} = D' , \tag{2-19}$$

$$\frac{\partial v'}{\partial x} = \zeta' , \tag{2-20}$$

$$\frac{\partial \phi'}{\partial x} = RT' , \tag{2-21}$$

$$D' + \frac{\partial \dot{z}'}{\partial z} = 0 . \tag{2-22}$$

The use of primes to denote perturbation quantities will be discontinued. All quantities used in the remainder of

the paper will be perturbation quantities unless otherwise noted.

The mean state is assumed to be in hydrostatic and geostrophic balance. The term $\partial\bar{T}/\partial y$ in the first law of thermodynamics can be evaluated by taking $\partial/\partial y$ of the hydrostatic equation and substituting for $\partial\bar{\phi}/\partial y$ from the geostrophic relation, $\partial\bar{\phi}/\partial y = -f\bar{u}$. Thus,

$$\frac{\partial\bar{T}}{\partial y} = -\frac{f}{\bar{R}}\frac{\partial\bar{u}}{\partial Z} . \qquad (2\text{-}23)$$

Geostrophic balance of the mean state at the surface implies

$$\frac{\partial\bar{\phi}_s}{\partial y} = -f\bar{u}_{sfc} . \qquad (2\text{-}24)$$

The expressions (2-23) and (2-24) are substituted into equations (2-17) and (2-18), respectively.

A singlewave spectral representation is used in the x-direction, with wave number $\mu = 2\pi/L$, where L is the wavelength in the x-direction. The perturbation quantities have the form

$$\zeta'(x,Z,t) = A_1(Z,t)\cos\mu x + A_2(Z,t)\sin\mu x , \qquad (2\text{-}25)$$

$$D'(x,Z,t) = D_1(Z,t)\cos\mu x + D_2(Z,t)\sin\mu x , \qquad (2\text{-}26)$$

$$T'(x,Z,t) = T_1(Z,t)\cos\mu x + T_2(Z,t)\sin\mu x , \qquad (2\text{-}27)$$

$$\phi_s'(x,t) = S_1(t)\cos \mu x + S_2(t)\sin \mu x \ , \tag{2-28}$$

$$u'(x,Z,t) = U_1(Z,t)\cos \mu x + U_2(Z,t)\sin \mu x \ , \tag{2-29}$$

$$v'(x,Z,t) = V_1(Z,t)\cos \mu x + V_2(Z,t)\sin \mu x \ , \tag{2-30}$$

$$\dot{Z}'(x,Z,t) = W_1(Z,t)\cos \mu x + W_2(Z,t)\sin \mu x \ , \tag{2-31}$$

$$\phi'(x,Z,t) = H_1(Z,t)\cos \mu x + H_2(Z,t)\sin \mu x \ , \tag{2-32}$$

$$Q'(x,Z,t) = Q_1(Z,t)\cos \mu x + Q_2(Z,t)\sin \mu x \ , \tag{2-33}$$

$$MTS'(x,t) = MTS_1(t)\cos \mu x + MTS_2(t)\sin \mu x \ . \tag{2-34}$$

The relations (2-25)-(2-34) are substituted into equations (2-15)-(2-22). The prognostic and diagnostic equations are separated into equations for the cosine and sine terms. The resultant prognostic equations are

$$\frac{\partial A_1}{\partial t} = -fD_1 - \bar{u}\mu A_2 - \beta V_1 \ , \tag{2-35}$$

$$\frac{\partial A_2}{\partial t} = -fD_2 + \bar{u}\mu A_1 - \beta V_2 \ , \tag{2-36}$$

$$\frac{\partial D_1}{\partial t} = fA_1 - \bar{u}\mu D_2 - \beta U_1 - \mu \frac{d\bar{u}}{dZ} W_2 + \mu^2 H_1 \ , \tag{2-37}$$

$$\frac{\partial D_2}{\partial t} = fA_2 + \bar{u}\mu D_1 - \beta U_2 + \mu \frac{d\bar{u}}{dZ} W_1 + \mu^2 H_2 , \quad (2\text{-}38)$$

$$\frac{\partial T_1}{\partial t} = -\bar{u}\mu T_2 + \frac{f}{R} \frac{d\bar{u}}{dZ} V_1 - \frac{\partial \bar{T}}{\partial Z} W_1 + Q_1 , \quad (2\text{-}39)$$

$$\frac{\partial T_2}{\partial t} = \bar{u}\mu T_1 + \frac{f}{R} \frac{d\bar{u}}{dZ} V_2 - \frac{\partial \bar{T}}{\partial Z} W_2 + Q_2 , \quad (2\text{-}40)$$

$$\frac{\partial S_1}{\partial t} = -\bar{u}\mu S_2 + f\bar{u}V_1 - R\bar{T}W_1 + MTS_1 , \quad (2\text{-}41)$$

$$\frac{\partial S_2}{\partial t} = \bar{u}\mu S_1 + f\bar{u}V_2 - R\bar{T}W_2 + MTS_2 . \quad (2\text{-}42)$$

The resultant diagnostic equations for u and v are

$$U_1 = -\frac{D_2}{\mu} , \quad (2\text{-}43)$$

$$U_2 = \frac{D_1}{\mu} , \quad (2\text{-}44)$$

$$V_1 = -\frac{A_2}{\mu} , \quad (2\text{-}45)$$

$$V_2 = \frac{A_1}{\mu} . \quad (2\text{-}46)$$

Geopotential values above the surface are obtained by integrating the hydrostatic equation from the surface ($Z = Z_0$) to height Z:

$$H_1 = R \int_{Z_0}^{Z} T_1(Z,t)dZ + S_1 \quad (2\text{-}47)$$

$$H_2 = R \int_{Z_0}^{Z} T_2(Z,t)dZ + S_2 \qquad (2\text{-}48)$$

The vertical velocity is calculated by integrating the continuity equation from the top of the atmosphere ($Z = Z_T$) down to height Z. The upper boundary condition, $\dot{Z} = 0$ at $Z = Z_T$, is used. This boundary condition is not exact, but some form of it is used in most numerical models. The diagnostic equations for the vertical velocity are

$$W_1 = \int_{Z}^{Z_T} D_1(Z,t)dZ \ , \qquad (2\text{-}49)$$

$$W_2 = \int_{Z}^{Z_T} D_2(Z,t)dZ \ . \qquad (2\text{-}50)$$

Equations (2-35)-(2-50) are the prognostic and diagnostic equations that govern all six numerical models. Using the given basic state and the one-wave spectral perturbation quantities, the governing equations reduce to functions of Z and t. The models are effectively one-dimensional.

To display the results of each model, the sine and cosine amplitudes of each variable are combined to determine the amplitude and phase of a single cosine wave in the x-direction. A typical variable has the form

$$Y(x,Z,t) = A(Z,t)\cos(\mu x - \delta) \ , \qquad (2\text{-}51)$$

where the amplitude is A(Z,t) and the phase is $\delta(Z,t)$. The amplitude and phase are calculated at each level for all variables.

C. TIME DIFFERENCING

Two forward time steps are taken to start each model and then leapfrog time differencing is used. The leapfrog scheme is employed because of its ease to code. A Robert filter is used to reduce the amplitude of the computational mode generated by the leapfrog time differencing. The filter is discussed by Haltiner and Williams, 1980. For a prognostic variable F, calculate $\bar{F}_{n-1}$, the average value of F at time step $(n-1)\Delta t$, using equation (2-52). Using the unaveraged values at time step $n\Delta t$, compute the tendency $(\frac{\partial F}{\partial t})_n$ from its predictive equation. The predicted value at time step $(n+1)\Delta t$ is calculated using equation (2-53).

$$\bar{F}_{n-1} = F_{n-1} + \gamma(F_n - 2F_{n-1} + \bar{F}_{n-2}) , \qquad (2\text{-}52)$$

where γ is a weighting function.

$$F_{n+1} = \bar{F}_{n-1} + 2\Delta t(\frac{\partial F}{\partial t})_n \qquad (2\text{-}53)$$

In all thesis experiments, $\gamma = 0.05$ is used. The time step for each experiment is calculated in the model by requiring, for computational stability,

$$\nu\Delta t = \frac{1}{2} , \qquad (2\text{-}54)$$

where $\nu = \mu c$, and c is the typical phase speed of an external gravity wave.

D. VERTICAL GRIDS

Each of the models uses one of three vertical grids. The three ways of distributing the variables over discrete levels are depicted in Figure 1. The staggered levels are represented by the dashed lines in Figure 1. Notice that the heights at which the variables are defined change between the three grids. The notation used in this paper to denote the staggered and unstaggered levels is consistent with the conventions used in the coded models. The height of the unstaggered levels is denoted as Z'. The height of the staggered levels is denoted as Z. In the models, both Z'_1 and Z_1 are defined to be the surface of the earth. It is assumed that the staggered level Z_i is exactly in the middle of the layer between Z'_{i-1} and Z'_i. This distinction is important because the models can have layers with unequal depth. Thus, the height of the staggered levels is defined relative to the height of the unstaggered levels.

A finite difference model is written for each of the grid structures. The models are denoted as DFM-A, FDM-B and FDM-C. Similarly, finite element models using the three grids are indicated by FEM-A, FEM-B and FEM-C.

E. FINITE DIFFERENCE MODELS

The only differences in the equations between the three FDM models are the approximations of terms involving $d\bar{u}/dZ$ and $\partial\bar{T}/\partial Z$ in the prognostic equations and the approximations of the integral in the diagnostic geopotential equation. Centered difference approximations are used, except at the boundaries where one-sided differences are employed. The finite difference approximations used in the prognostic equations are listed in Appendix A.

F. FINITE ELEMENT MODELS

1. FEM-C

The unstaggered FEM model is the simplest of the three FEM models. Each of the dependent variables is expanded into a finite series in terms of the eigenfunctions $\phi_j(Z)$. The eigenfunctions for this model are depicted in Figure 2. The eigenfunction expansion for a typical term is

$$A_l(Z,t) = \sum_{j=1}^{N+1} A_l^j(t)\,\phi_j(Z) \quad . \tag{2-55}$$

The finite element approximations for the vorticity, divergence and thermodynamic equations are derived by substituting the eigenfunction expansion for each dependent variable into equations (2-35)-(2-40). Each equation is multiplied by $\phi_i(Z)$ and integrated with respect to Z from the bottom to

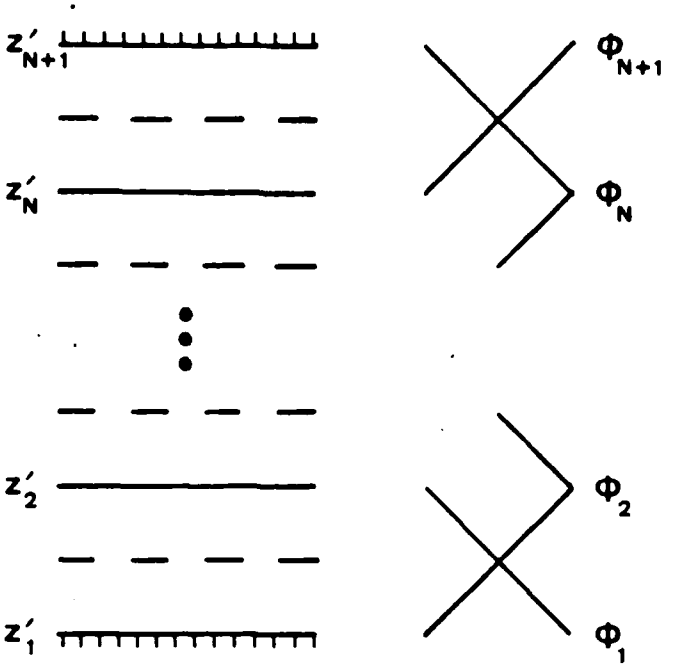

Figure 2. Eigenfunctions defined at unstaggered levels (solid lines) for grid C. Dashed lines represent staggered levels.

the top of the atmosphere. Each term in the equations is the finite sum of separate integrals. Only the integrals of overlapping eigenfunctions are nonzero. The resultant equations, listed in Appendix B, are matrix equations. For an N-layer model, the variables are calculated at N+1 discrete levels and the variable can be represented as a column vector of length N+1. Thus, the forecast equations for vorticity, divergence and potential temperature become vector equations which contain four (N+1) × (N+1) matrices multiplying appropriate vectors.

The mass matrix for this model is defined by

$$\underline{\underline{M}} = \sum_{j=i-1}^{i+1} \int_{Z_0}^{Z_T} \phi_j(Z)\phi_i(Z)dZ, \quad \text{for } i = 1,\ldots,N+1 . \qquad (2\text{-}56)$$

The matrix $\underline{\underline{N}}$ is defined for terms multiplied by $\bar{u}$,

$$\underline{\underline{N}} = \sum_{j=i-1}^{i+1} \sum_{k=i-1}^{i+1} \bar{u}_j \int_{Z_0}^{Z_T} \phi_j(Z)\phi_k(Z)\phi_i(Z)dZ,$$

$$\text{for } i = 1,\ldots,N+1 . \qquad (2\text{-}57)$$

The matrix $\underline{\underline{P}}$ is defined for terms multiplied by $d\bar{u}/dZ$,

$$\underline{\underline{P}} = \sum_{j=i-1}^{i+1} \sum_{k=i-1}^{i+1} \bar{u}_j \int_{Z_0}^{Z_T} \frac{d\phi_j}{dZ} \phi_k(Z)\phi_i(Z)dZ,$$

$$\text{for } i = 1,\ldots,N+1 . \qquad (2\text{-}58)$$

The matrix $\underline{\underline{R}}$ is defined for terms multiplied by $\partial\bar{T}/\partial Z$,

$$\underline{\underline{R}} = \sum_{j=i-1}^{i+1} \sum_{k=i-1}^{i+1} \bar{T}_j \int_{Z_0}^{Z_T} \frac{d\phi_j}{dZ} \phi_k(Z)\phi_i(Z)dZ,$$

$$\text{for } i = 1,\ldots,N+1 . \qquad (2\text{-}59)$$

The method to evaluate the terms of matrices (2-56)-(2-59) and the resultant formulas for the matrix elements are listed in Appendix C.

The vorticity, divergence and thermodynamic equations, written in matrix (indicated by a double underline) and vector (indicated by a single underline) form are

$$\underline{\underline{M}}\cdot\frac{d}{dt}(\underline{A1}) = \underline{\underline{M}}\cdot(-f\cdot\underline{D1} - \beta\cdot\underline{V1}) - \mu\cdot\underline{\underline{N}}\cdot\underline{A2} \ , \tag{2-60}$$

$$\underline{\underline{M}}\cdot\frac{d}{dt}(\underline{A2}) = \underline{\underline{M}}\cdot(-f\cdot\underline{D2} - \beta\cdot\underline{V2}) + \mu\cdot\underline{\underline{N}}\cdot\underline{A1} \ , \tag{2-61}$$

$$\underline{\underline{M}}\cdot\frac{d}{dt}(\underline{D1}) = \underline{\underline{M}}\cdot(f\cdot\underline{A1} - \beta\underline{U1}) - \mu\cdot\underline{\underline{N}}\cdot\underline{D2} - \mu\cdot\underline{\underline{P}}\cdot\underline{W2} + \mu^2\cdot\underline{\underline{M}}\cdot\underline{H1} \ , \tag{2-62}$$

$$\underline{\underline{M}}\cdot\frac{d}{dt}(\underline{D2}) = \underline{\underline{M}}\cdot(f\cdot\underline{A2} - \beta\underline{U2}) + \mu\cdot\underline{\underline{N}}\cdot\underline{D1} + \mu\cdot\underline{\underline{P}}\cdot\underline{W2} + \mu^2\cdot\underline{\underline{M}}\cdot\underline{H2} \ , \tag{2-63}$$

$$\underline{\underline{M}}\cdot\frac{d}{dt}(\underline{T1}) = -\mu\cdot\underline{\underline{N}}\cdot\underline{T2} + (\frac{f}{R})\cdot\underline{\underline{P}}\cdot\underline{V1} - \underline{\underline{R}}\cdot\underline{W1} + \underline{\underline{M}}\cdot\underline{Q1} \ , \tag{2-64}$$

$$\underline{\underline{M}}\cdot\frac{d}{dt}(\underline{T2}) = \mu\cdot\underline{\underline{N}}\cdot\underline{T1} + (\frac{f}{R})\cdot\underline{\underline{P}}\cdot\underline{V2} - \underline{\underline{R}}\cdot\underline{W2} + \underline{\underline{M}}\cdot\underline{Q2} \ . \tag{2-65}$$

Equations (2-60)-(2-65) are simplified by multiplying each equation by $\underline{\underline{M}}^{-1}$ and applying the Robert filter. The matrices $\underline{\underline{M}}^{-1}\cdot\underline{\underline{N}}$, $\underline{\underline{M}}^{-1}\cdot\underline{\underline{P}}$, $\underline{\underline{M}}^{-1}\cdot\underline{\underline{R}}$ are constants. They are constructed in the initialization subroutine and stored for use in the forecast subroutine. The matrices are multiplied by the appropriate vectors with values for time level $n\Delta t$. The

resultant forecast equations are vector equations and the forecast value for the i-th vertical level is the sum of values in the i-th location of each vector in the equation. The prognostic equations for the vorticity, divergence and potential temperature vectors are

$$\underline{A1}_{n+1} = \underline{A1BAR}_{n-1} + 2\Delta t(-f\cdot\underline{D1} - \beta\cdot\underline{V1} - \mu\cdot\underline{\underline{M}}^{-1}\cdot\underline{\underline{N}}\cdot\underline{A2})_n , \quad (2\text{-}66)$$

$$\underline{A2}_{n+1} = \underline{A2BAR}_{n-1} + 2\Delta t(-f\cdot\underline{D2} - \beta\cdot\underline{V2} + \mu\cdot\underline{\underline{M}}^{-1}\cdot\underline{\underline{N}}\cdot\underline{A1})_n , \quad (2\text{-}67)$$

$$\underline{D1}_{n+1} = \underline{D1BAR}_{n-1} + 2\Delta t(f\cdot\underline{A1} - \beta\cdot\underline{U1} - \mu\cdot\underline{\underline{M}}^{-1}\cdot\underline{\underline{N}}\cdot\underline{D2} - \mu\cdot\underline{\underline{M}}^{-1}\cdot\underline{\underline{P}}\cdot\underline{W2} + \mu^2\underline{H1})_n , \quad (2\text{-}68)$$

$$\underline{D2}_{n+1} = \underline{D2BAR}_{n-1} + 2\Delta t(f\cdot\underline{A2} - \beta\cdot\underline{U2} + \mu\cdot\underline{\underline{M}}^{-1}\cdot\underline{\underline{N}}\cdot\underline{D1} + \mu\cdot\underline{\underline{M}}^{-1}\cdot\underline{\underline{P}}\cdot\underline{W1} + \mu^2\underline{H2})_n , \quad (2\text{-}69)$$

$$\underline{T1}_{n+1} = \underline{T1BAR}_{n-1} + 2\Delta t(-\mu\cdot\underline{\underline{M}}^{-1}\cdot\underline{\underline{N}}\cdot\underline{T2} + (\frac{f}{R})\cdot\underline{\underline{M}}^{-1}\cdot\underline{\underline{P}}\cdot\underline{V1} - \underline{\underline{M}}^{-1}\cdot\underline{\underline{R}}\cdot\underline{W1} + \underline{Q1})_n , \quad (2\text{-}70)$$

$$\underline{T2}_{n+1} = \underline{T2BAR}_{n-1} + 2\Delta t(\mu\cdot\underline{\underline{M}}^{-1}\cdot\underline{\underline{N}}\cdot\underline{T1} + (\frac{f}{R})\cdot\underline{\underline{M}}^{-1}\cdot\underline{\underline{P}}\cdot\underline{V2} - \underline{\underline{M}}^{-1}\cdot\underline{\underline{R}}\cdot\underline{W2} + \underline{Q2})_n , \quad (2\text{-}71)$$

where the subscripts n+1, n, n-1, refer to the values of the vectors at time step $(n+1)\Delta t$, $n\Delta t$, and $(n-1)\Delta t$, respectively.

The surface geopotential and the diagnostic variables are calculated using the same equations that are used in the unstaggered model FDM-C.

2. FEM-A

The FEM-A model defines vertical velocity at the unstaggered levels in terms of the eigenfunctions $\psi_j(Z)$. The other variables are defined at the staggered levels in terms of the eigenfunctions $\phi_j(Z)$. The eigenfunctions for this model are depicted in Figure 3.

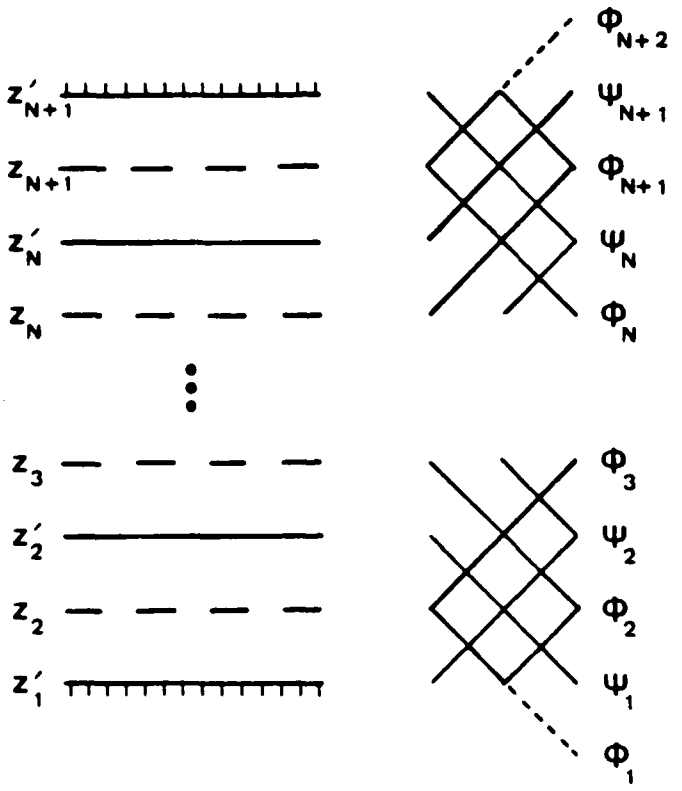

Figure 3. Eigenfunctions for grids A and B. Egienfunctions $\psi(Z)$ are defined for the unstaggered levels (solid lines at height Z') and $\phi(Z)$ are defined for the staggered levels (dashed lines at height Z).

The finite element approximations for the vorticity, divergence and thermodynamic equations are derived using the method described for the FEM-C model. The resultant Galerkin formulation of the equations, listed in Appendix D, are matrix equations. The mass matrix, $\underline{\underline{M}}$, and the matrix, $\underline{\underline{N}}$, for terms of the form $\bar{u}$ multiplied by variables defined at the nodal points of $\phi_j(Z)$ have the same formulas as $\underline{\underline{M}}$ and $\underline{\underline{N}}$ in the FEM-C model, equations (2-56) and (2-57). However, the eigenfunctions $\phi_j(Z)$ are not defined at the same levels in both models. The matrix $\underline{\underline{Q}}$ is defined for terms of the form $\frac{d\bar{u}}{dZ}\cdot V$,

$$\underline{\underline{Q}} = \sum_{j=i-1}^{i+1} \sum_{k=i-1}^{i+1} \bar{u}_j \int_{Z_0}^{Z_T} \frac{d\phi_j}{dZ} \phi_k \phi_i dZ \ . \tag{2-72}$$

The matrix $\underline{\underline{P}}$ is defined for terms of the form $\frac{d\bar{u}}{dZ}\cdot W$,

$$\underline{\underline{P}} = \sum_{j=i-1}^{i+1} \sum_{k=i-2}^{i+1} \bar{u}_j \int_{Z_0}^{Z_T} \frac{d\phi_j}{dZ} \psi_k \phi_i dZ \ . \tag{2-73}$$

The matrix $\underline{\underline{R}}$ is defined for terms of the form $\frac{\partial\bar{T}}{\partial Z}\cdot W$,

$$\underline{\underline{R}} = \sum_{j=i-1}^{i+1} \sum_{k=i-2}^{i+1} \bar{T}_j \int_{Z_0}^{Z_T} \frac{d\phi_j}{dZ} \psi_k \phi_i dZ \ . \tag{2-74}$$

The staggered eigenfunctions present three general problems for evaluating the elements of the five matrices.

First, for an N-layer model, portions of eigenfunctions $\phi_1(Z)$ and $\phi_{N+2}(Z)$ are defined in the model atmosphere but the physical meaning of contributions from those terms is unclear. The contributions are included in the first two rows and the last row of each matrix. Second, only portions of eigenfunctions $\phi_2(Z)$ and $\phi_{N+1}(Z)$ are defined in the model atmosphere. To describe the incomplete sides of both eigenfunctions an assumption must be made about the value of ϕ_2 at the surface and ϕ_{N+1} at the top of the atmosphere. Last, the equations derived for the general elements of each matrix are more complex than the formulas for the model FEM-C. The complexity of these equations makes it much more difficult to evaluate the elements in the first two and last two rows of each matrix.

Assumptions are made and procedures are developed in an attempt to resolve these problems. In this model the mean state variables, $\bar{u}$ and $\bar{T}$, are defined only at the N staggered levels. However, $\bar{u}$ and $\bar{T}$ values defined at the nodal points of $\phi_1(Z)$ and $\phi_{N+2}(Z)$ are important in the Galerkin formulation of the $d\bar{u}/dZ$ and $\partial\bar{T}/\partial Z$ terms. In my thesis experiments, the values of $\bar{u}$ and $\bar{T}$ are defined at the surface and top of the atmosphere; they are not defined at the nodal points of $\phi_1(Z)$ and $\phi_{N+2}(Z)$ becuase these points are outside the model atmosphere. For constant shear with height, $\bar{u}$ and $\bar{T}$ are defined at the boundaries such that the shear in the two half layers at the boundaries is the same as the shear in the other layers.

The contributions from the perturbation quantities defined at the nodal points of $\phi_1(Z)$ and $\phi_{N+2}(Z)$ are not included in these experiments. To be consistent with the other N-layer models, all perturbation quantities are defined as column vectors of length N+1 even though all quantities, except vertical velocity, are defined at only N levels. The values of each perturbation at its lowest staggered level are stored as the second element in its column vector; zero is stored as the first element, which corresponds to the contribution from $\phi_1(Z)$. To evaluate the staggered eigenfunctions defined in the layers between the surface and Z_2, and Z_{N+1} and the top of the atmosphere, it is assumed that the value at the boundaries of those eigenfunctions is one-half. Thus, three-fourths of the eigenfunctions $\phi_2(Z)$ and $\phi_{N+2}(Z)$ are defined in the model atmosphere.

The equations for the general elements of the five matrices are evaluated by substituting into equations (2-56)-(2-57) and (2-72)-(2-74) the formulas for $\phi_{i+1}(Z)$, $\phi_i(Z)$, $\phi_{i-1}(Z)$, $\psi_{i+1}(Z)$, $\psi_i(Z)$, $\psi_{i-1}(Z)$, and $\psi_{i-2}(Z)$ terms of the local coordinate $\xi = Z - Z_i$. The equations for these eigenfunctions defined for the levels 1, 2, i, and N+1 are listed in Appendix E. The equations for the elements of the first two rows and the last row of the matrices $\underline{\underline{P}}$, $\underline{\underline{Q}}$, and $\underline{\underline{R}}$ are derived using the formulas for levels 1, 2, and N+1. However, the corresponding rows of matrices $\underline{\underline{M}}$ and $\underline{\underline{N}}$ were not calculated using these formulas because the model results for the

barotropic experiment were not constant with height when the elements in those three rows of both $\underline{\underline{M}}$ and $\underline{\underline{N}}$ were calculated using these formulas. The reason for this is not clear. The equations for the general elements of $\underline{\underline{M}}$ and $\underline{\underline{N}}$ are simple enough to allow the terms in the affected three rows of each matrix to be deduced by reason. The equations for the elements of all five matrices are listed in Appendix F.

The prognostic matrix equations for vorticity, divergence and temperature, listed in Appendix D, are simplified in a manner similar to the method described for the FEM-C model. The final form of the forecast equations for the vorticity and divergence vectors are the same as for model FEM-C, equations (2-66)-(2-69). The thermodynamic vector equations are

$$\underline{T1}_{n+1} = \underline{T1BAR}_{n-1} + 2\Delta t \cdot [\underline{Q1} - \mu \cdot \underline{\underline{M}}^{-1} \cdot \underline{\underline{N}} \cdot \underline{T2} + (\frac{f}{R}) \cdot \underline{\underline{M}}^{-1} \cdot \underline{Q} \cdot \underline{V1} - \underline{\underline{M}}^{-1} \cdot \underline{\underline{R}} \cdot \underline{W1}]_n , \quad (2\text{-}75)$$

$$\underline{T2}_{n+1} = \underline{T2BAR}_{n-1} + 2\Delta t \cdot [\underline{Q2} + \mu \cdot \underline{\underline{M}}^{-1} \cdot \underline{\underline{N}} \cdot \underline{T1} + (\frac{f}{R}) \underline{\underline{M}}^{-1} \cdot \underline{Q} \cdot \underline{V2} - \underline{\underline{M}}^{-1} \cdot \underline{\underline{R}} \cdot \underline{W2}]_n . \quad (2\text{-}76)$$

The six forecast equations are solved at levels two to N+1. The surface geopotential and the diagnostic variables are calculated using the corresponding equations in model FEM-A.

3. FEM-B

The FEM-B model defines vertical velocity, potential temperature, mean state potential temperature and diabatic heating at the unstaggered levels in terms of the eigenfunctions $\psi_j(Z)$. The other variables are defined at the staggered levels in terms of the eigenfunctions $\phi_j(Z)$. The eigenfunctions are the same as defined for the FEM-A model, shown in Figure 3.

The finite element approximations for the vorticity, divergence and thermodynamic equations are derived by substituting the eigenfunction expansion for each dependent variable into equations (2-35)-(2-40). The vorticity and divergence equations are multiplied by $\phi_i(Z)$ and integrated with respect to Z from the bottom to the top of the atmosphere. The resultant Galerkin formulation of the vorticity and divergence equations are the same as those derived for model FEM-A. The matrices in those equations, $\underline{\underline{M}}$, $\underline{\underline{N}}$, and $\underline{\underline{P}}$, are the same as defined for FEM-A, equations (2-56)-(2-57) and (2-73). The thermodynamic equations are multiplied by $\psi_i(Z)$ because potential temperature is defined at the unstaggered levels. As before, the equations are integrated through the depth of the atmosphere. The resultant equations are listed in Appendix G. Four additional matrices are defined for the two thermodynamic equations. The mass matrix $\underline{\underline{S}}$ is

$$\underline{\underline{S}} = \sum_{j=i-1}^{i+1} \int_{Z_0}^{Z_T} \psi_j(Z)\psi_i(Z)dZ \ . \qquad (2\text{-}77)$$

The matrix $\underline{\underline{Q}}$ is defined for terms of the form $\frac{d\bar{u}}{dZ}\cdot V$,

$$\underline{\underline{Q}} = \sum_{j=i-1}^{i+2} \sum_{k=i-1}^{i+2} \bar{u}_j \int_{Z_0}^{Z_T} \phi_j(Z)\phi_k(Z)\psi_i(Z)dZ \ . \qquad (2\text{-}78)$$

The matrix $\underline{\underline{R}}$ is defined for terms of the form $\frac{\partial\bar{T}}{\partial Z}\cdot W$,

$$\underline{\underline{R}} = \sum_{j=i-1}^{i+1} \sum_{k=i-1}^{i+1} \bar{T}_j \int_{Z_0}^{Z_T} \frac{d\psi_j}{dZ} \psi_k(Z)\psi_i(Z)dZ \ . \qquad (2\text{-}79)$$

The matrix $\underline{\underline{T}}$ is defined for terms of the form $\bar{u}\cdot T$,

$$\underline{\underline{T}} = \sum_{j=i-1}^{i+2} \sum_{k=i-1}^{i+1} \bar{u}_j \int_{Z_0}^{Z_T} \phi_j(Z)\psi_k(Z)\psi_i(Z)dZ \ . \qquad (2\text{-}80)$$

As discussed in the FEM-A model description, the staggered finite elements present problems for evaluating the elements of the matrices. In this model $\bar{u}$ is defined at the surface, the top of the atmosphere, and at the N staggered levels. The mean state temperature, $\bar{T}$, is defined at the unstaggered levels so special definitions for it are not needed. Also, the contributions from the perturbation quantities defined at the nodal points of $\phi_1(Z)$ and $\phi_{N+2}(Z)$ are not included in the model FEM-B model experiments. The staggered eigenfunctions, $\phi_i(Z)$, are evaluated at the boundaries using the assumptions discussed in the previous section.

The elements of matrices $\underline{\underline{S}}$, $\underline{\underline{Q}}$, $\underline{\underline{R}}$, and $\underline{\underline{T}}$ are evaluated by substituting formulas for $\phi_{i+2}(Z)$, $\phi_{i+1}(Z)$, $\phi_i(Z)$, $\phi_{i-1}(Z)$, $\psi_{i+1}(Z)$, $\psi_i(Z)$ and $\psi_{i-1}(Z)$, defined in terms of the local coordinate $\eta = Z - Z_i'$, into equations (2-77)-(2-80). Formulas for these eigenfunctions are listed in Appendix H. The equations for the matrix elements are listed in Appendix I.

The forecast matrix equations for vorticity, divergence and temperature are simplified in a manner similar to the method described for model FEM-C. The final form of the vorticity and divergence vector equations are the same as for model FEM-C, equations (2-66)-(2-69). The thermodynamic vector equations are

$$\underline{T1}_{n+1} = \underline{T1BAR}_{n-1} + 2\Delta t[\underline{Q1} - \mu\cdot\underline{\underline{S}}^{-1}\cdot\underline{\underline{T}}\cdot\underline{T2} + (\frac{f}{R})\cdot\underline{\underline{S}}^{-1}\cdot\underline{\underline{Q}}\cdot\underline{V1} - \underline{\underline{S}}^{-1}\cdot\underline{\underline{R}}\cdot\underline{W1}]_n , \quad (2\text{-}81)$$

$$\underline{T2}_{n+1} = \underline{T2BAR}_{n-1} + 2\Delta t[\underline{Q2} + \mu\cdot\underline{\underline{S}}^{-1}\underline{\underline{T}}\cdot\underline{T1} + (\frac{f}{R})\cdot\underline{\underline{S}}^{-1}\cdot\underline{\underline{Q}}\cdot\underline{V2} - \underline{\underline{S}}^{-1}\cdot\underline{\underline{R}}\cdot\underline{W2}]_n . \quad (2\text{-}82)$$

The vorticity and divergence equations are solved at levels two to N+1. The thermodynamic equations are solved at all unstaggered levels. The surface geopotential and the diagnostic variables are calculated using the corresponding equations in model FDM-B.

III. EXPERIMENTS AND RESULTS

Three experiments are performed with each model; an initial perturbation in the meridional flow, flow over mountain topography and flow with a diabatic heat source. The first two experiments are performed with each model defined with six and then sixty layers. The heating experiment is repeated with six, twelve and sixty-layer models. The analytic solution of each experiment has not been derived. For each experiment, the 60-layer model results are intercompared to determine if the models are converging to the same solution. The standard of comparison for each six-layer model is its corresponding 60-layer solution. Temperature and divergence profiles are examined in each experiment.

Several parameters are defined identically in each experiment. The vertical coordinate, Z, is defined between zero and one (1000-368 mb) and the vertical levels are equally spaced. The x-wavelength is 4,000 kilometers. The time step is 17.7 minutes. The Coriolis parameter is defined at 45 degrees latitude. There is no vertical shear in the $\bar{u}$ field and $\bar{u}$ = 10.0 meters/second (m/s). The mean state potential temperature increases with height from its surface value of 310.0 Kelvin (K).

A. ROSSBY WAVE EXPERIMENT

Rossby waves are generated in each model using an initial perturbation, v' = 5.0 m/s, in the cosine term of the

meridional flow. All other perturbations are initially zero. There is no diabatic heat source and no mountain topography. The latitudinal variation of the Coriolis parameter, β, is defined at 45 degrees latitude. The forecast length of this experiment is 96 hours.

1. Sixty-Layer Models

The 60-layer FDM-A, FDM-B, FDM-C, and FEM-C models converge to the same temperature and divergence solutions (Figures 4-7). It should be noted that the phase of each variable is defined between zero and 360 degrees. There is a discontinuity in the phase profile if the phase passes through zero degrees. The height at which the temperature phase discontinuity in model FDM-A occurs differs from the other three models because temperature is defined at the staggered levels in FDM-A. The four models represent the same physical solution, which is called the consensus solution.

The FEM-B temperature amplitude is slightly larger than the consensus amplitude (5%) and an amplitude oscillation is present in the lowest three layers of the atmosphere (Figure 8). The jagged profile may be caused by the terms in the matrices which represent contributions from the eigenfunctions near the lower boundary of the model. There is a discontinuity between the temperature phases in the lowest two layers of the FEM-B profile (Figure 9). Apart from this feature, the general shape of the phase profile is similar to the consensus, although the phase is five degrees less and passes through

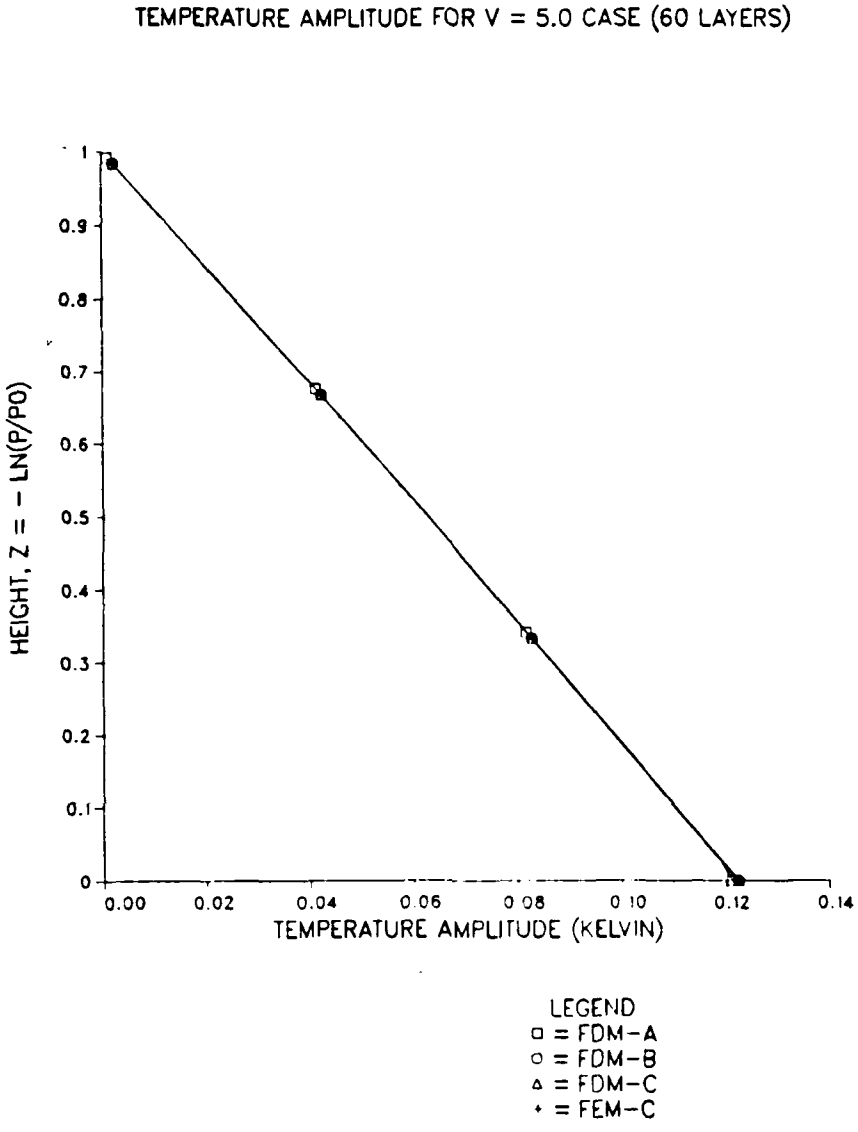

Figure 4. Sixty-layer Rossby-wave experiment at 96 hours. Temperature amplitude profiles are compared for models FDM-A, FDM-B, FDM-C, and FEM-C.

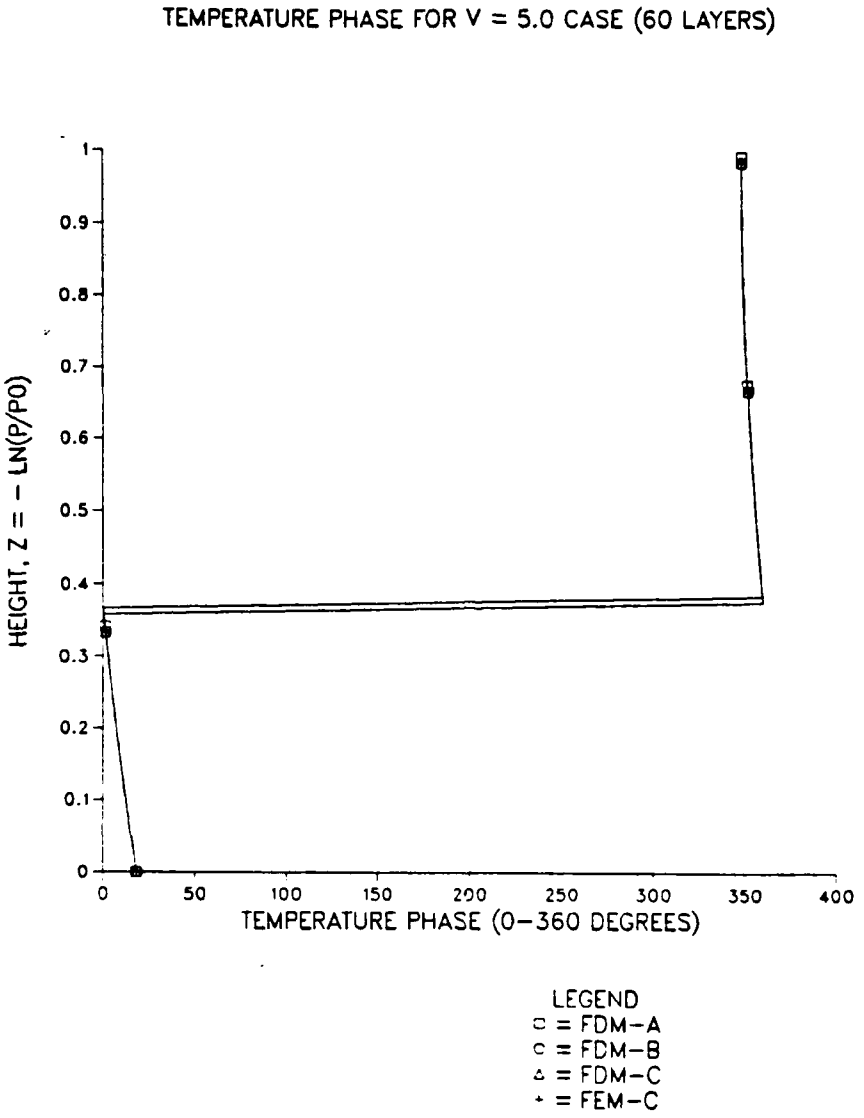

Figure 5. As in Fig. 4 but for temperature phase.

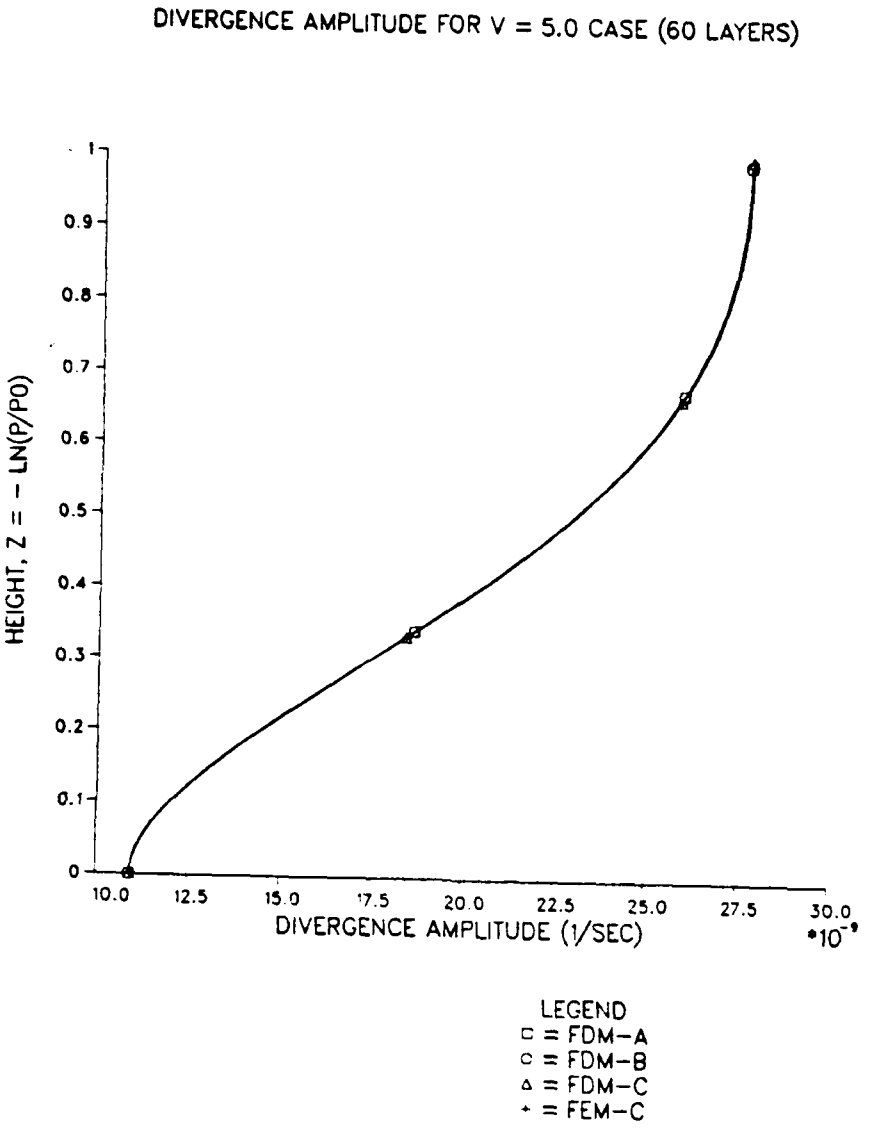

Figure 6. As in Fig. 4 but for divergence amplitude.

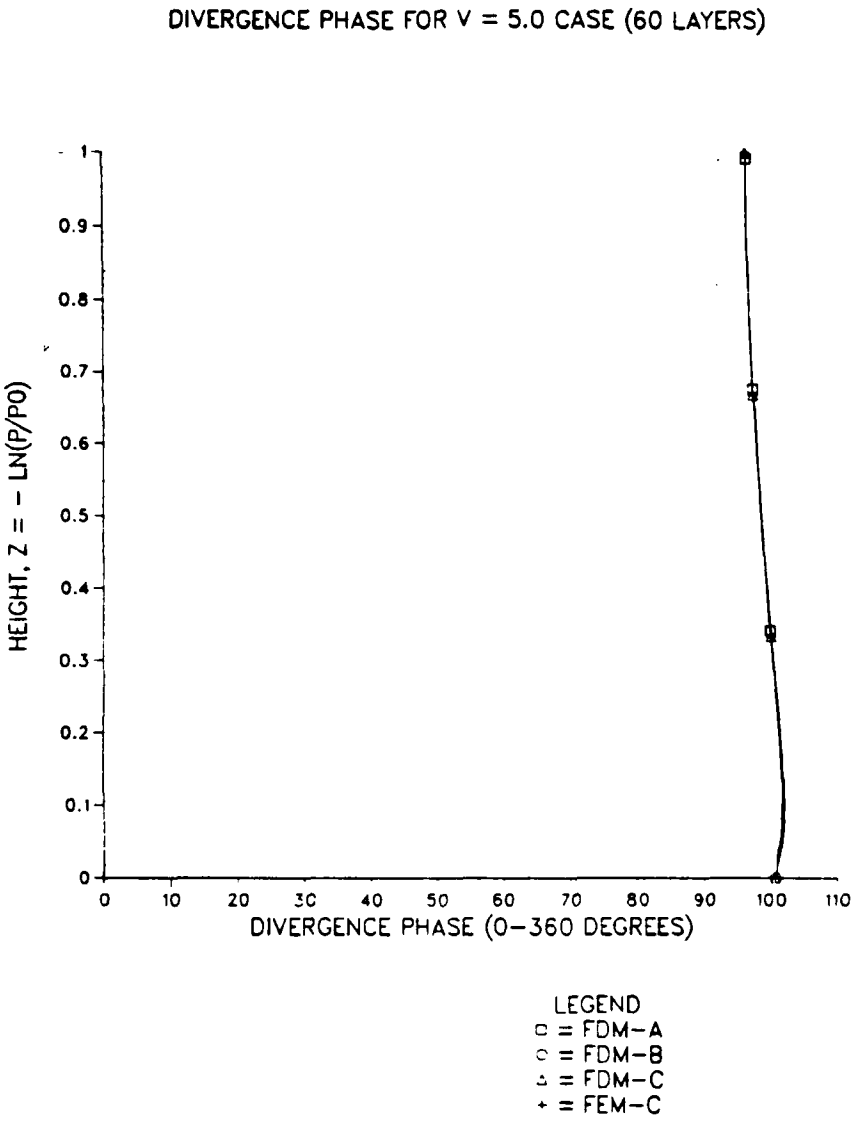

Figure 7. As in Fig. 4 but for divergence phase.

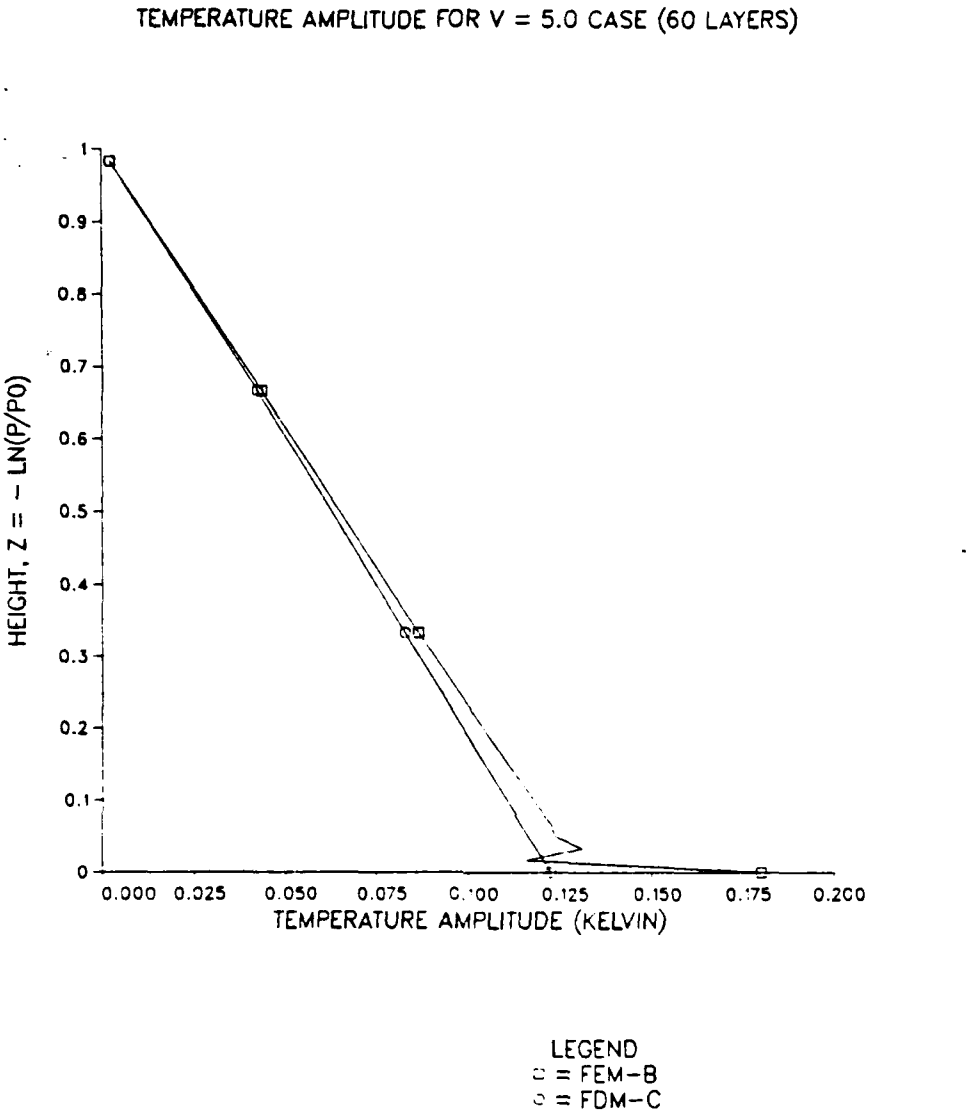

Figure 8. Sixty-layer Rossby wave experiment at 96 hours. FEM-B temperature amplitude profile is compared with the temperature amplitude profile of FDM-C, which represents the consensus profile.

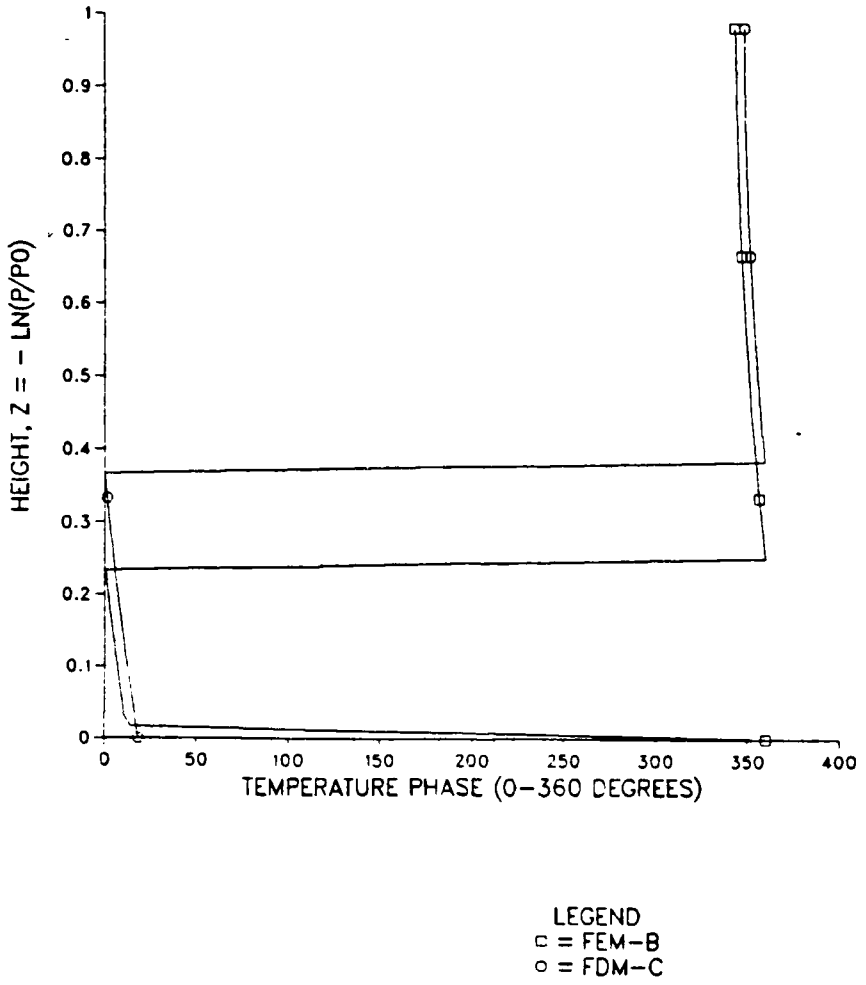

Figure 9. As in Fig. 8 but for temperature phase.

zero at a lower level than the consensus. The divergence amplitude of model FEM-B is within five percent of the consensus (Figure 10) but its phase profile (Figure 11) is quite different from the consensus.

The model FEM-A temperature and divergence amplitudes vary significantly from the consensus. The temperature amplitude profile (Figure 12) has a large amplitude oscillation in the lowest three levels above the surface, possibly caused by the choice of eigenfunction representations used to evaluate elements of the first two rows of the matrices. The FEM-A temperature amplitude is larger than the consensus throughout the atmosphere. The temperature phase passes through zero at a lower level and is five degrees less than the consensus (Figure 13). The maximum FEM-A divergence amplitude occurs near the middle of the atmosphere and its magnitude is ten percent less than the maximum of the consensus (Figure 14). The consensus divergence phase is nearly constant with height, but the phase profile for model FEM-A steadily decreases with height (Figure 15).

2. Six-Layer Models

The comparison of six and sixty-layer profiles for variables defined at staggered levels may be initially misleading. The first staggered level in a six-layer model occurs at Z = 0.0833. The lowest staggered level in a 60-layer model is defined at Z = 0.0083, which may be mistaken for the surface in the graphs. When the values of a six-layer model

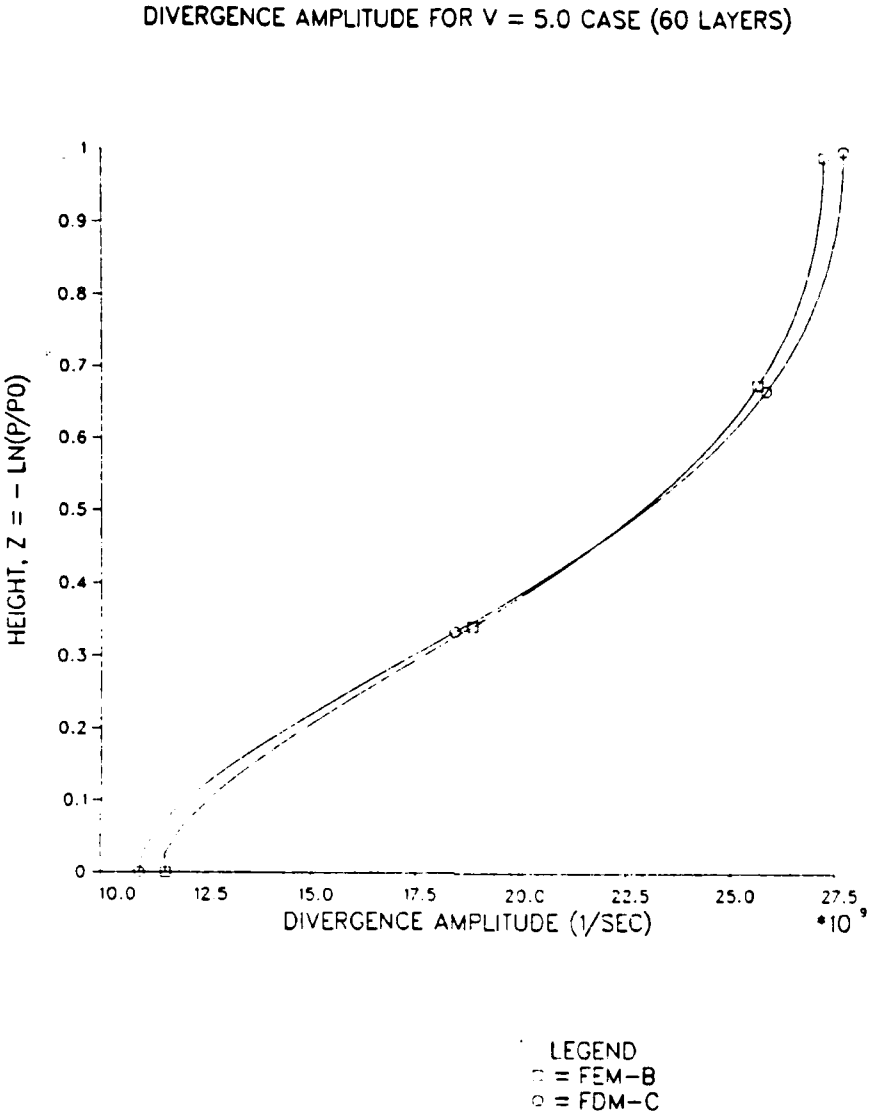

Figure 10. As in Fig. 8 but for divergence amplitude.

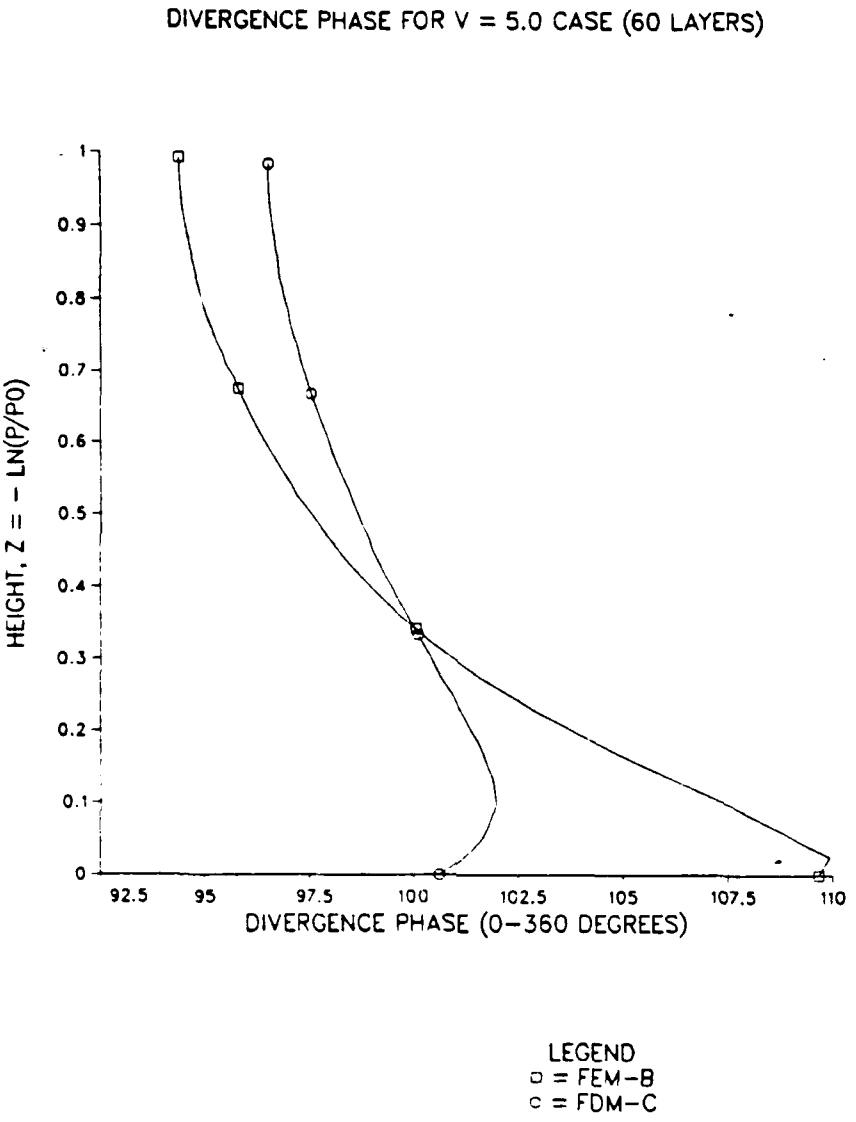

Figure 11. As in Fig. 8 but for divergence phase.

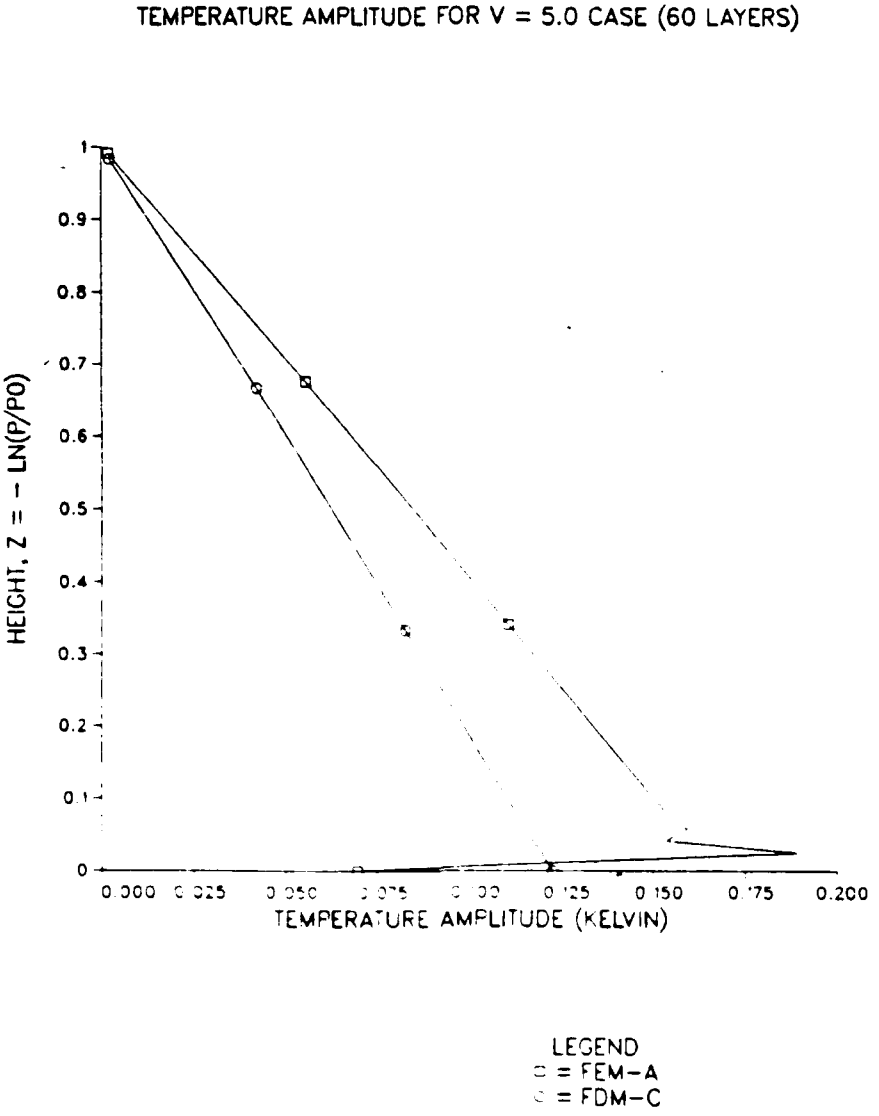

Figure 12. As in Fig. 8 but for model FEM-A compared with the consensus, FDM-C.

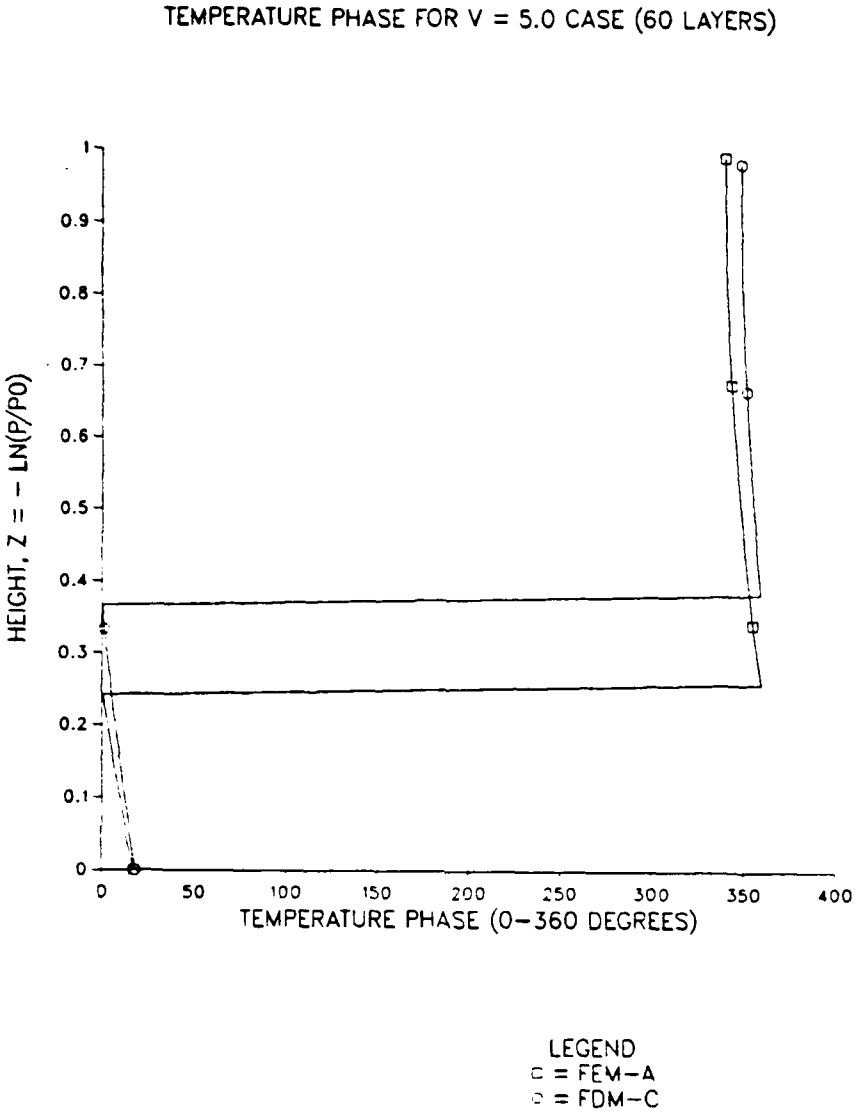

Figure 13. As in Fig. 12 but for temperature phase.

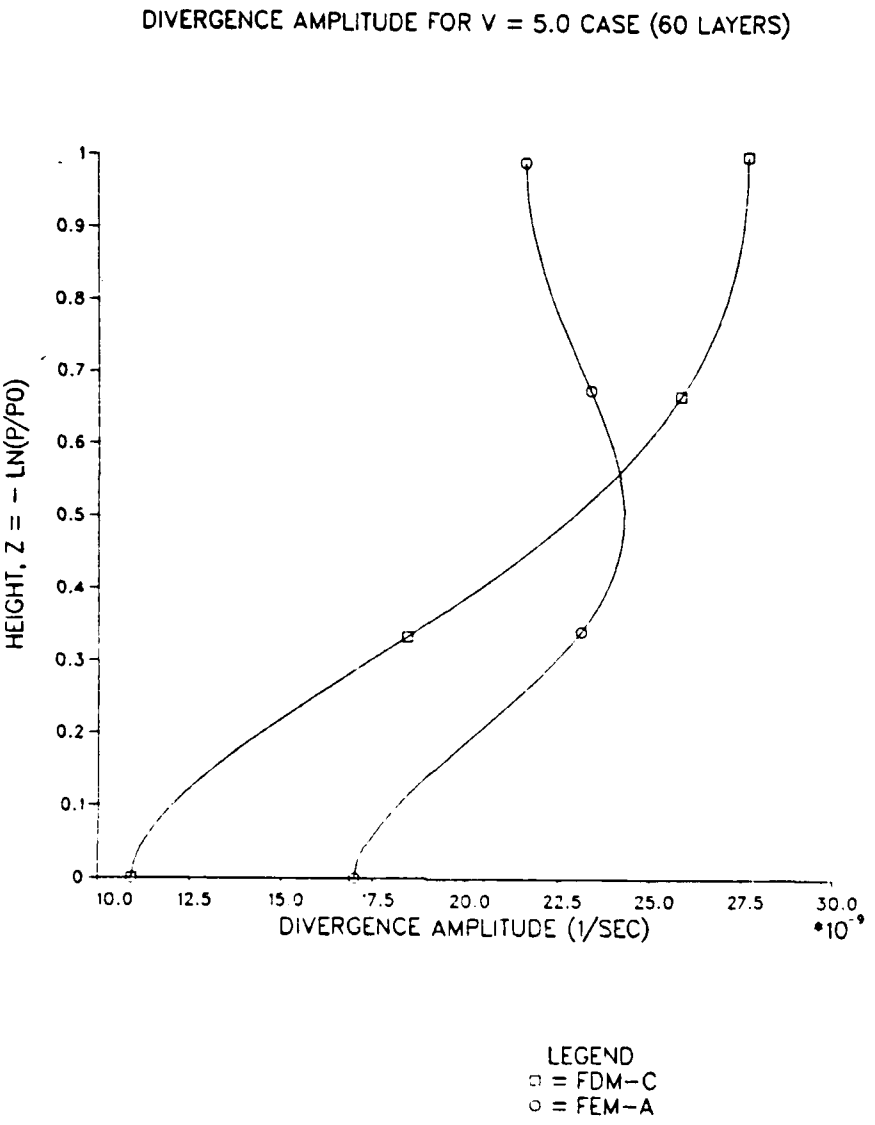

Figure 14. As in Fig. 12 but for divergence amplitude.

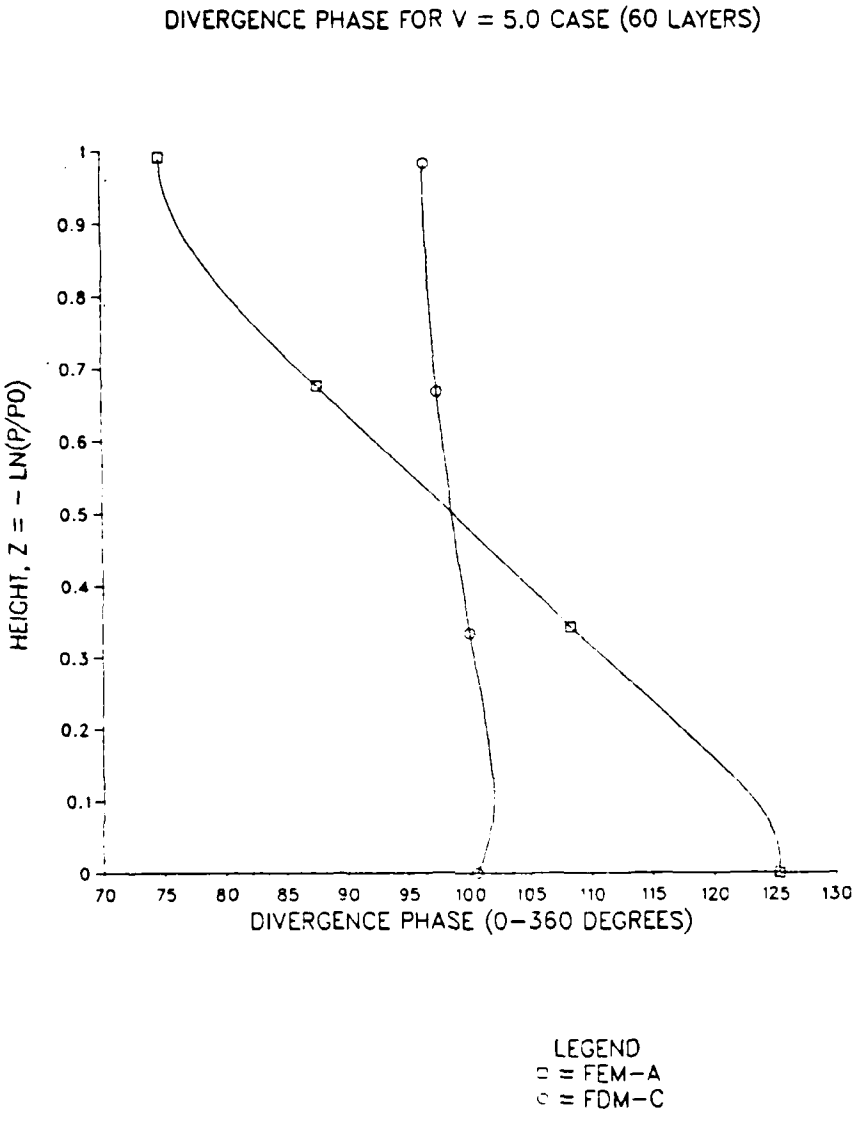

Figure 15. As in Fig. 12 but for divergence phase.

coincide with a 60-layer profile, the models are considered to represent the same physical solution, even though the six-layer model has a smaller vertical domain for staggered variables.

The temperature amplitude profiles of the six-layer FDM-A, FDM-B, FDM-C and FEM-C models are identical with their corresponding 60-layer results (Figures 16-19). The previously discussed problems in the lowest layers of models FEM-A and FEM-B are quite evident in their six-layer profiles. The temperature amplitude of FEM-B is virtually identical with its 60-layer profile above the first two layers (Figure 20). The six-layer FEM-A profile (Figure 21) does not agree with its 60-layer profile below Z = 0.50 (600 mb). The large amplitude oscillation in this profile destroys the integrity of the solution in a significant portion of the atmosphere.

The six-layer divergence amplitude profiles for the grid C models are identical with each other (Figures 22-23), and the divergence profiles for the grid B models are nearly the same (Figures 24-25). All four models approximate their corresponding 60-layer solutions with similar accuracy. The six-layer FDM-A model does not approximate the curvature of the consensus 60-layer divergence profile as well as the grid B and C models (Figure 26). The six-layer FEM-A model has difficulty approximating the location and magnitude of the mid-atmosphere divergence maximum of its 60-layer solution (Figure 27).

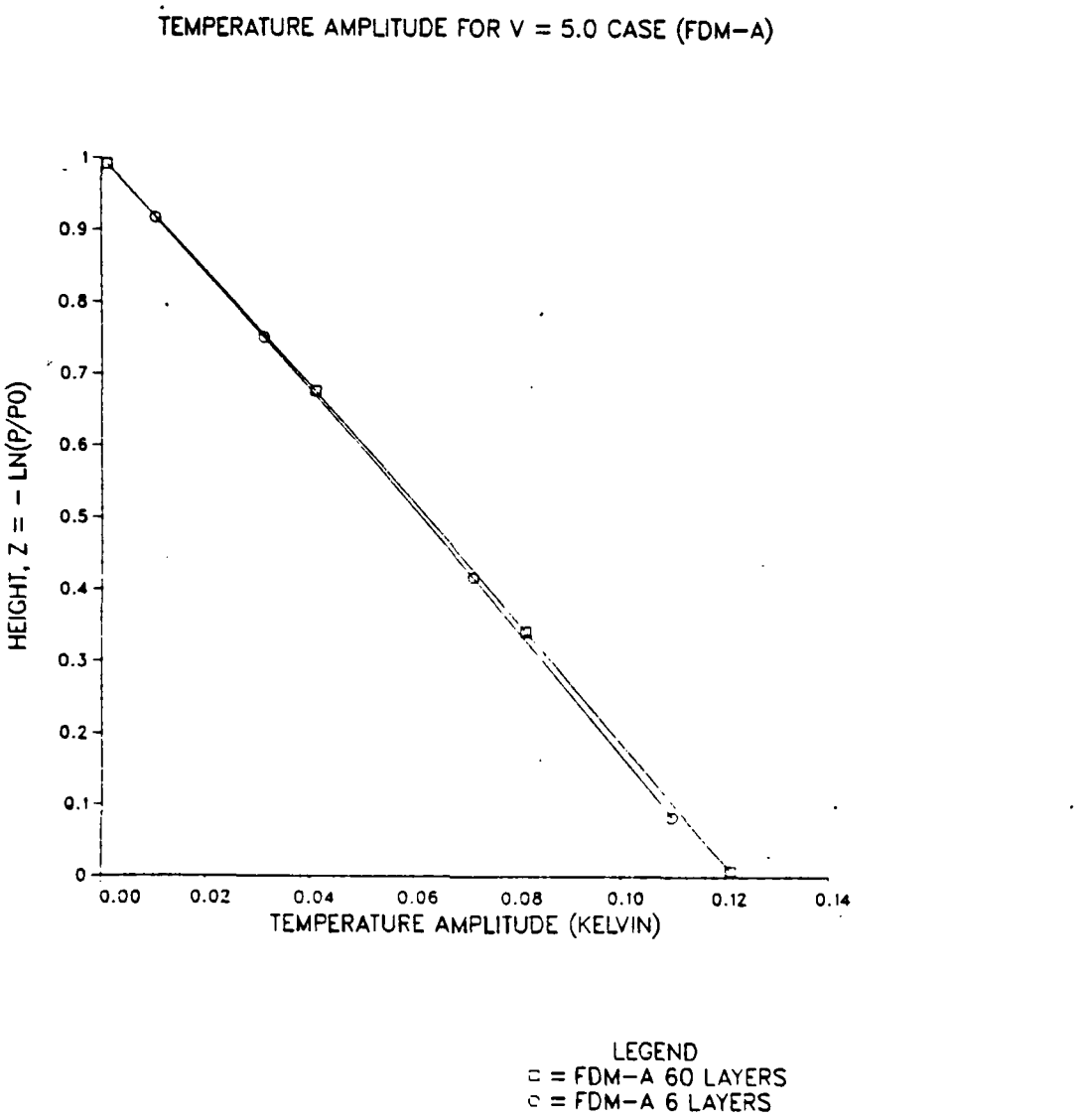

Figure 16. Six-layer Rossby wave experiment at 96 hours. Temperature amplitude profiles are compared for the six-layer and 60-layer FDM-A models.

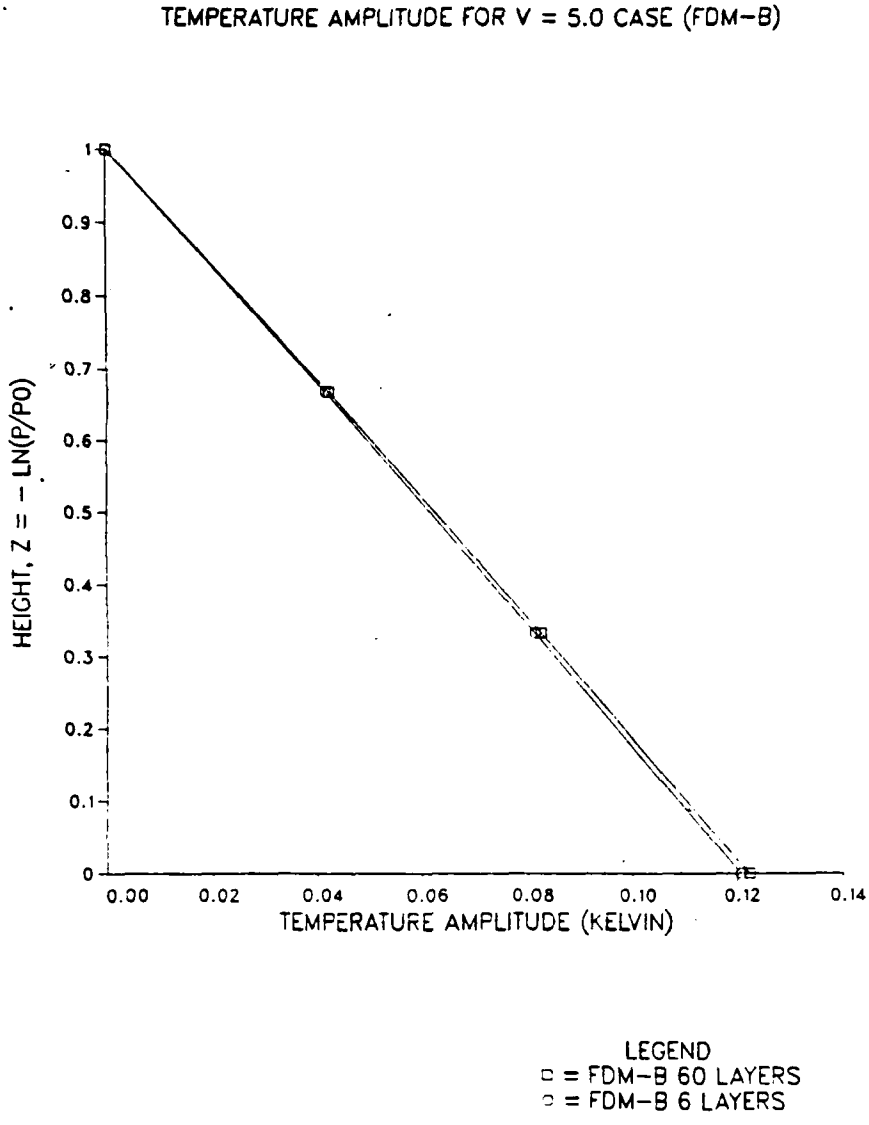

Figure 17. As in Fig. 16 but for model FDM-B.

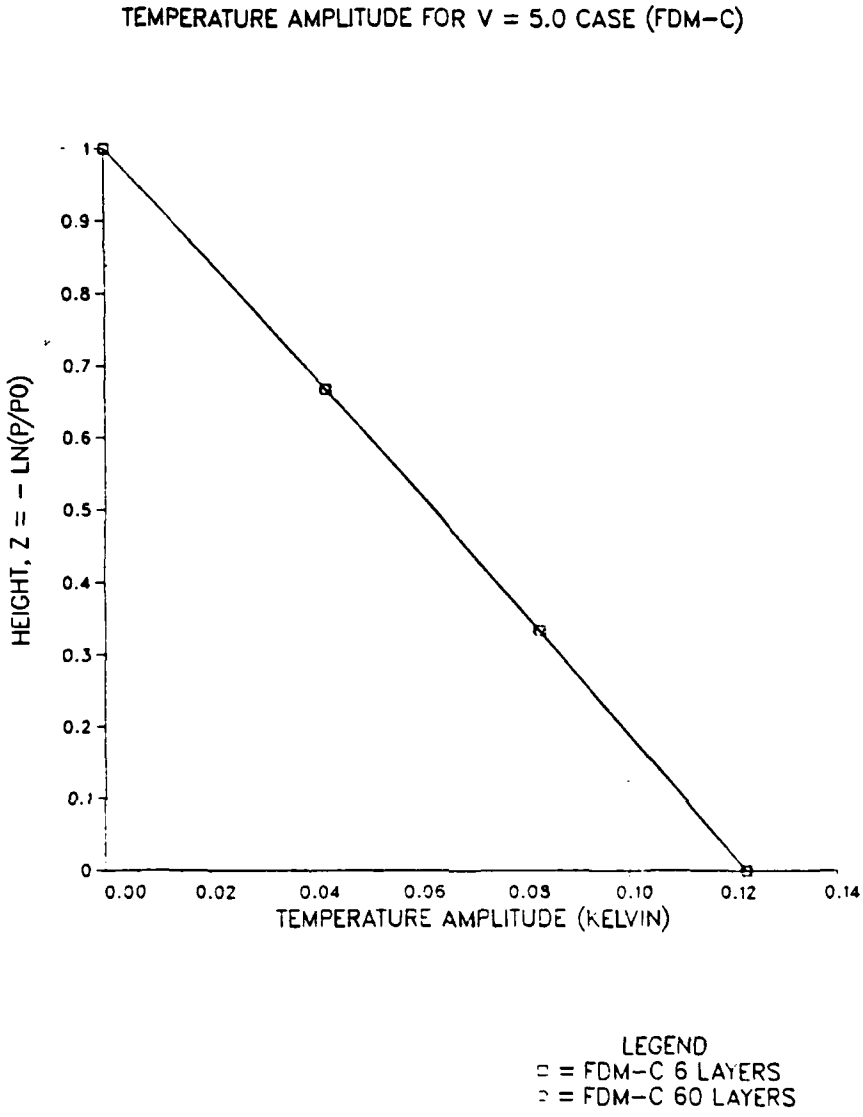

Figure 18. As in Fig. 16 but for model FDM-C.

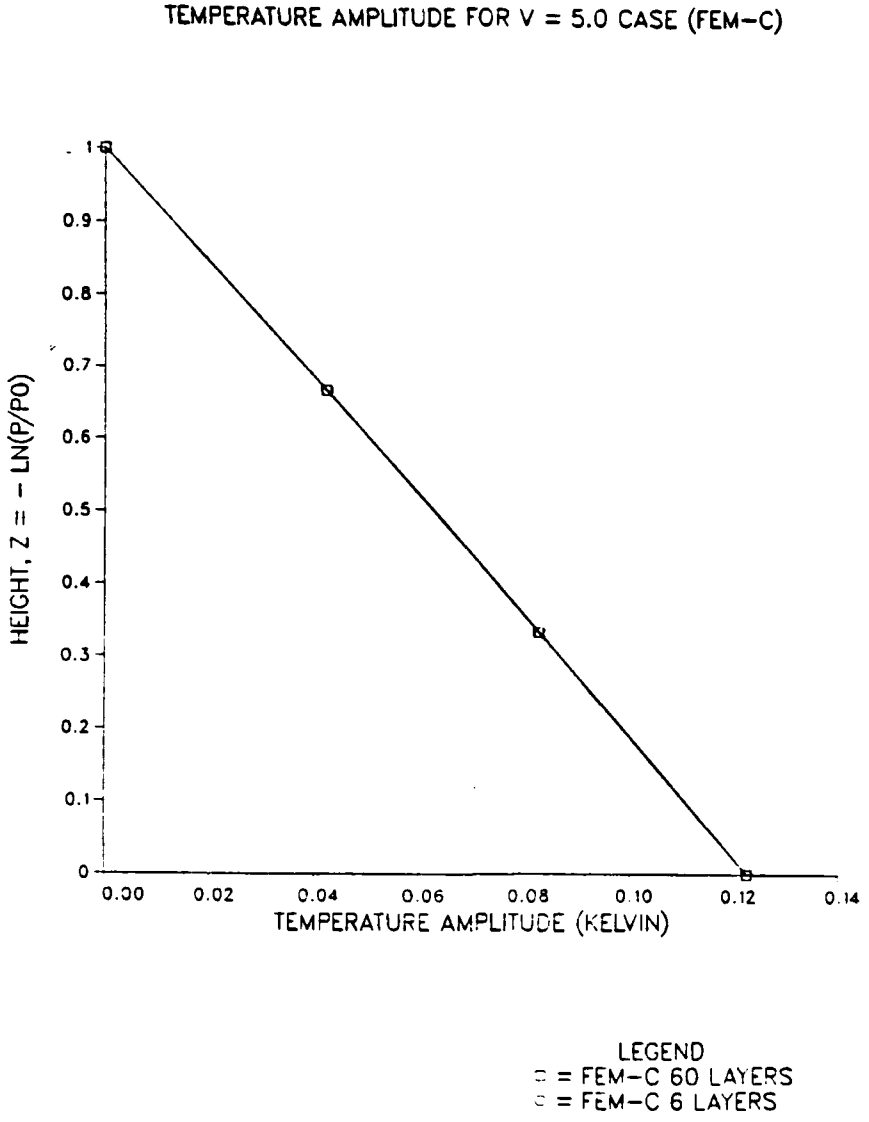

Figure 19. As in Fig. 16 but for model FEM-C.

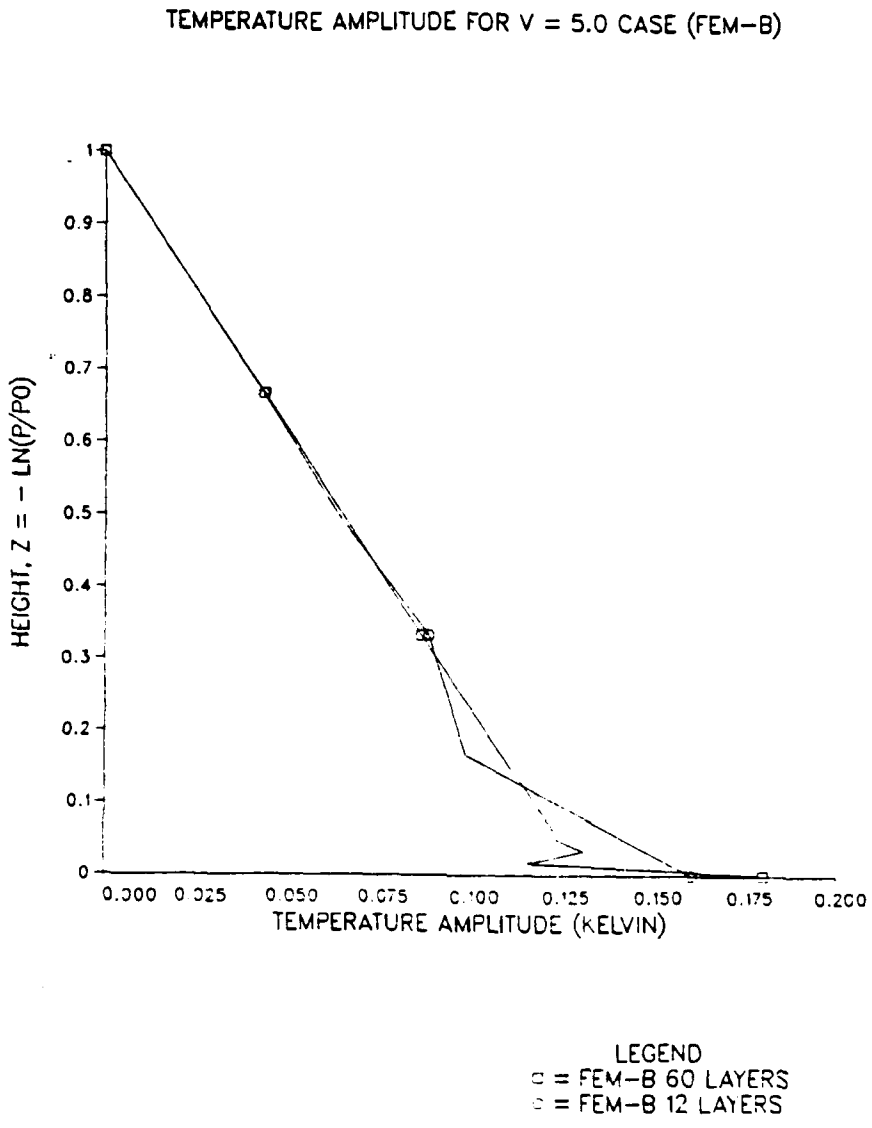

Figure 20. As in Fig. 16 but for model FEM-B.

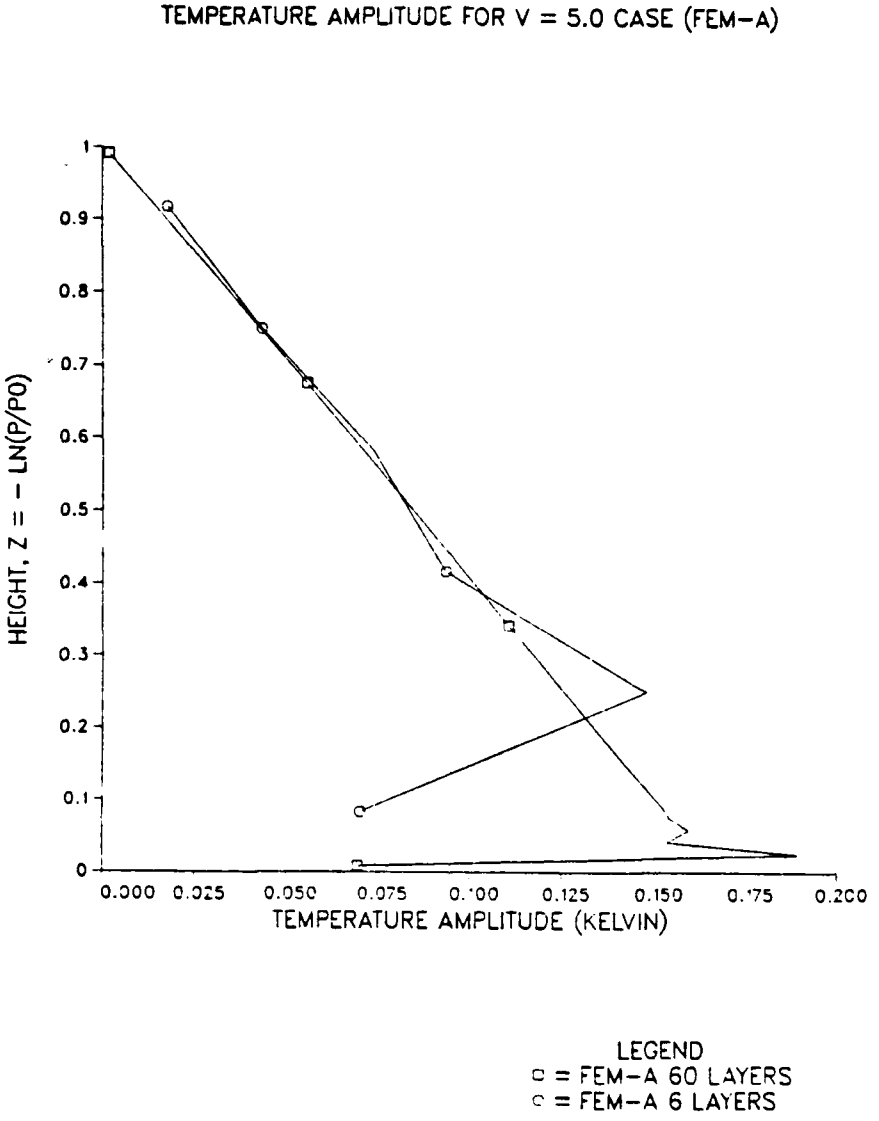

Figure 21. As in Fig. 16 but for model FEM-A.

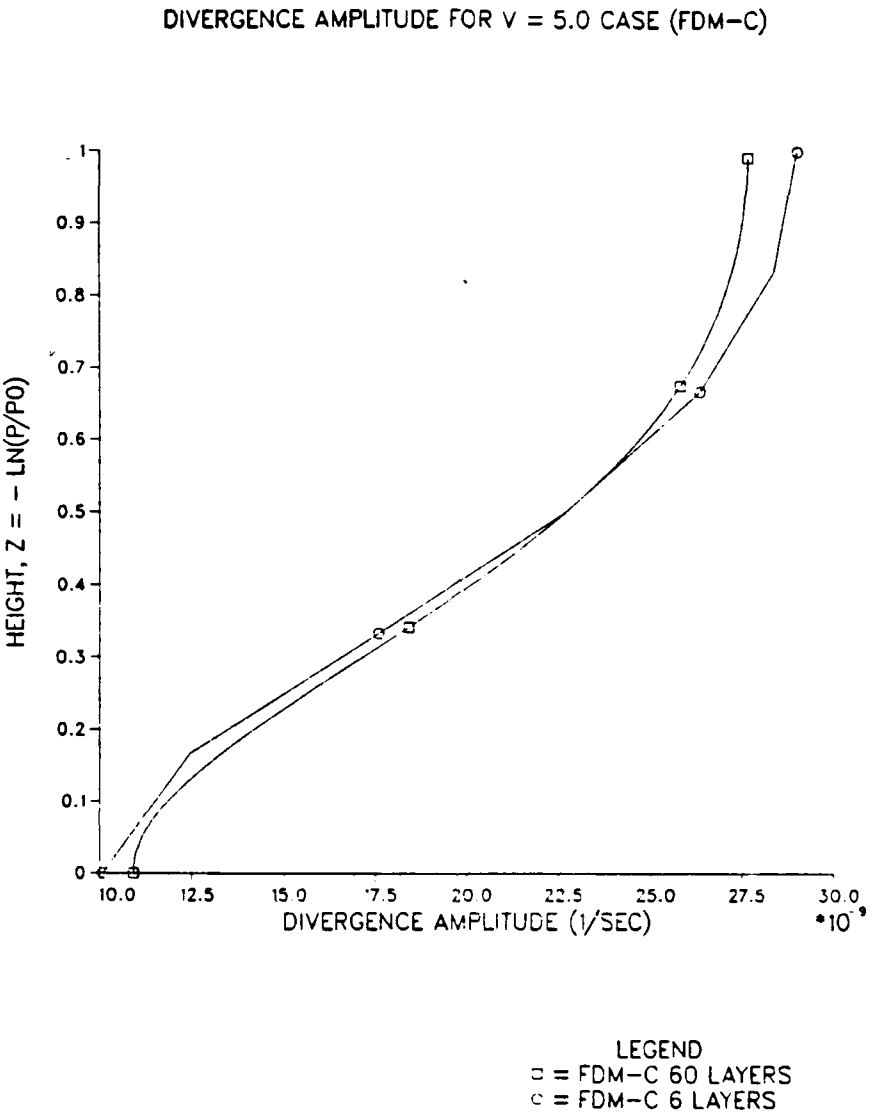

Figure 22. As in Fig. 16 but divergence amplitude of FDM-C.

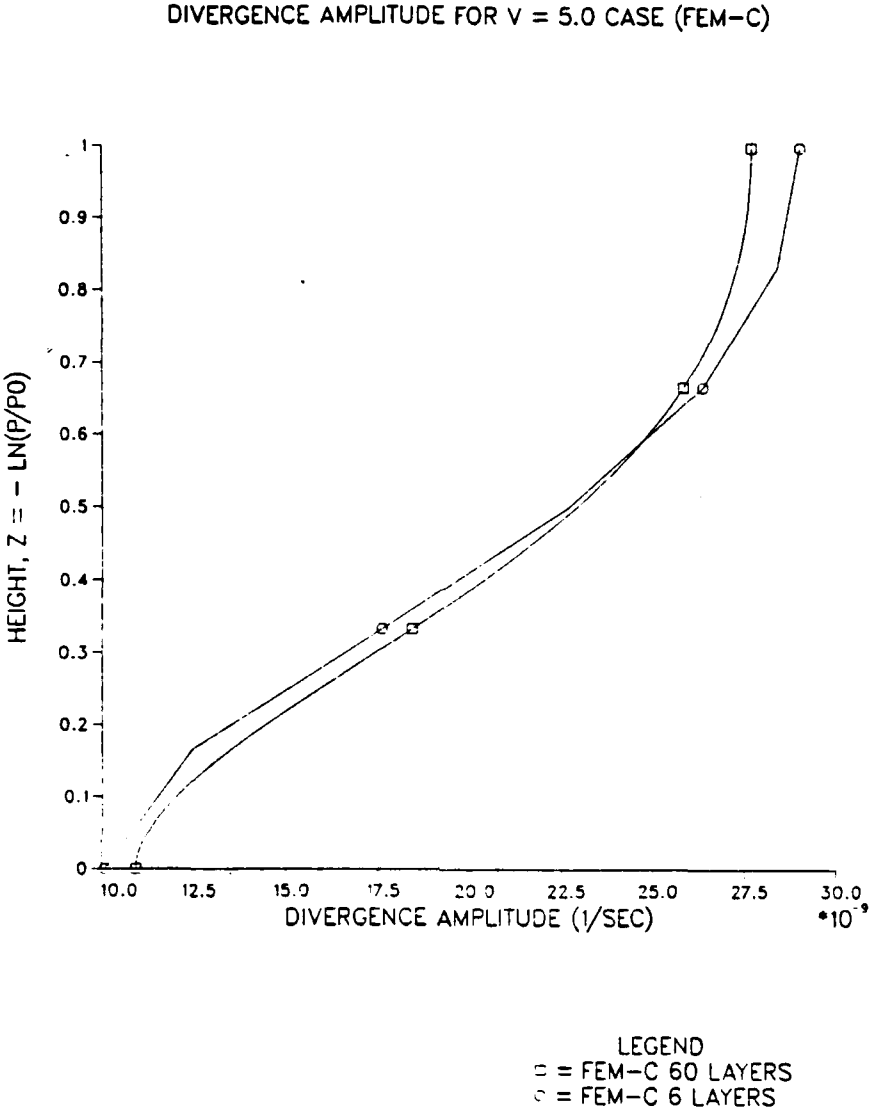

Figure 23. As in Fig. 22 but for model FEM-C.

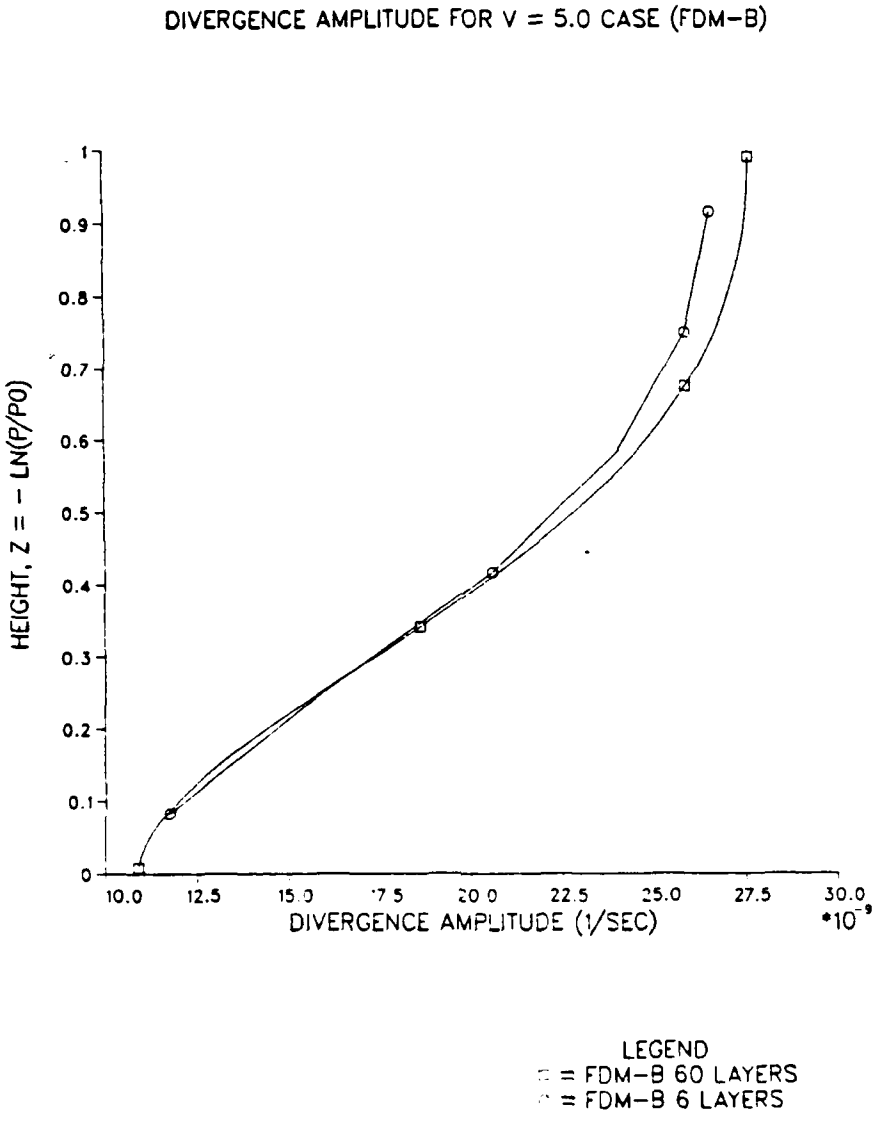

Figure 24. As in Fig. 22 but for model FDM-B.

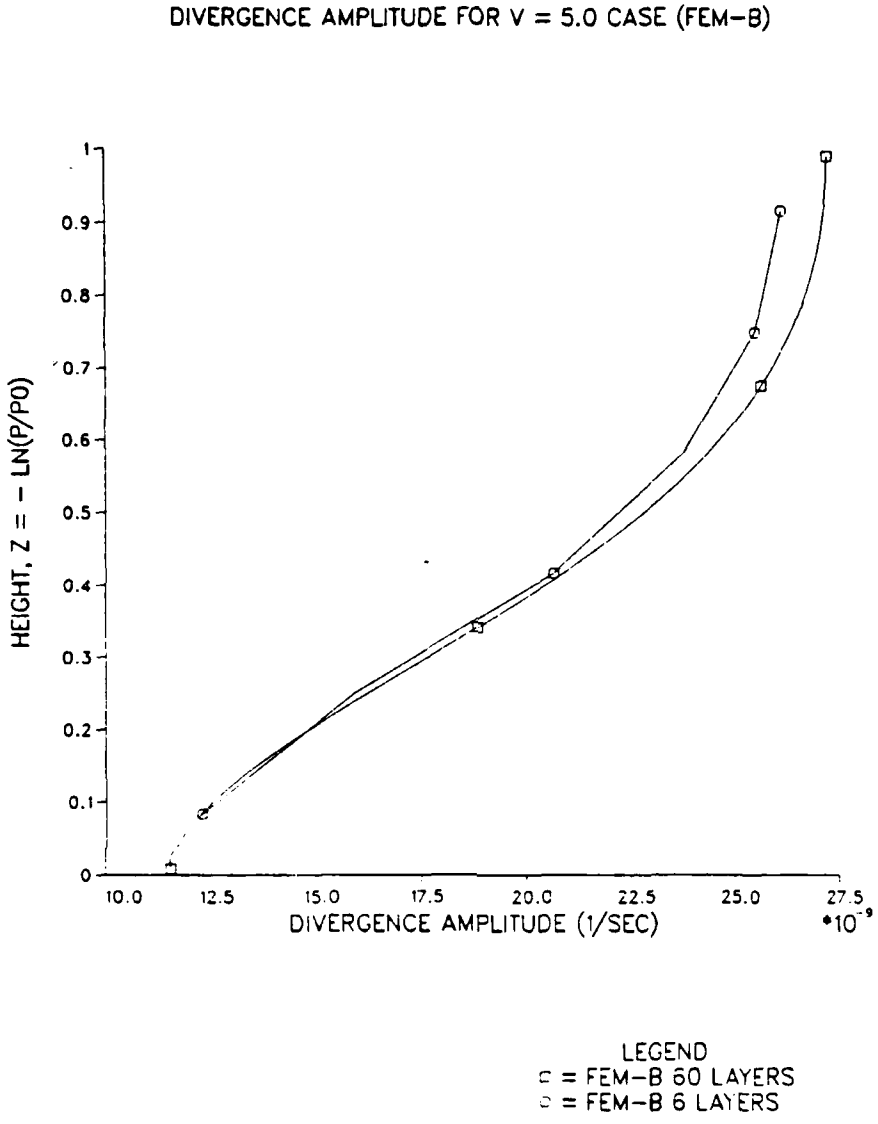

Figure 25. As in Fig. 22 but for model FEM-B.

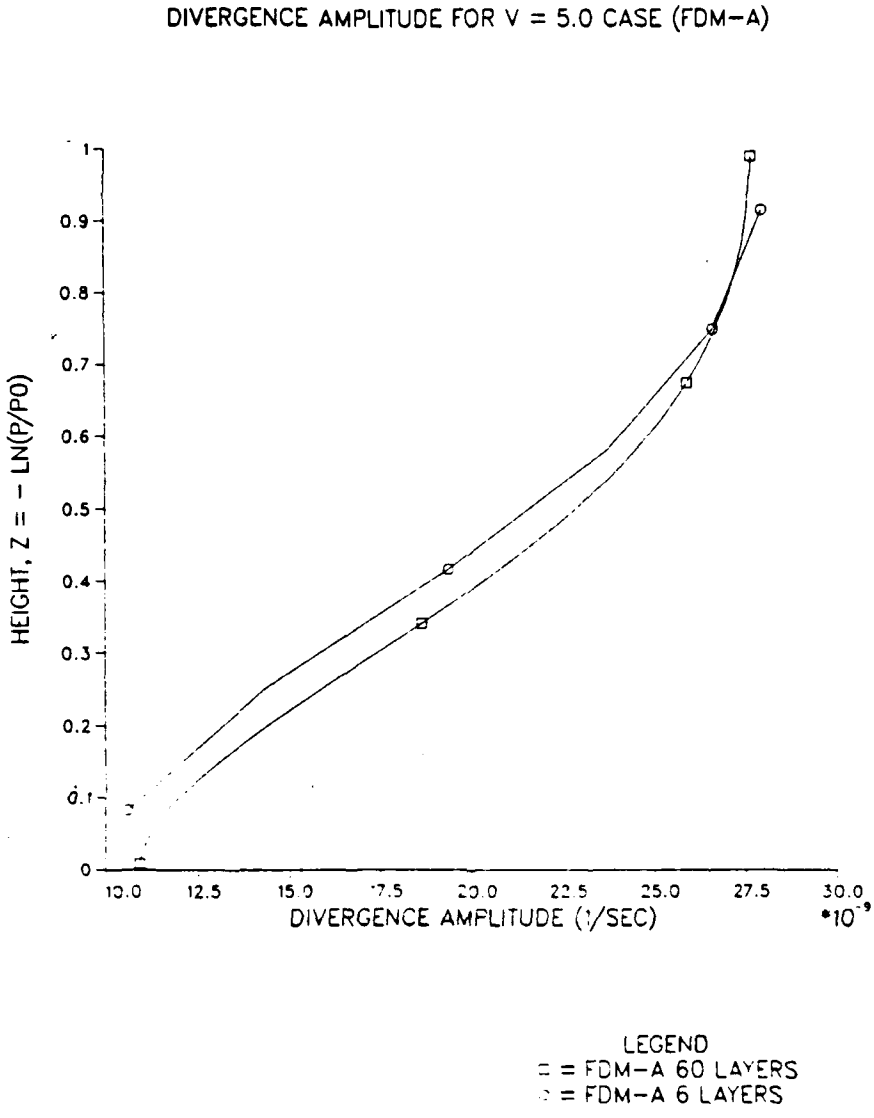

Figure 26. As in Fig. 22 but for model FDM-A.

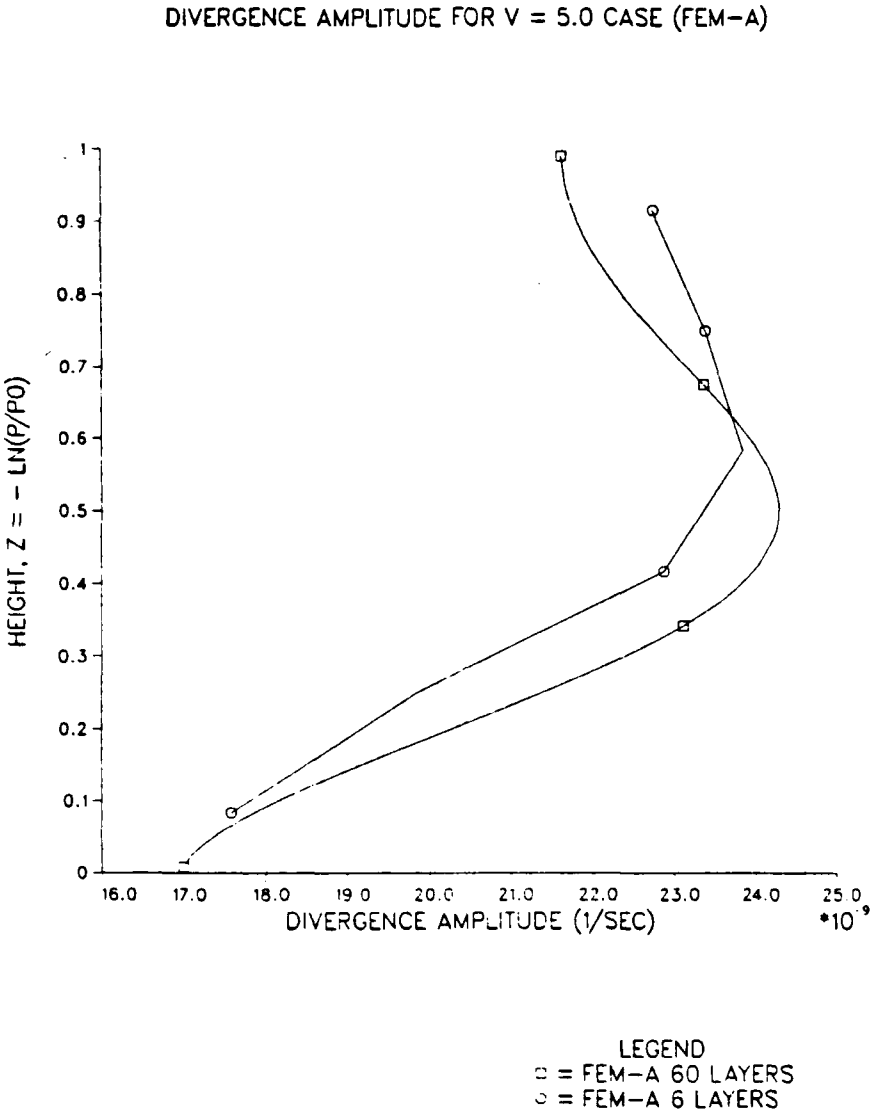

Figure 27. As in Fig. 22 but for model FEM-A.

B. MOUNTAIN TOPOGRAPHY EXPERIMENT

The forced vertical velocity term, MTS, in the surface geopotential forecast equation (2-3) is non-zero in this experiment. It represents the contribution to surface geopotential from air flowing over mountain topography which varies sinusoidally in the x-direction and has no variation in the y-direction. The mountain ridge-to-valley height difference is 1,500 meters. To reduce the trauma for the model, the mountains are gradually "built" to their full height over a period of 36 hours. Thus, the forced vertical velocity increases in the first 36 hours of the forecast period and is constant for the remainder of the 96-hour forecast period. The equations used to define the forced vertical velocity are included in Appendix J. Beta and all initial perturbations are zero in this experiment.

1. Sixty-Layer Models

The FDM-A, FDM-B, FDM-C, and FEM-C models converge to the same physical solution. The amplitude and phase profiles of temperature and divergence are depicted in Figures 28-31.

The FEM-B model again has a jagged temperature amplitude profile in the lowest two layers (Figure 32). The temperature amplitudes in the remainder of the atmosphere are within 5% of the consensus. The FEM-B temperature phase has oscillations in the bottom three layers and the top two layers of the profile (Figure 33), but the rest of the profile is

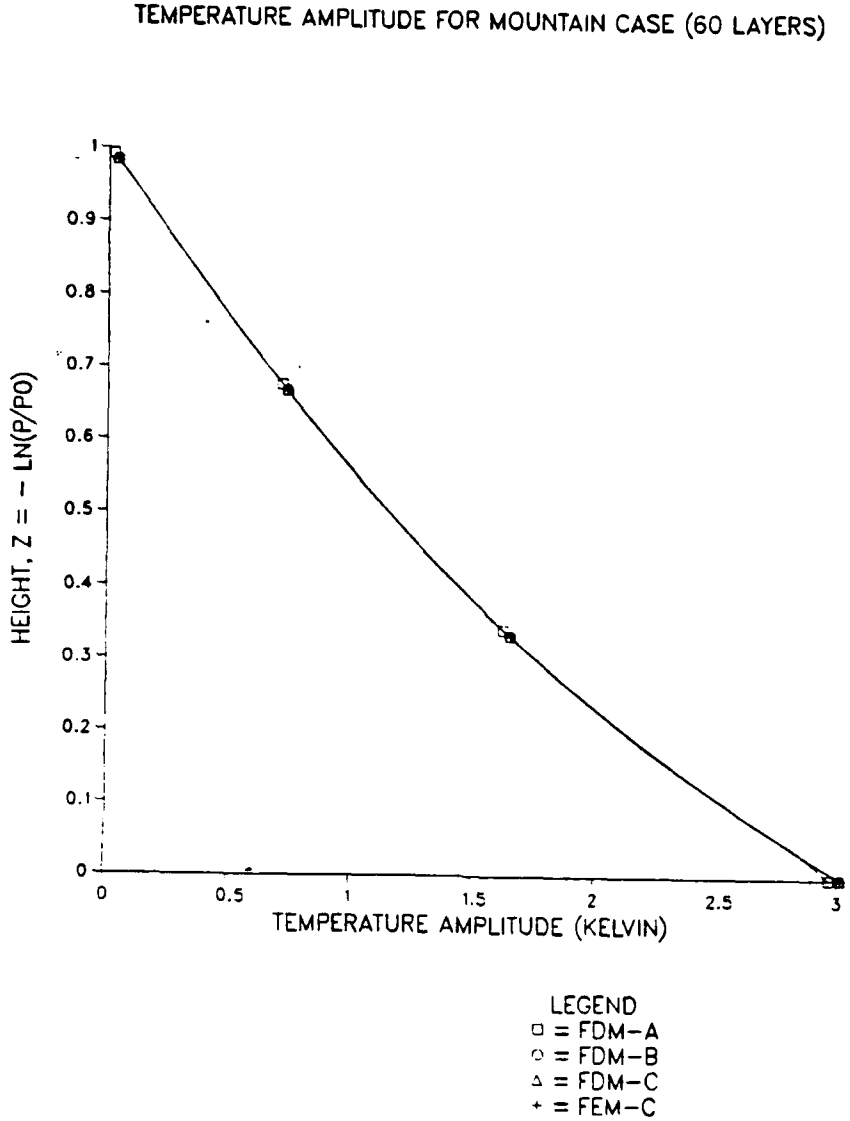

Figure 28. Sixty-layer mountain topography experiment at 96 hours. Temperature amplitude profiles are compared for models FDM-A, FDM-B, FDM-C, and FEM-C.

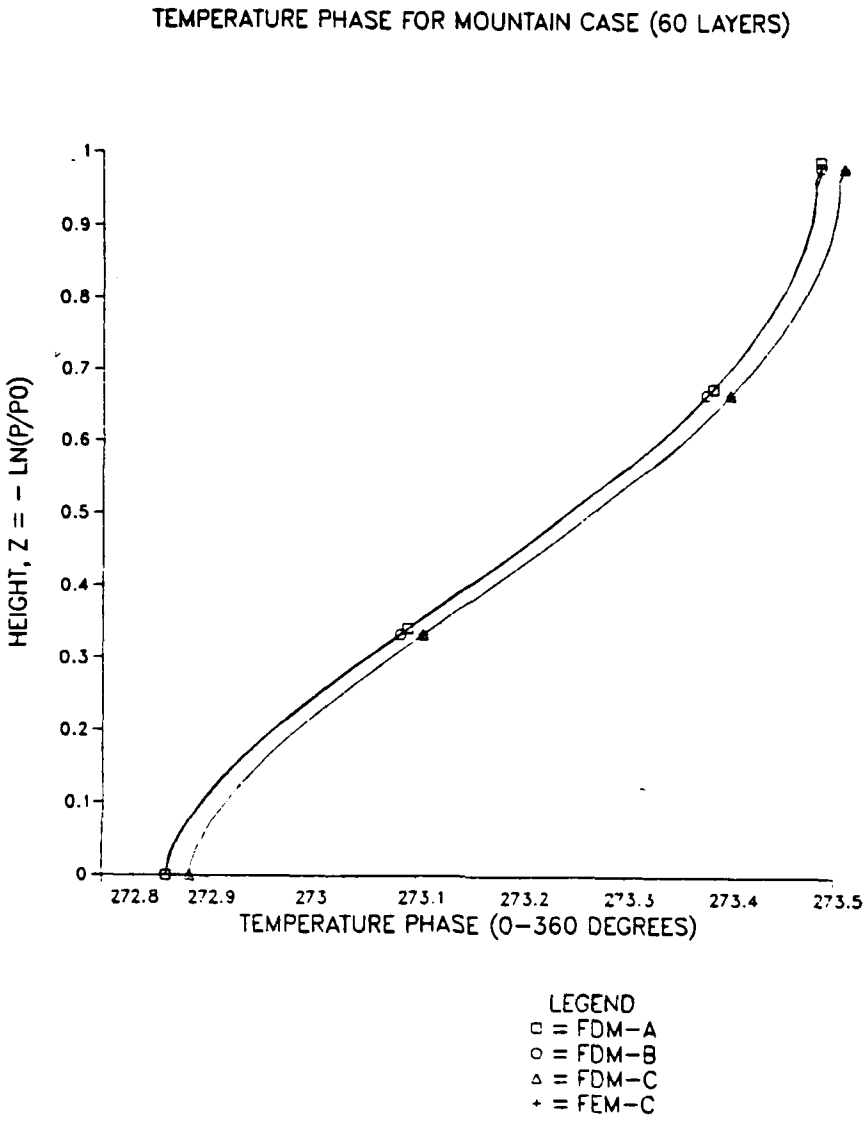

Figure 29. As in Fig. 28 but for temperature phase.

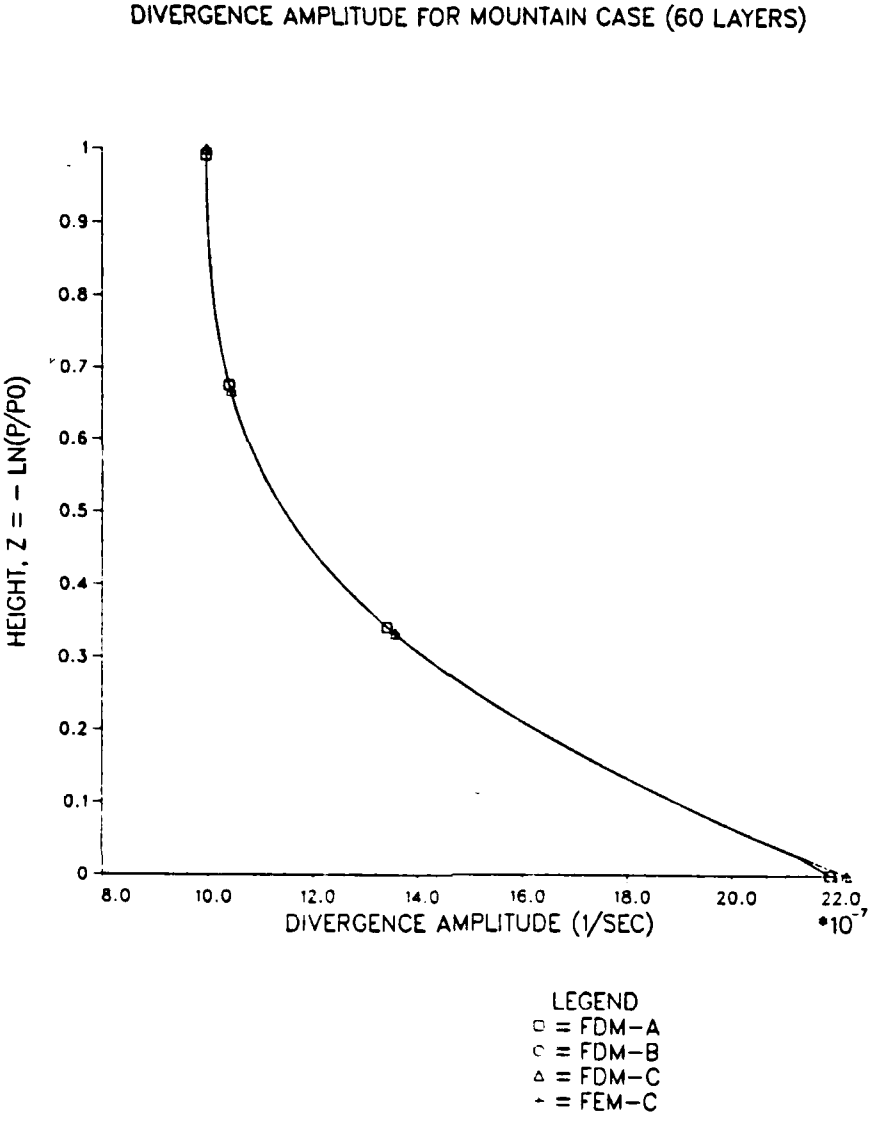

Figure 30. As in Fig. 28 but for divergence amplitude.

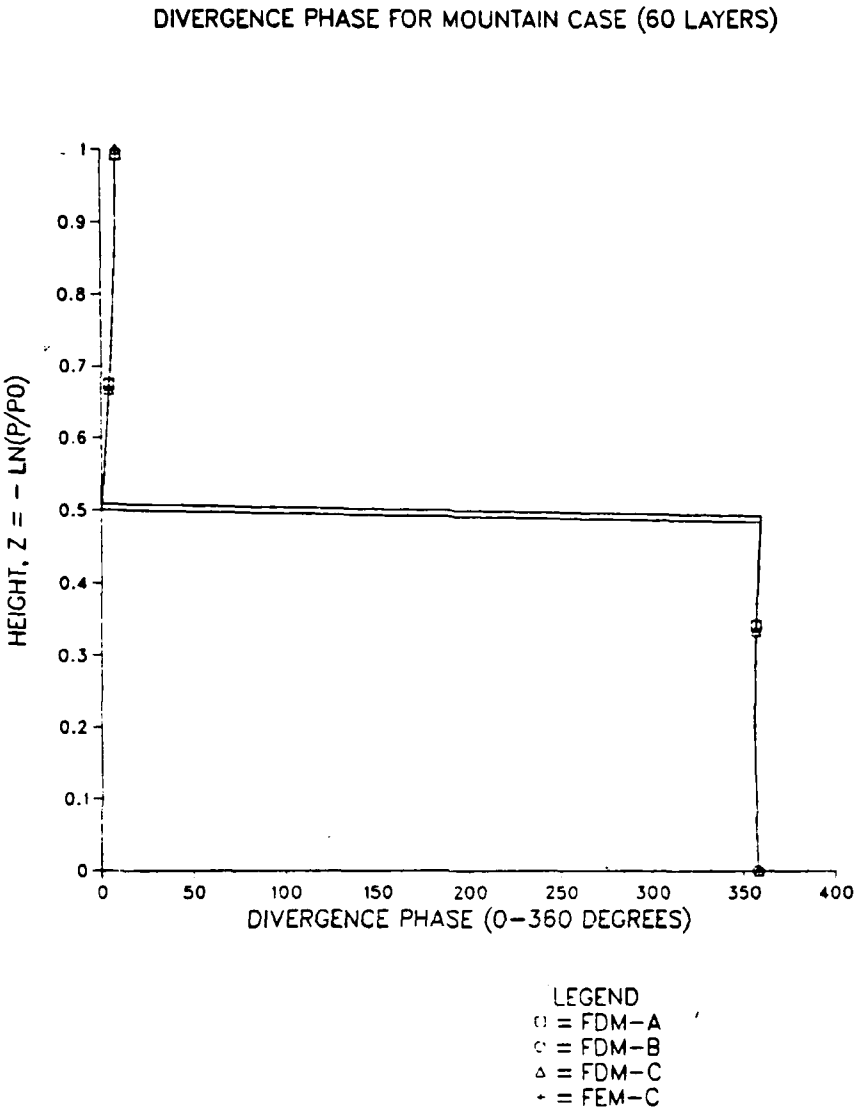

Figure 31. As in Fig. 28 but for divergence phase.

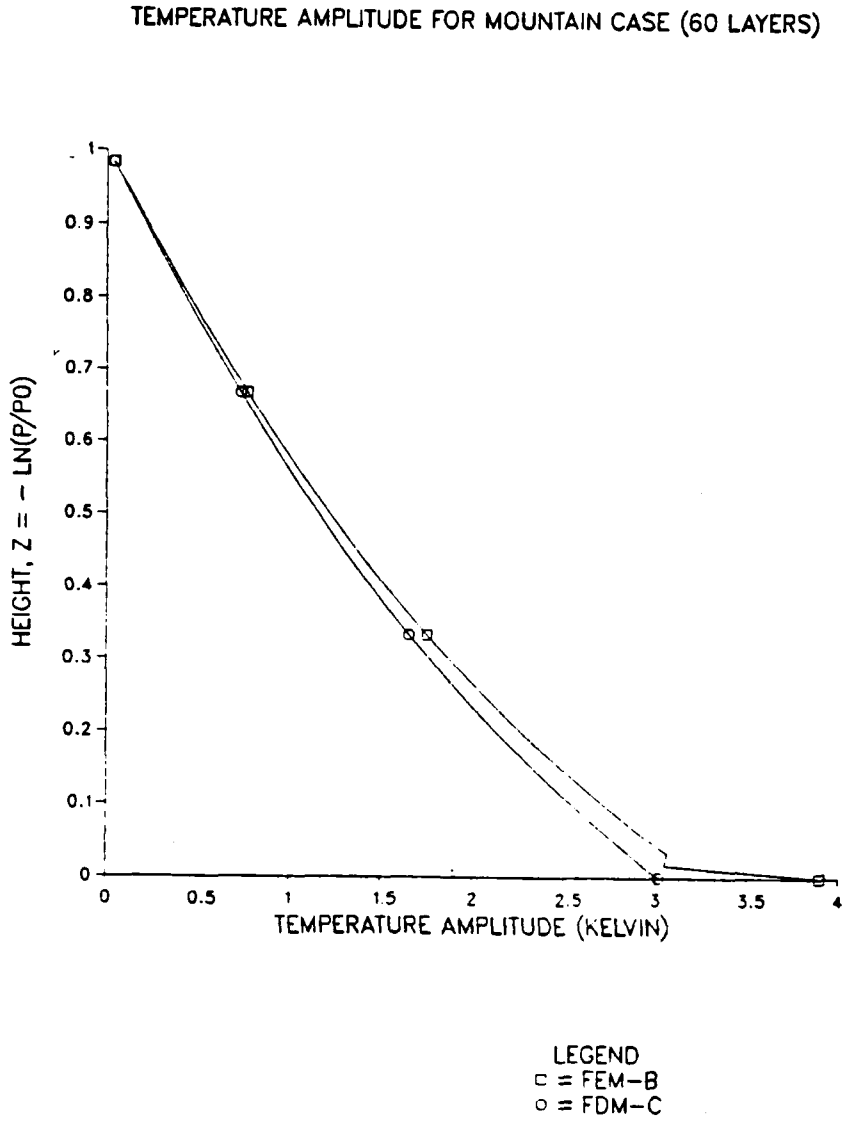

Figure 32. Sixty-layer mountain topography experiment at 96 hours. FEM-B temperature amplitude profile is compared with the temperature amplitude profile of FDM-C, which represents the consensus profile.

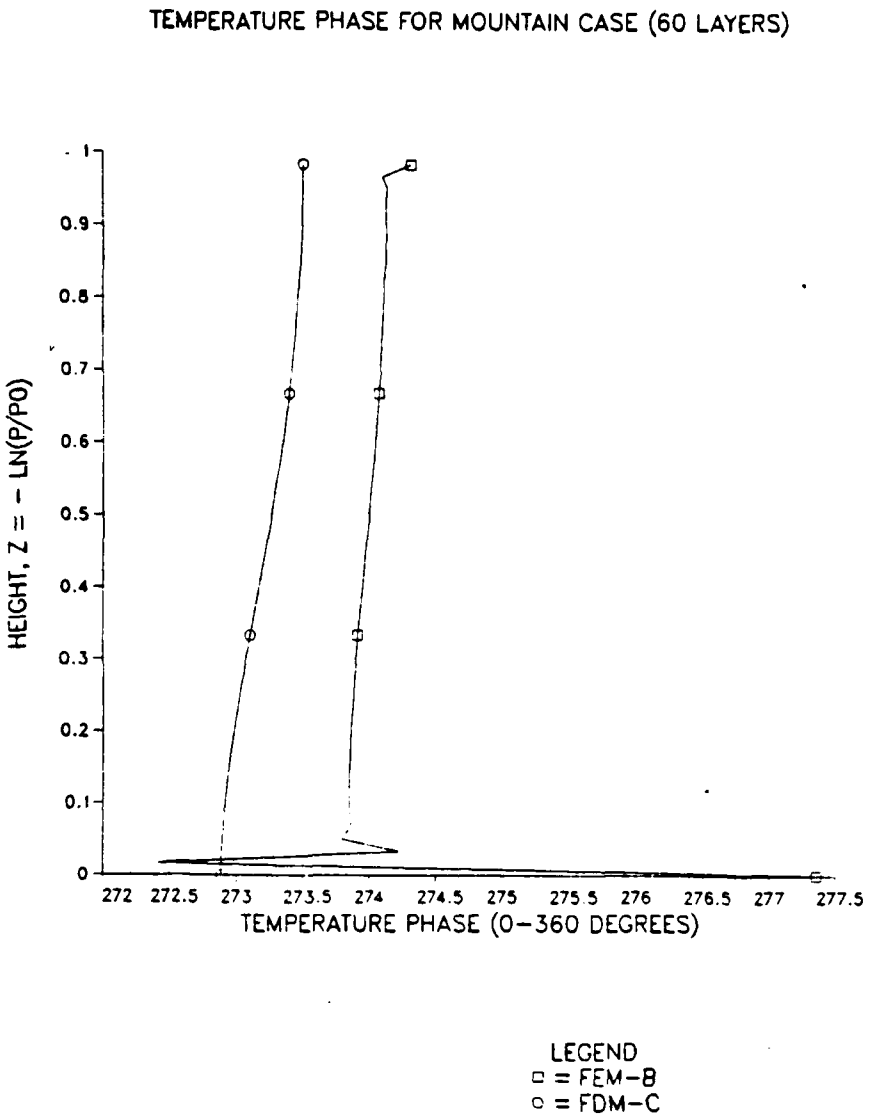

Figure 33. As in Fig. 32 but for temperature phase.

within one degree of the consensus phase. The FEM-B divergence amplitude and phase are identical with the consensus values.

An oscillation also exists in the lowest three layers of the temperature amplitude profile for model FEM-A (Figure 34). The amplitude is 30% higher than the consensus near the surface and this difference decreases with height. The temperature phases are nearly identical. The FEM-A divergence amplitude profile is similar to the consensus, but the amplitude does not decrease as fast with height as the consensus (Figure 35). The divergence phase profile for this model is the same as the consensus.

2. Six-Layer Models

The temperature amplitude profiles of the six-layer models FDM-A, FDM-B, FDM-C and FEM-C are identical with each other and also with the consensus solution (Figures 36-39). The six-layer staggered finite element models are nearly identical with their 60-layer solutions above the first two layers (Figures 40-41). The previously identified inadequate representations of the temperature amplitude in the lowest layers exist in this experiment. All six models approximate their 60-layer divergence amplitude profiles quite well (Figures 42-46), however the FEM-A model (Figure 47) does not approximate the curvature in the lower portion of its 60-layer profile as well as the other models.

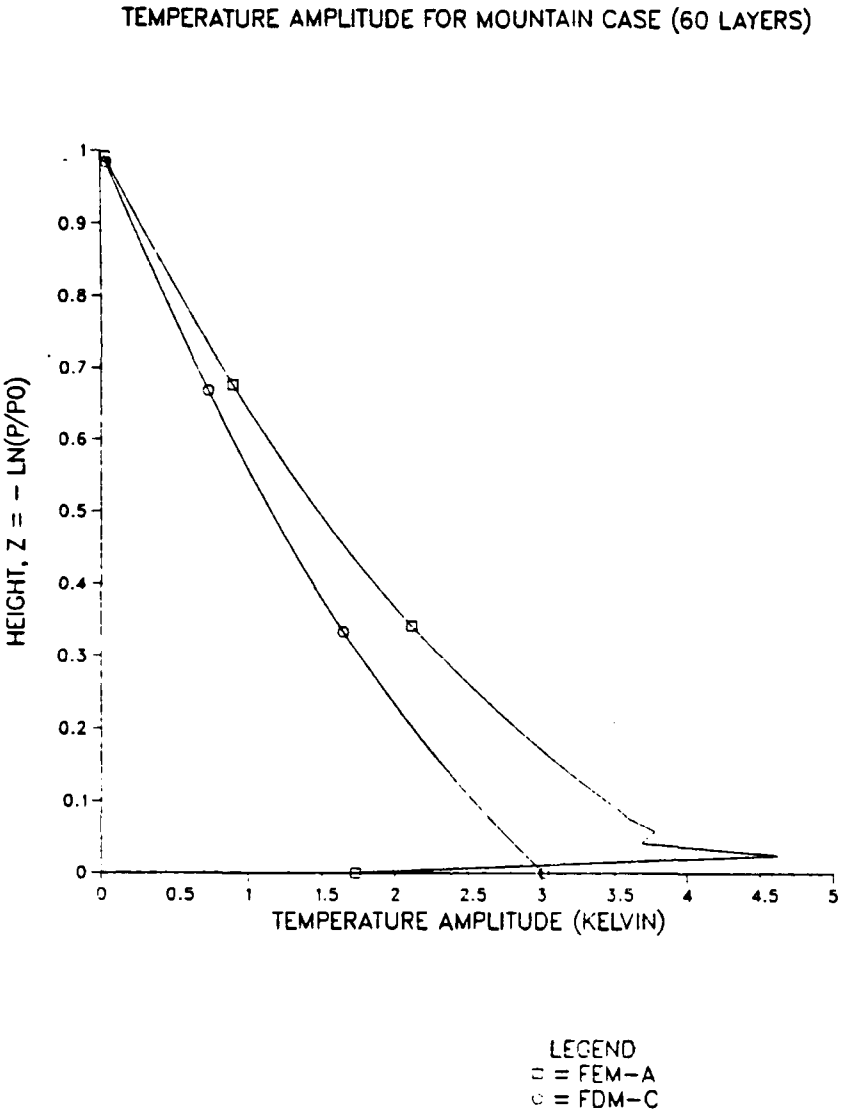

Figure 34. As in Fig. 32 but for model FEM-A compared with FDM-C.

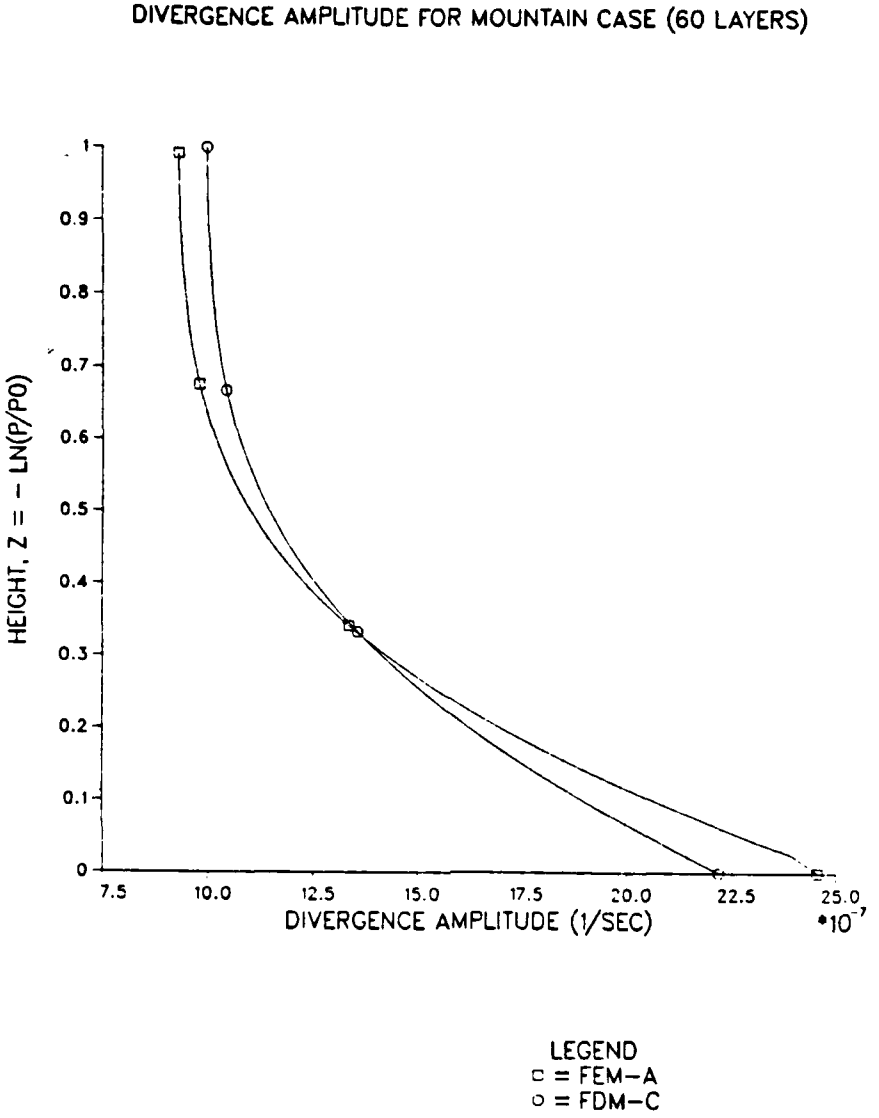

Figure 35. As in Fig. 34 but for divergence amplitude.

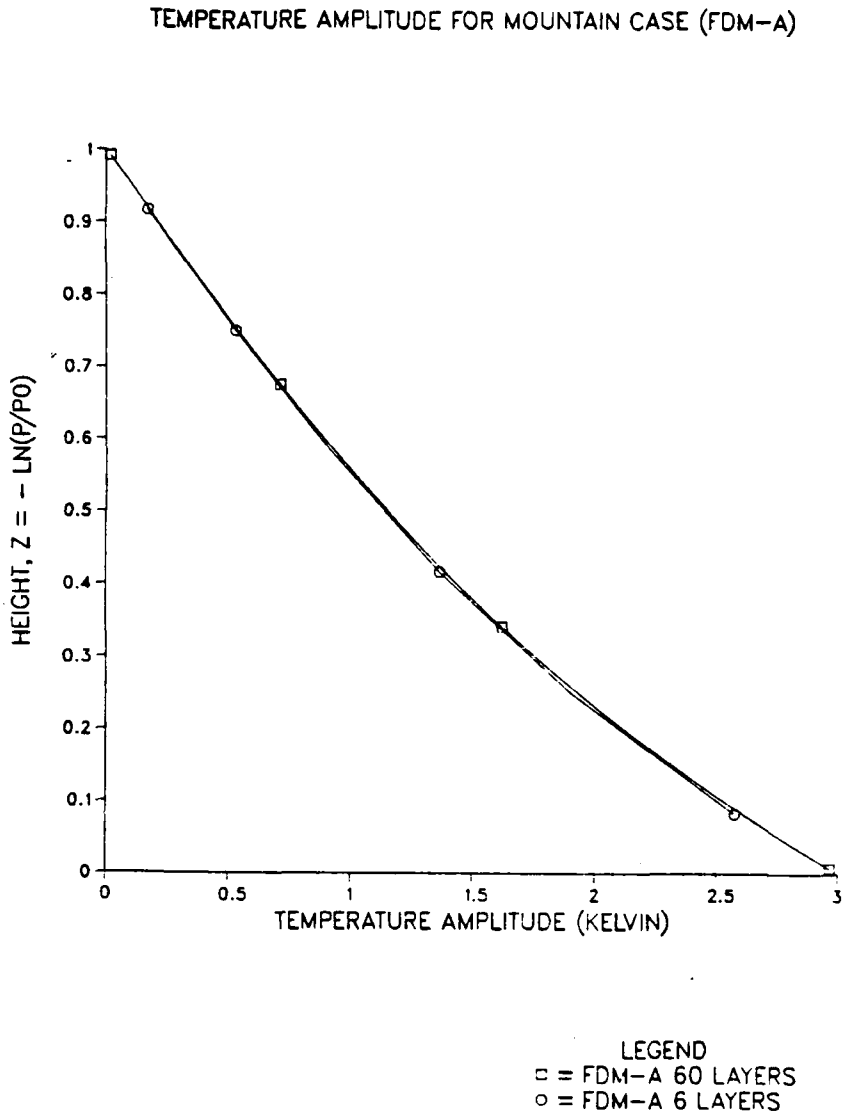

Figure 36. Six-layer mountain topography experiment at 96 hours. Temperature amplitude profiles are compared for the six-layer and 60-layer FDM-A models.

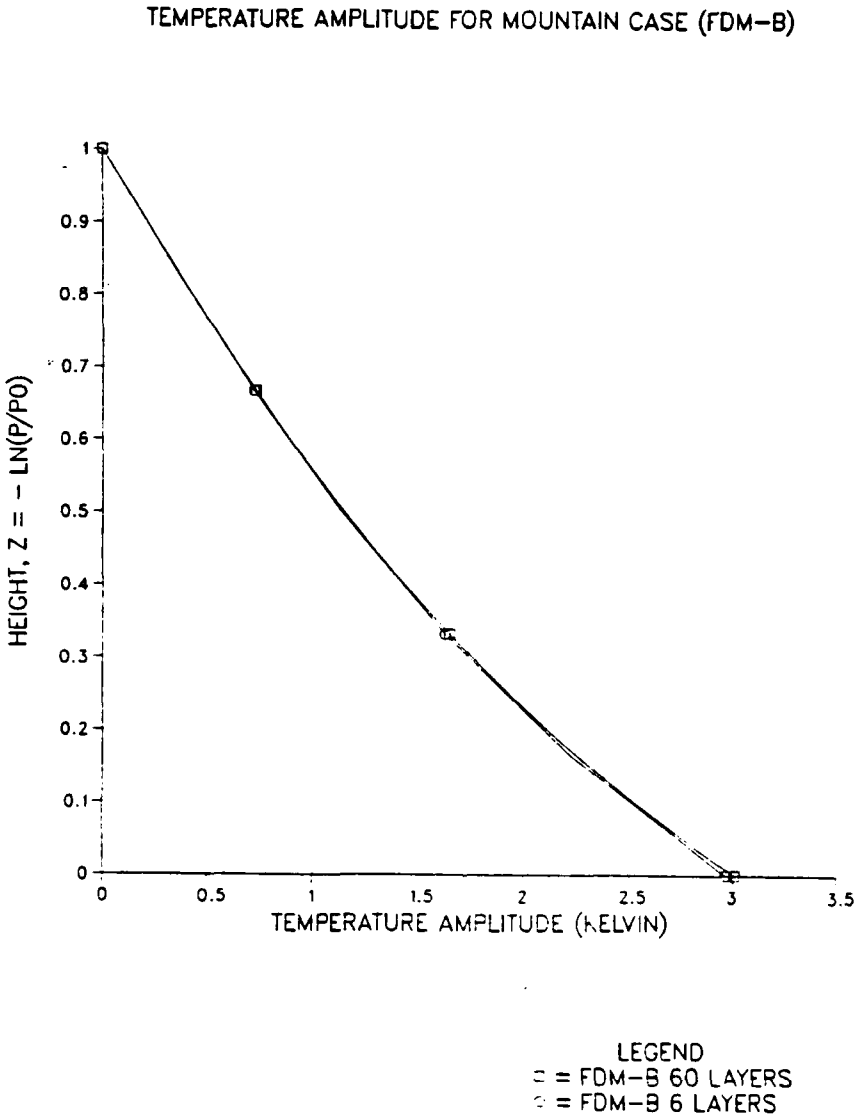

Figure 37. As in Fig. 36 but for model FDM-B.

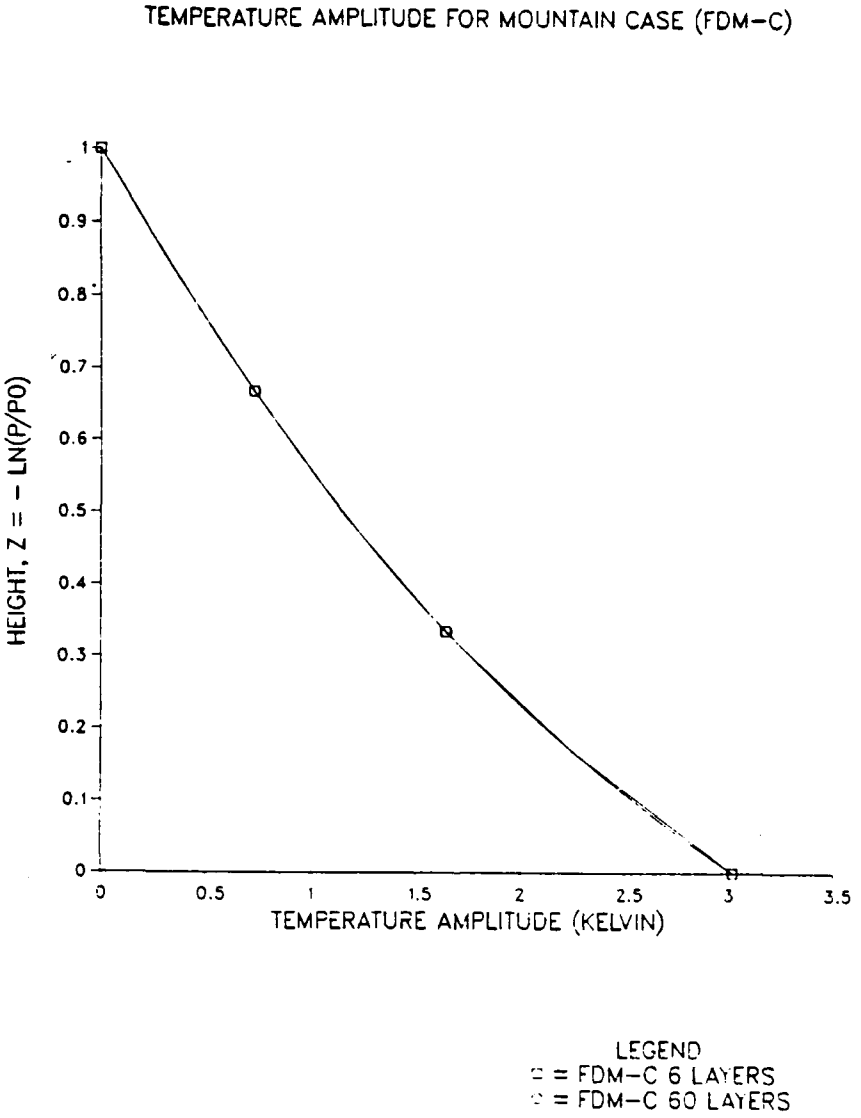

Figure 38. As in Fig. 36 but for model FDM-C.

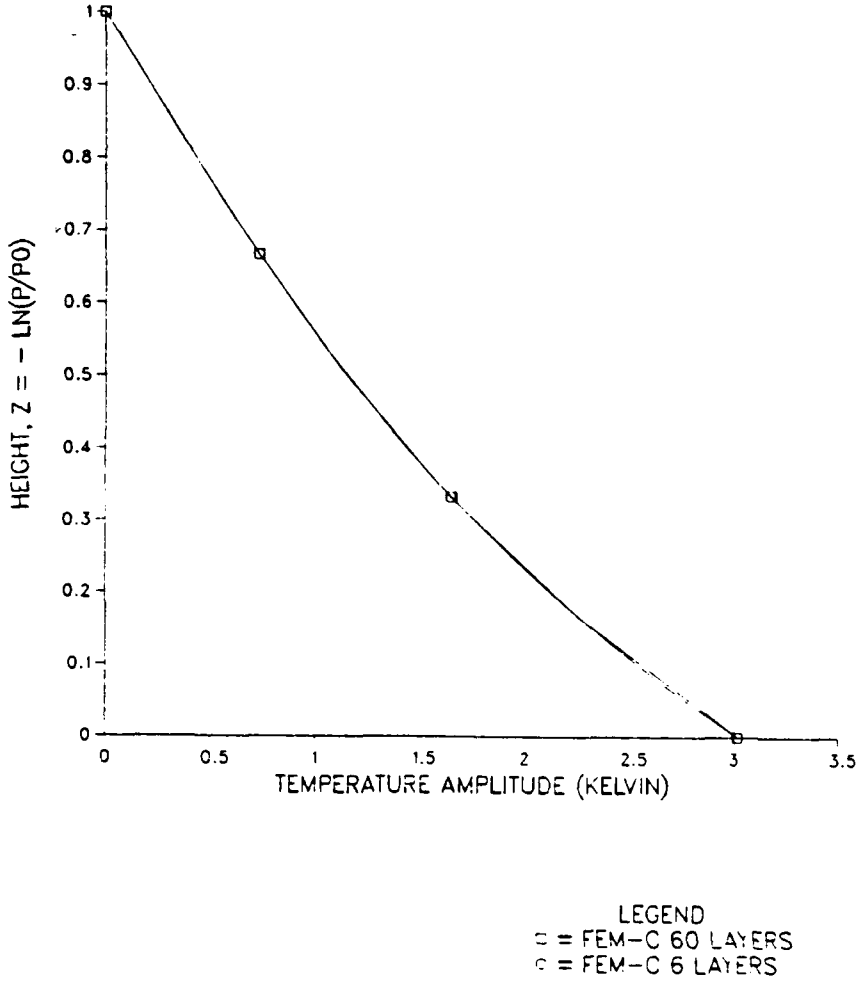

Figure 39. As in Fig. 36 but for model FEM-C.

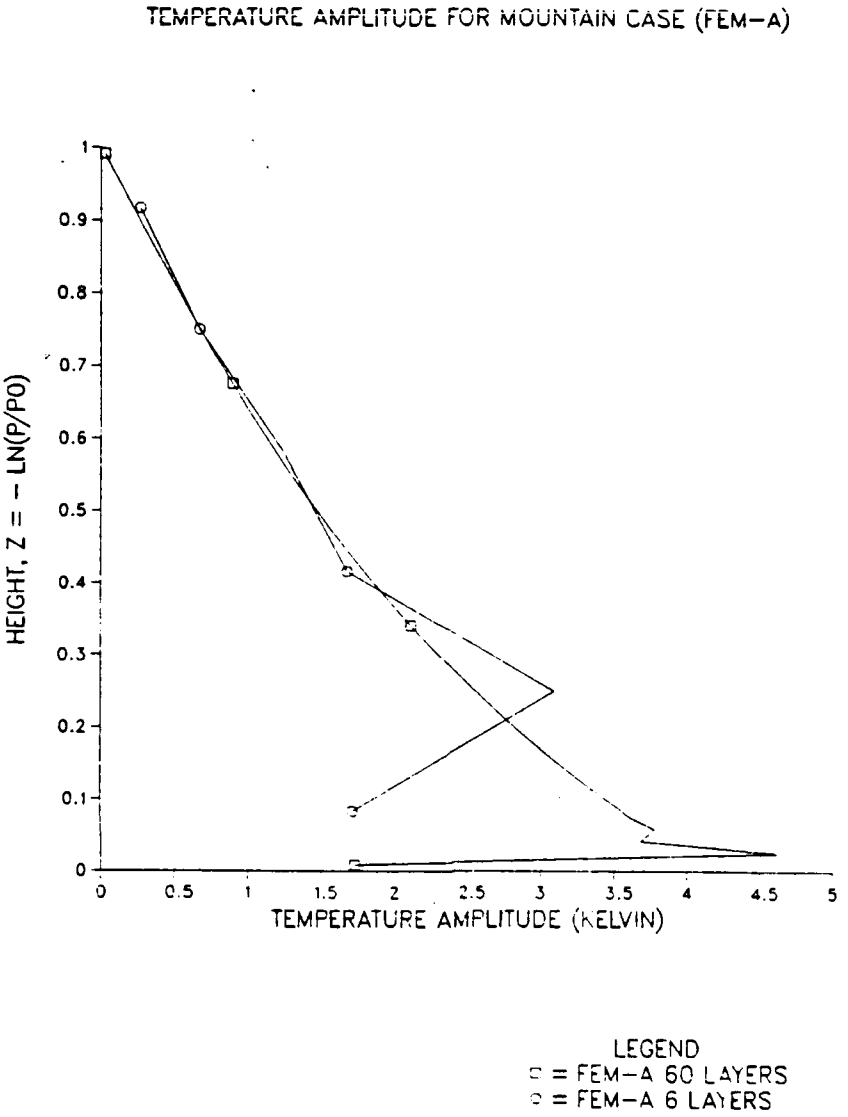

Figure 40. As in Fig. 36 but for model FEM-A.

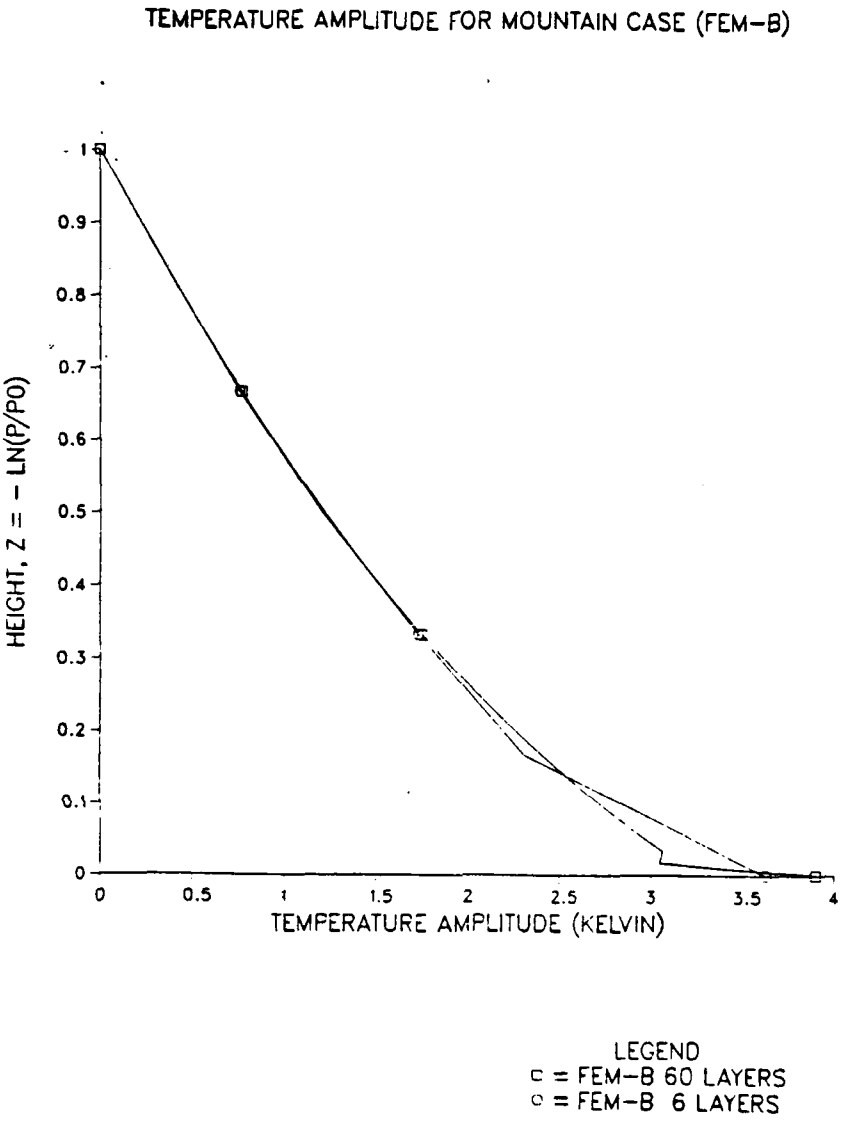

Figure 41. As in Fig. 36 but for model FEM-B.

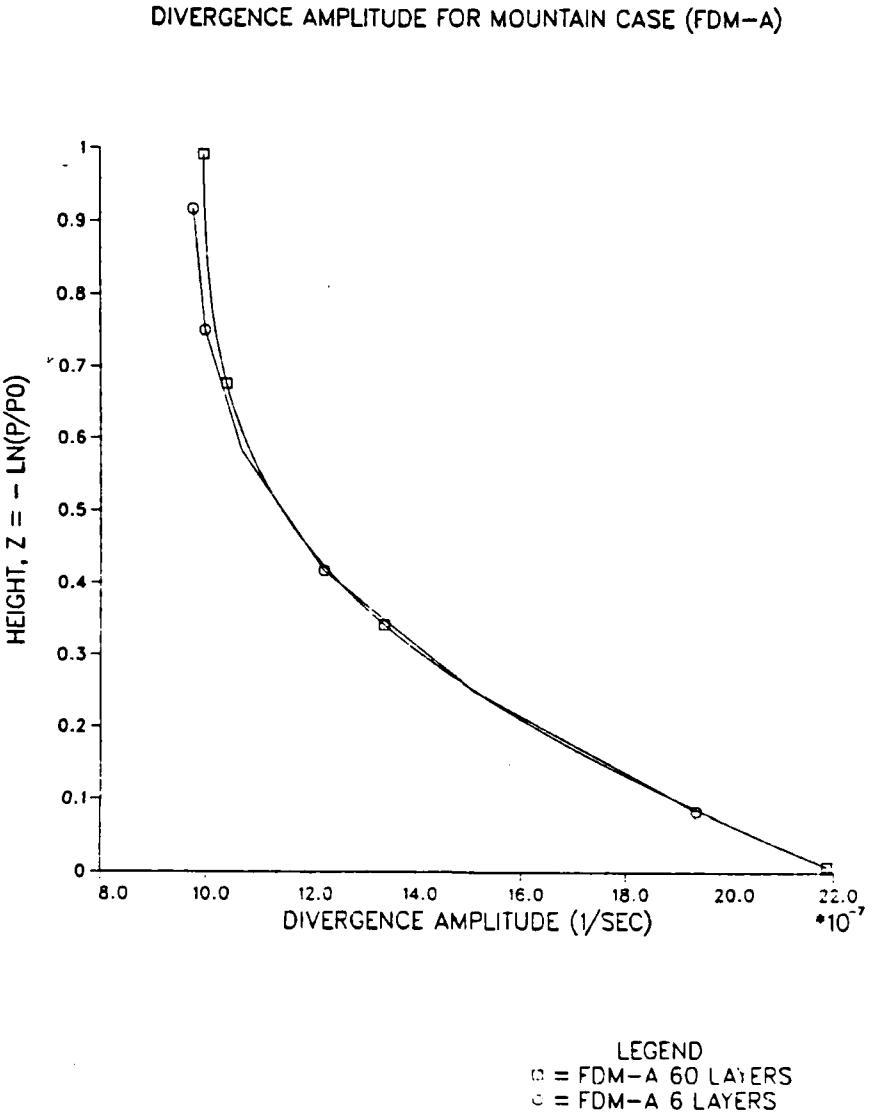

Figure 42. As in Fig. 36 but for divergence amplitude.

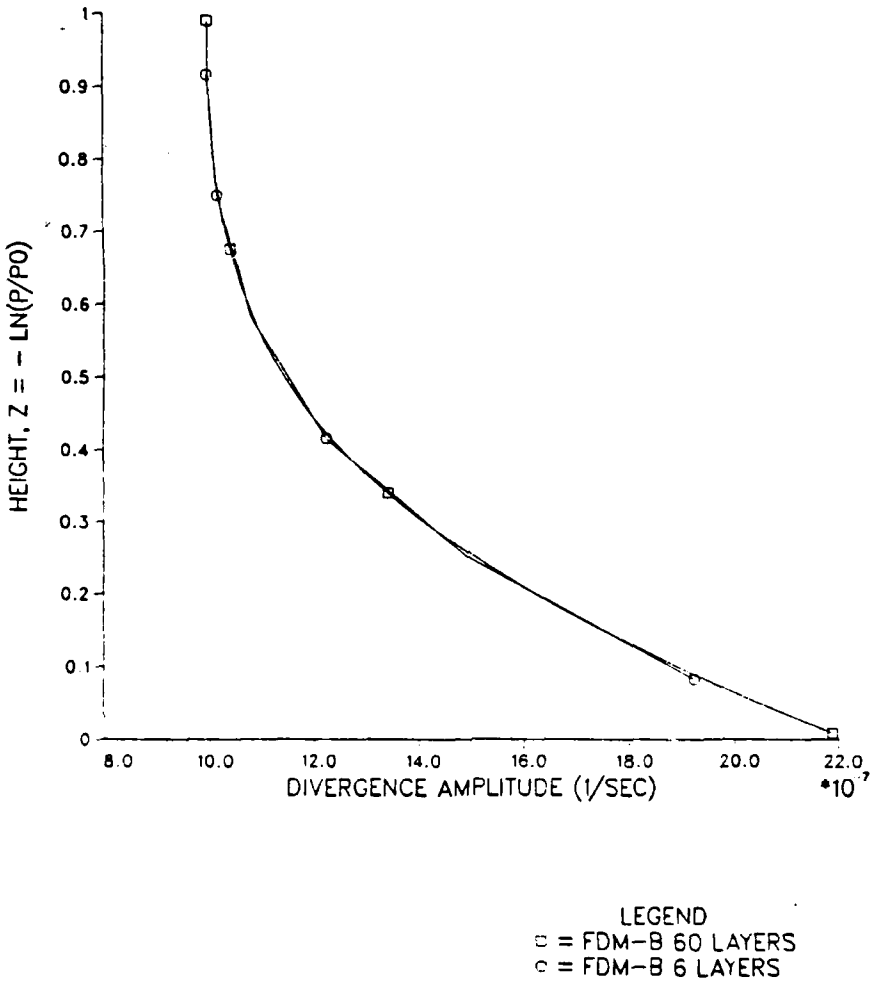

Figure 43. As in Fig. 36 but divergence amplitude for model FDM-B.

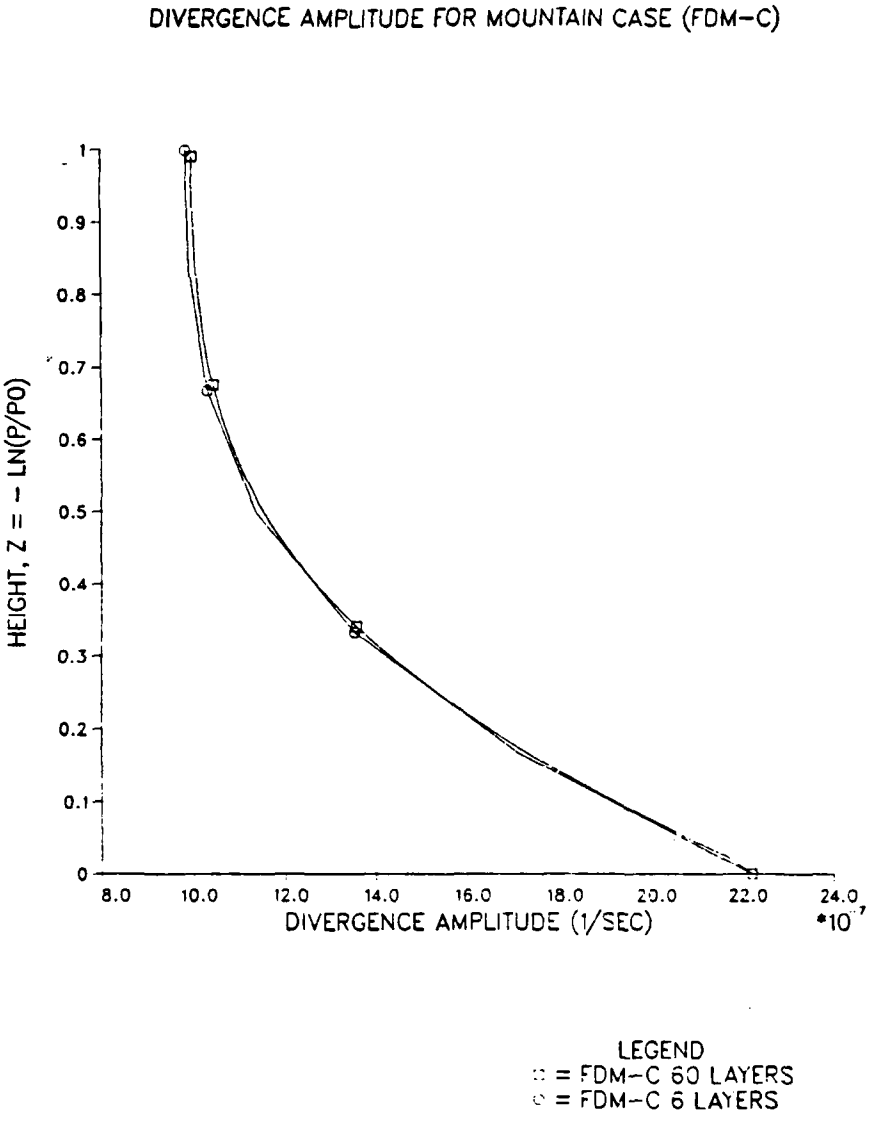

Figure 44. As in Fig. 36 but divergence amplitude for model FDM-C.

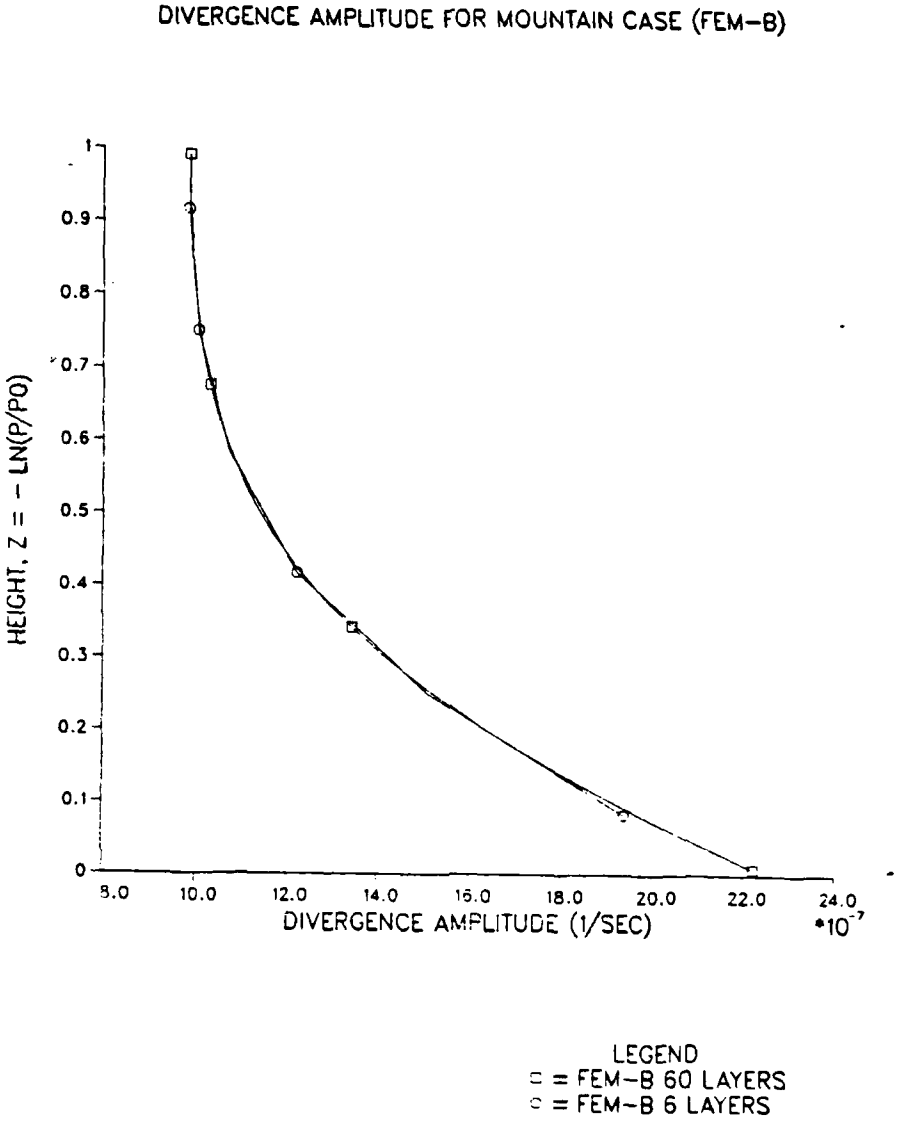

Figure 45. As in Fig. 36 but for divergence amplitude for model FEM-B.

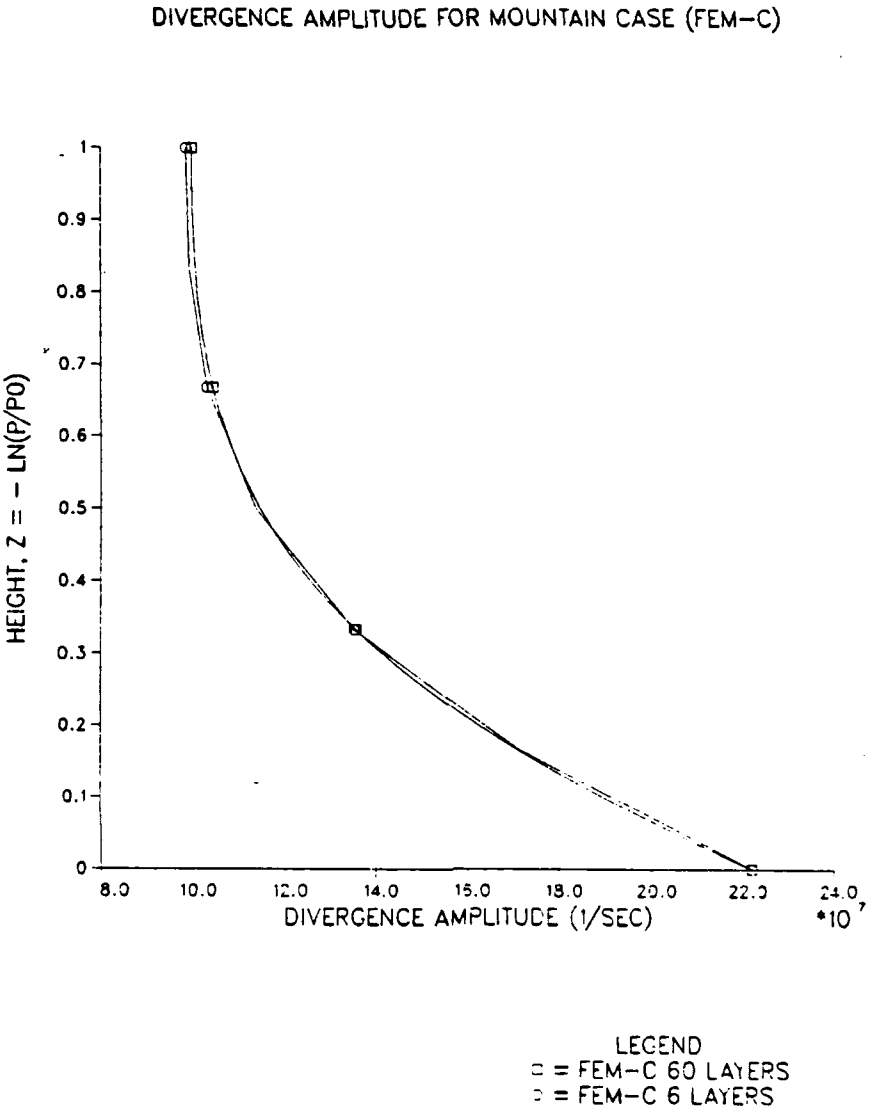

Figure 46. As in Fig. 36 but for divergence amplitude for model FEM-C.

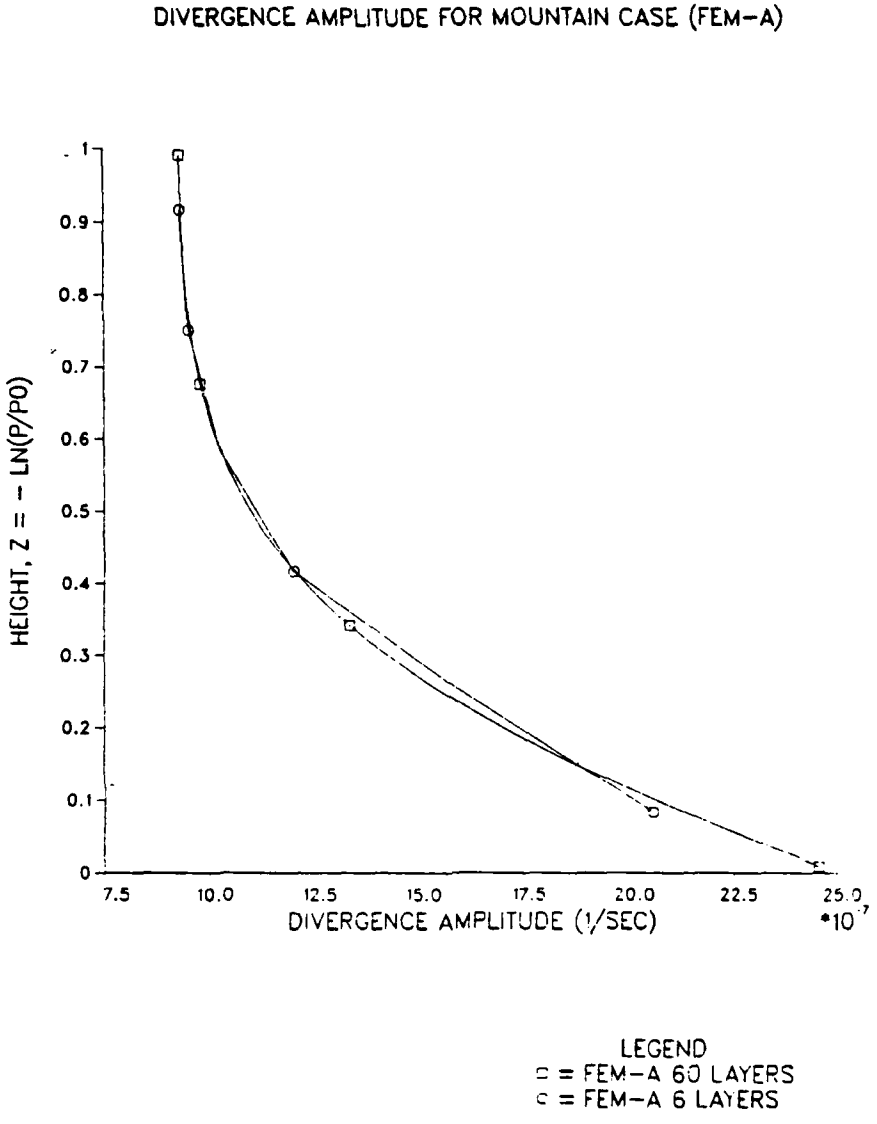

Figure 47. As in Fig. 36 but for divergence amplitude for model FEM-A.

C. DIABATIC HEATING EXPERIMENT

A diabatic heat source is defined in the layer between Z = 0.40 and Z = 0.60 (670-549 mb). The rate of heating is constant in time and varies in x and Z,

$$Q(x,Z,t) = \text{HEATING} \cdot \cos^2\left[\frac{(Z - Z_M)}{(Z_U - Z_L)}\right] \cdot \pi] \cdot \cos(\mu x) \ , \qquad (3\text{-}1)$$

where HEATING is 5.0 K/day, Z_M is the midpoint of the heated layer, and Z_L and Z_U are the lower and upper boundaries, respectively, of the heated layer. The diabatic heating vectors, Q1 and Q2, are defined in the initialization subroutine and stored for use in the forecast subroutine. Beta and all initial perturbations are zero. The forecast length is 12 hours.

1. Sixty-Layer Models

For the diabatic heating function defined in equation (3-1), the maximum heating occurs at Z = 0.50, the midpoint of the heated layer. The models defined using grids B and C define temperature and the heating functions at this point. The grid A models do not have temperature and diabatic heating defined at this point so the maximum rate of heating in these models is slightly less than in the other models, and the maximum heating occurs throughout one layer rather than occurring at one point. The heating rate at each level is listed in Appendix K for the six, twelve and sixty-layer staggered and unstaggered models.

The 60-layer profiles for the six models are quite similar, but the differences occur because the models are responding to different forcing. The temperature amplitude profiles for the B and C grids come to a sharp point at Z = 0.50 and the grid A models have a square-nosed profile around this point (Figures 48-50). The height in the atmosphere at which the model experiences the onset of forcing is slightly different between the grids. This explains the small-scale oscillation in the temperature amplitude profiles near the boundaries of the heated layer, Z = 0.40 and Z = 0.60. The previously identified temperature amplitude oscillations in the lowest layers of models FEM-A and FEM-B are not evident in this experiment. The temperature phase profiles are nearly identical, except that the grid A models do not have as sharp of a spike at the boundaries of the heated layer as the other grids (Figures 51-53). In summary, the 60-layer temperature profiles of all six models represent the same physical response to the diabatic heating.

Divergence is defined at the midpoint of the heated layer only in the grid C models. Consequently, the shape of the divergence amplitude profile for the grid C models is different than the other four models. The grid C profiles have a sharp point at Z = 0.50 (Figure 54). However, the minimum divergence is not symmetric around Z = 0.50 in the grid A and B models (Figures 55-57). The divergence amplitude is identical outside the heated layer for all models

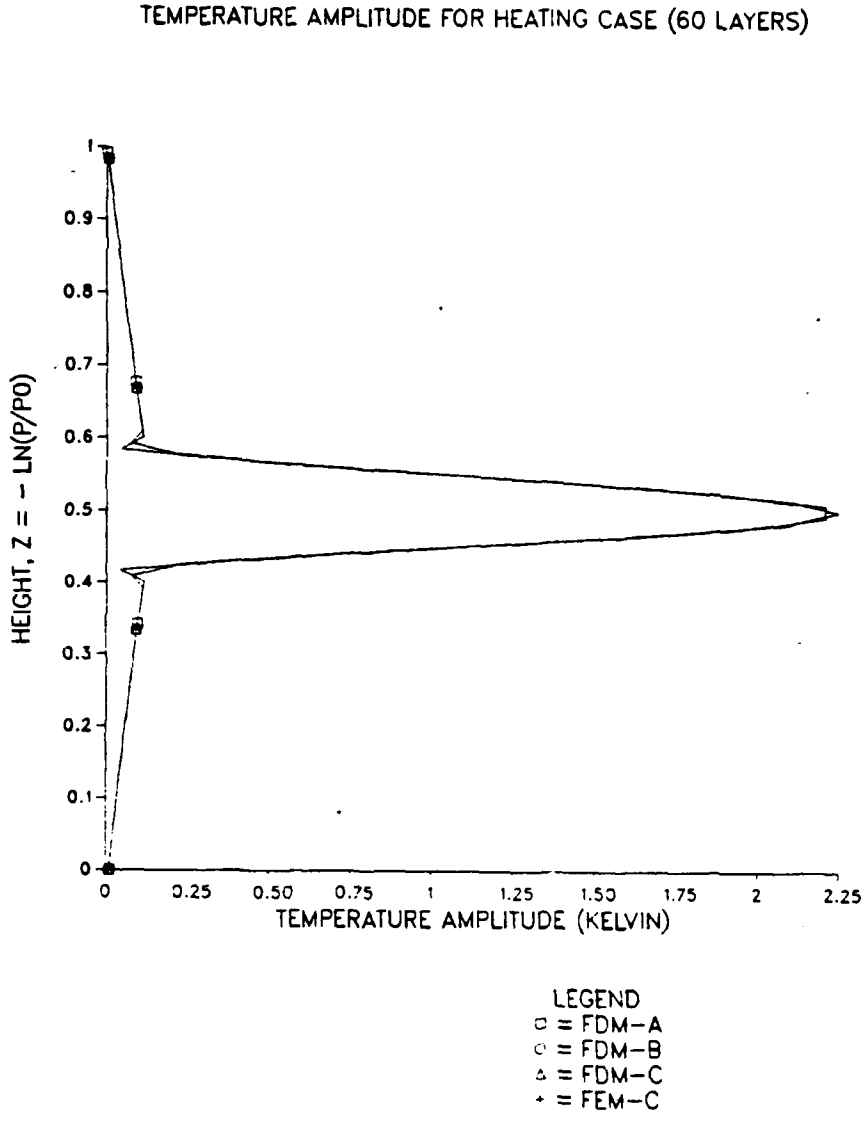

Figure 48. Sixty-layer diabatic heating experiment at 12 hours. Temperature amplitude profiles are compared for models FDM-A, FDM-B, FDM-C, and FEM-C.

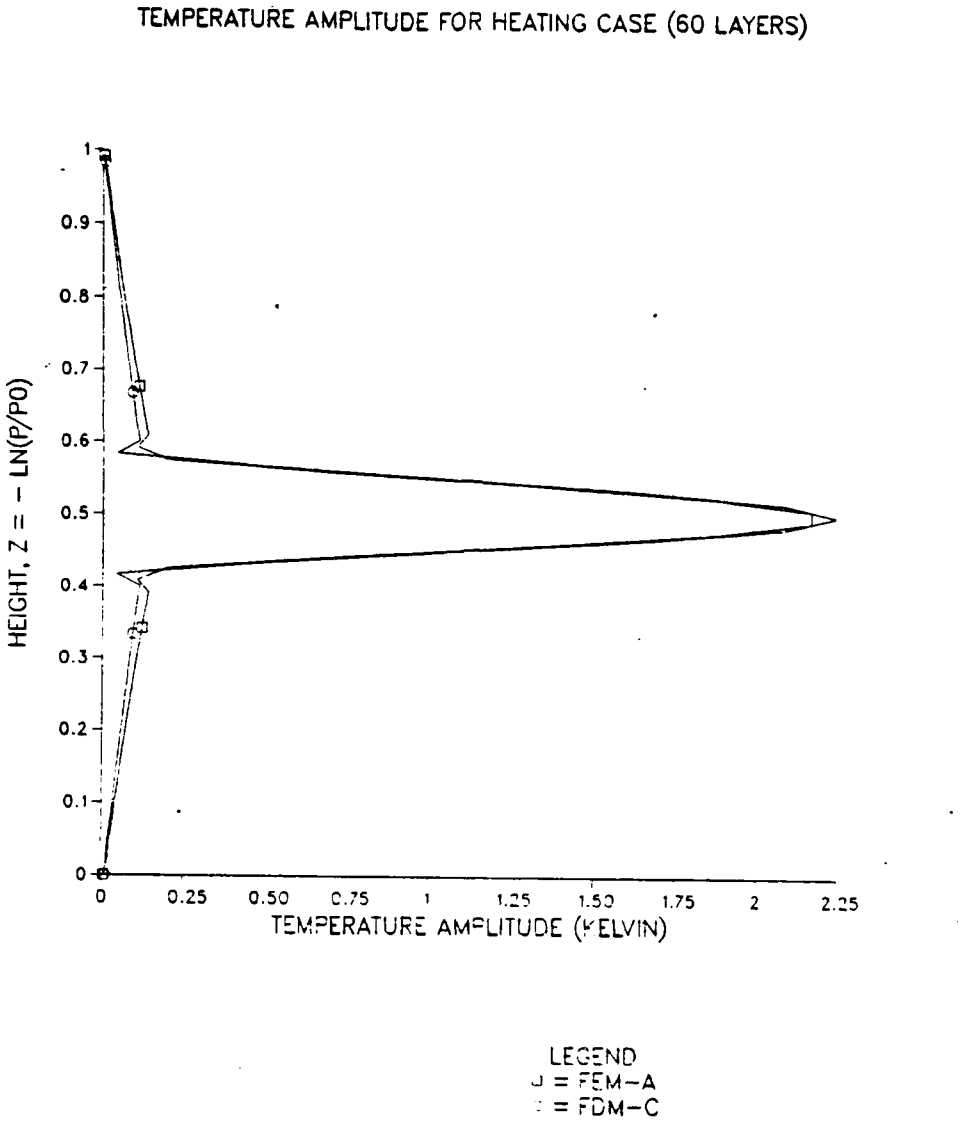

Figure 49. Sixty-layer diabatic heating experiment at 12 hours. FEM-A temperature amplitude profile is compared with the temperature amplitude profile of FDM-C, which represents the consensus profile.

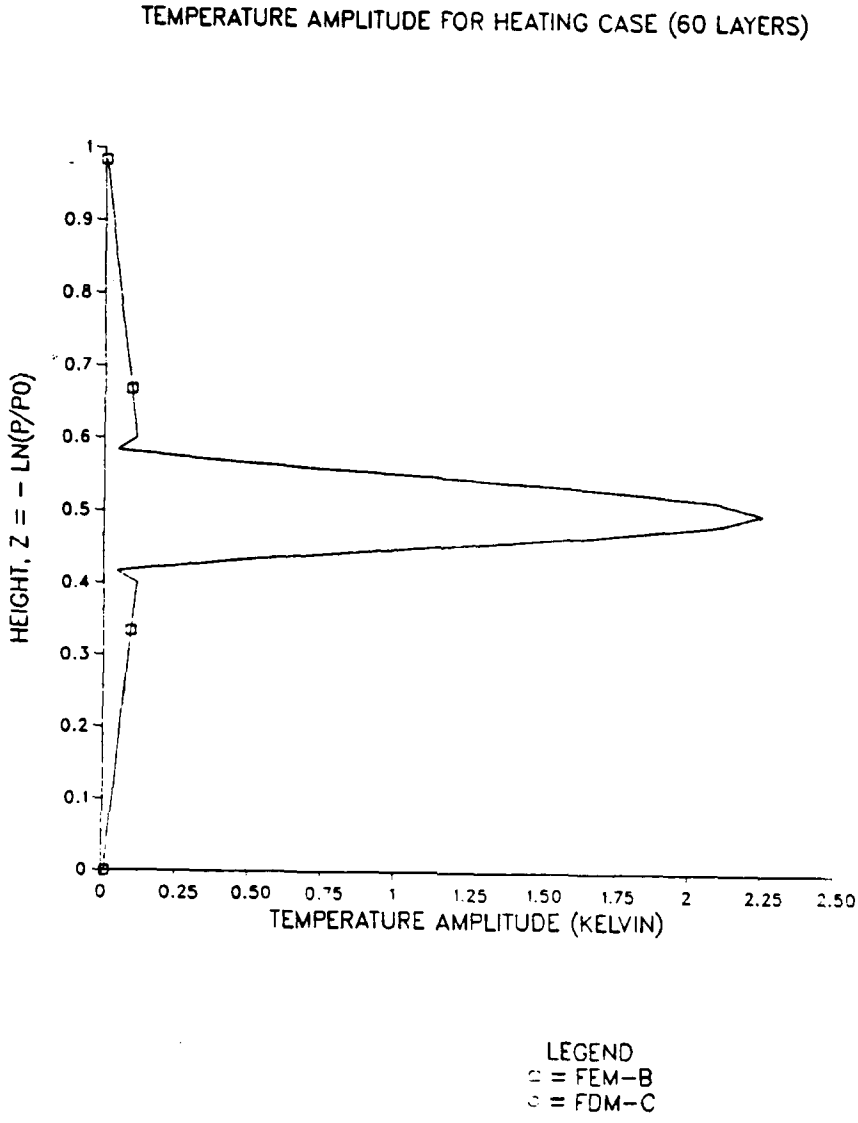

Figure 50. As in Fig. 49 but for model FEM-B compared with the consensus, FDM-C.

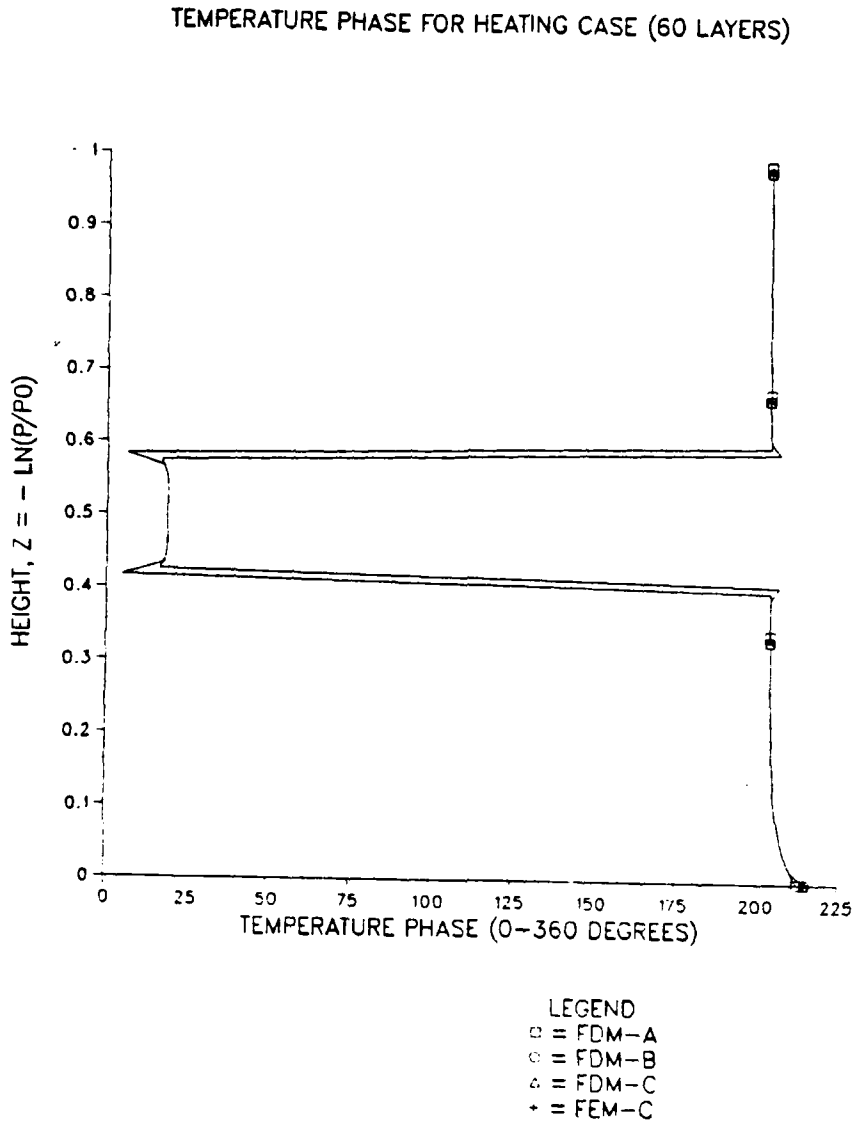

Figure 51. As in Fig. 48 but for temperature phase.

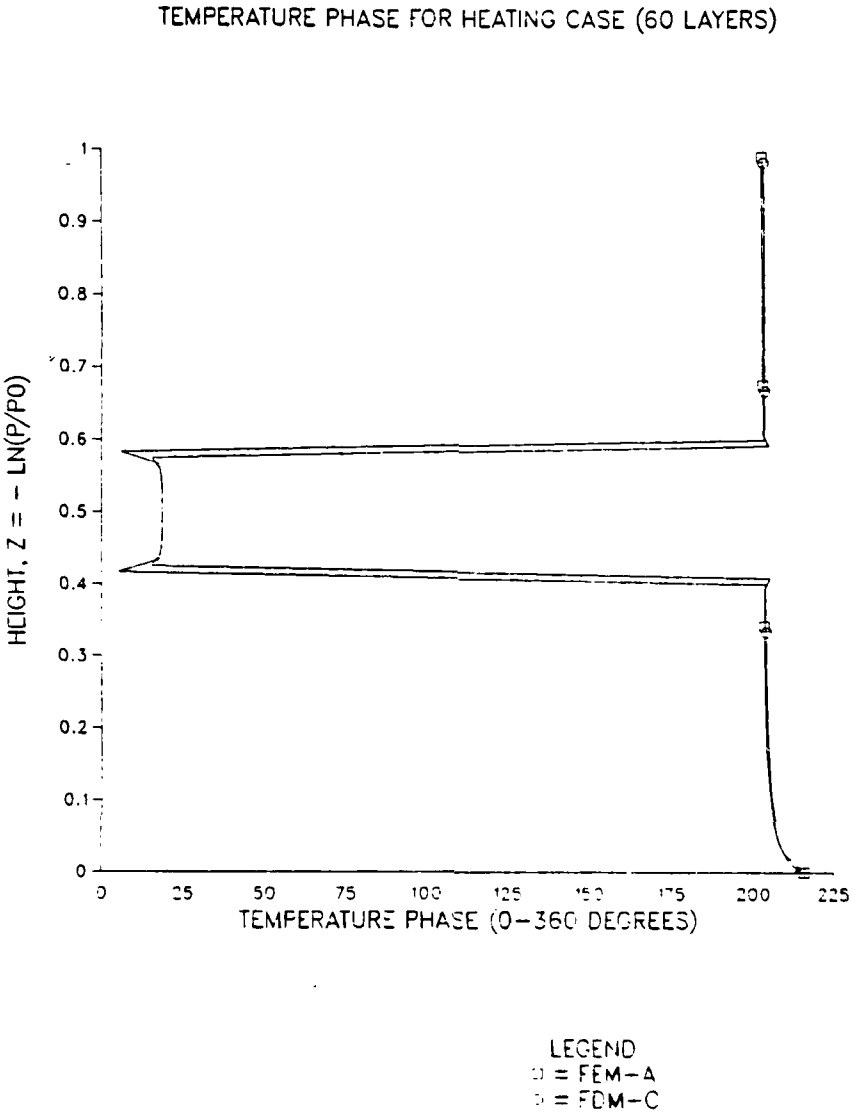

Figure 52. As in Fig. 49 but for temperature phase.

AD-A161 049 A COMPARISON OF SIX VERTICAL DISCRETIZATION SCHEMES(U) 2/2
NAVAL POSTGRADUATE SCHOOL MONTEREY CA M S JORDAN
SEP 85

UNCLASSIFIED F/G 12/1 NL

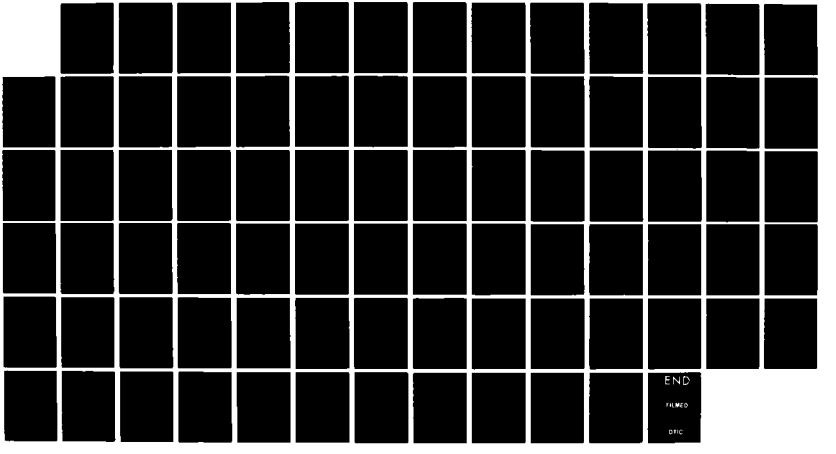

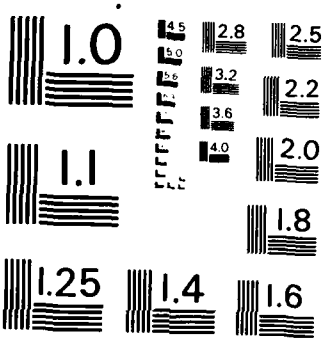

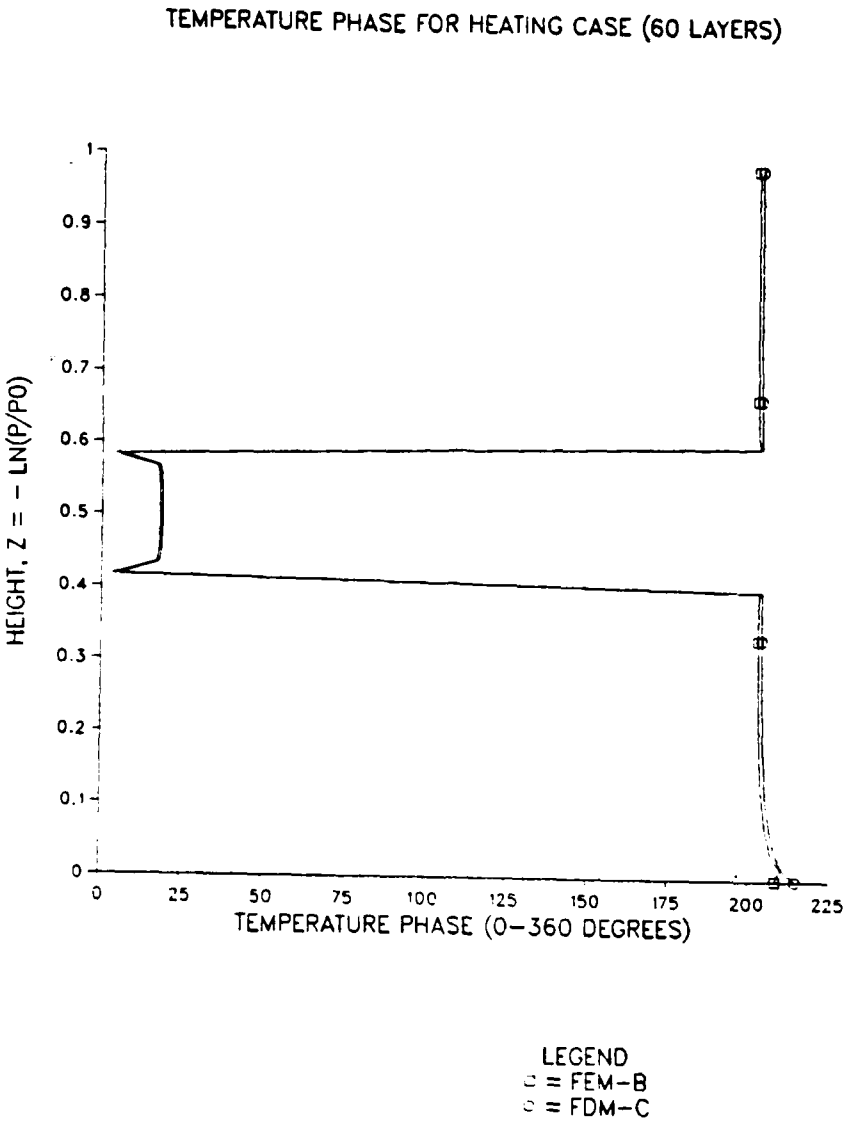

Figure 53. As in Fig. 50 but for temperature phase.

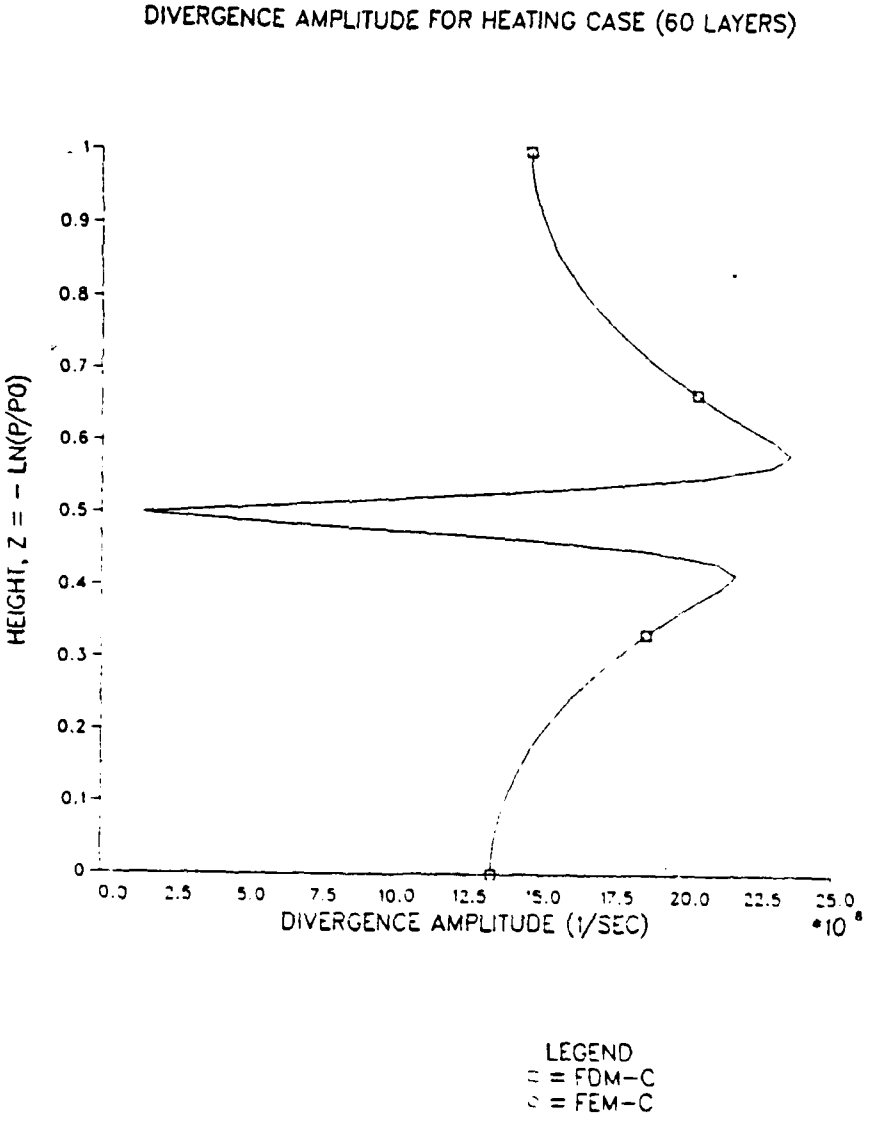

Figure 54. Sixty-layer diabatic heating experiment at 12 hours. Temperature amplitude models are compared for the two grid C models.

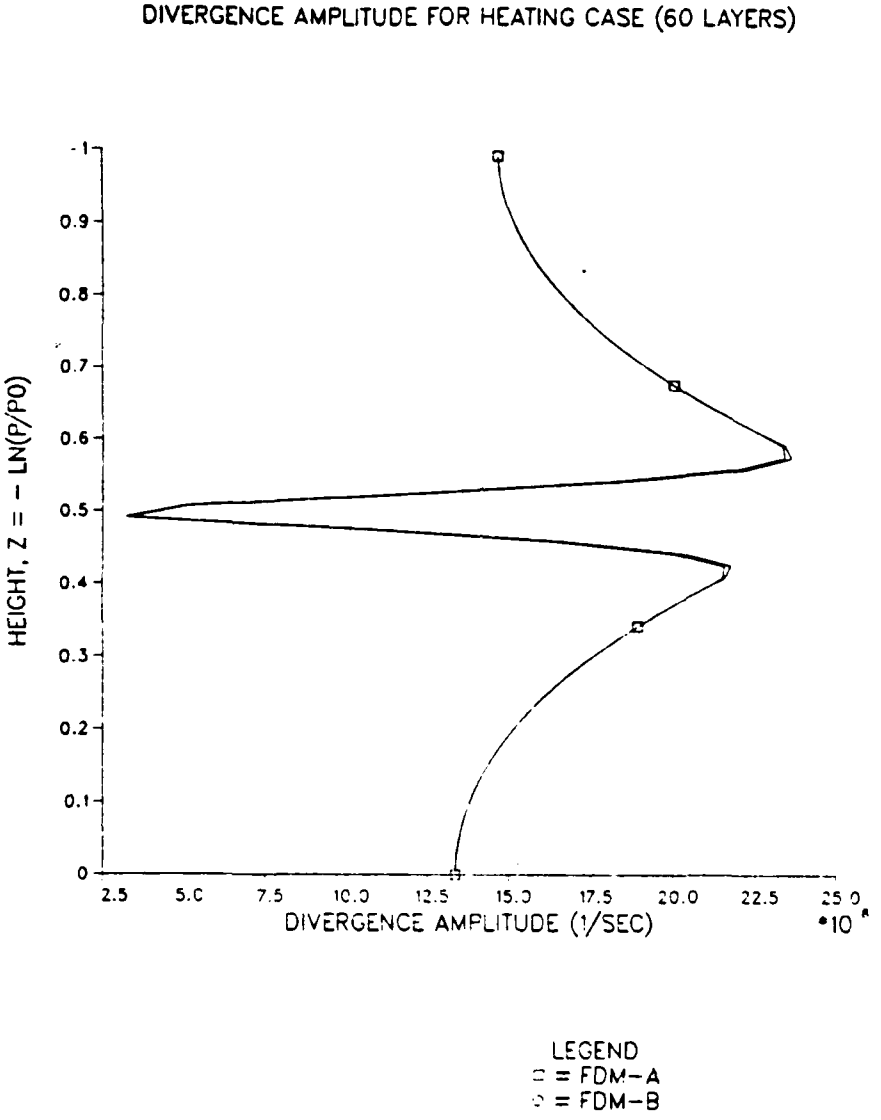

Figure 55. Sixty-layer diabatic heating experiment at 12 hours. Temperature amplitude profiles are compared for models FDM-A and FDM-B.

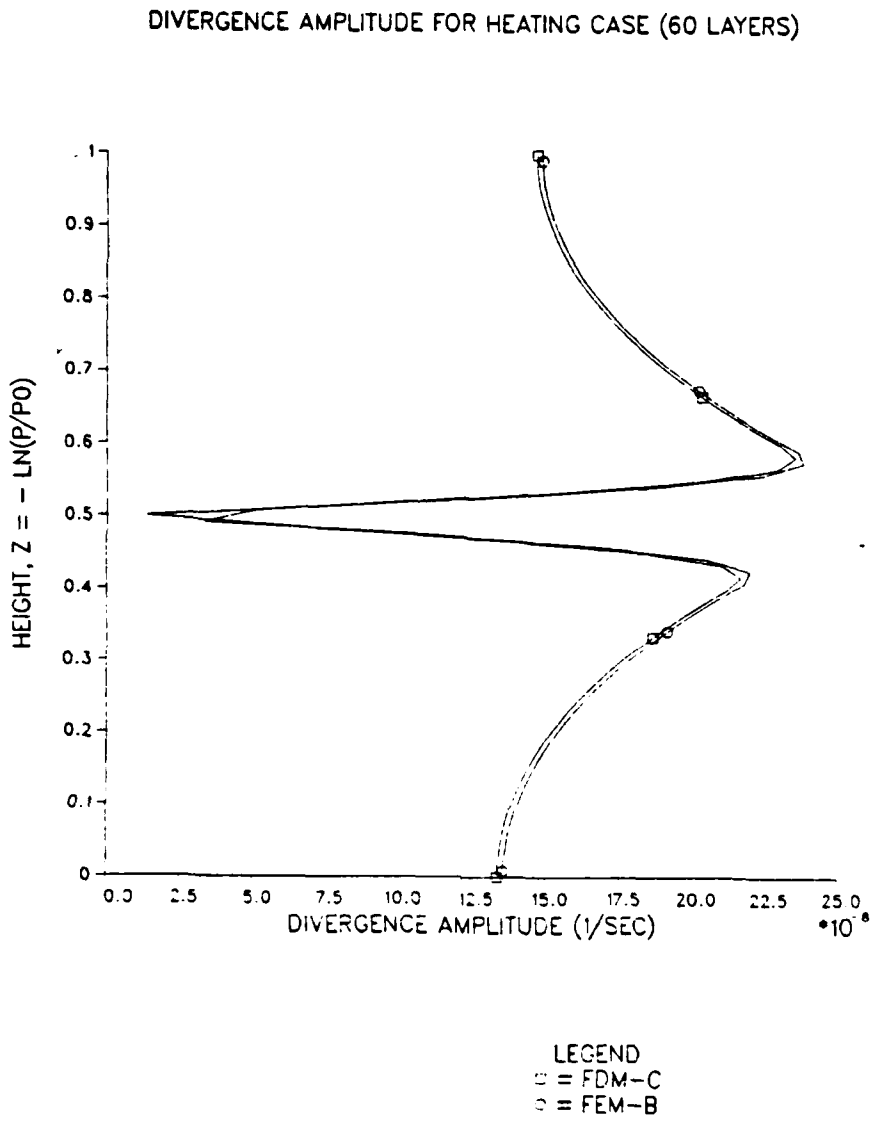

Figure 56. As in Fig. 55 but models FEM-B and FDM-C are compared.

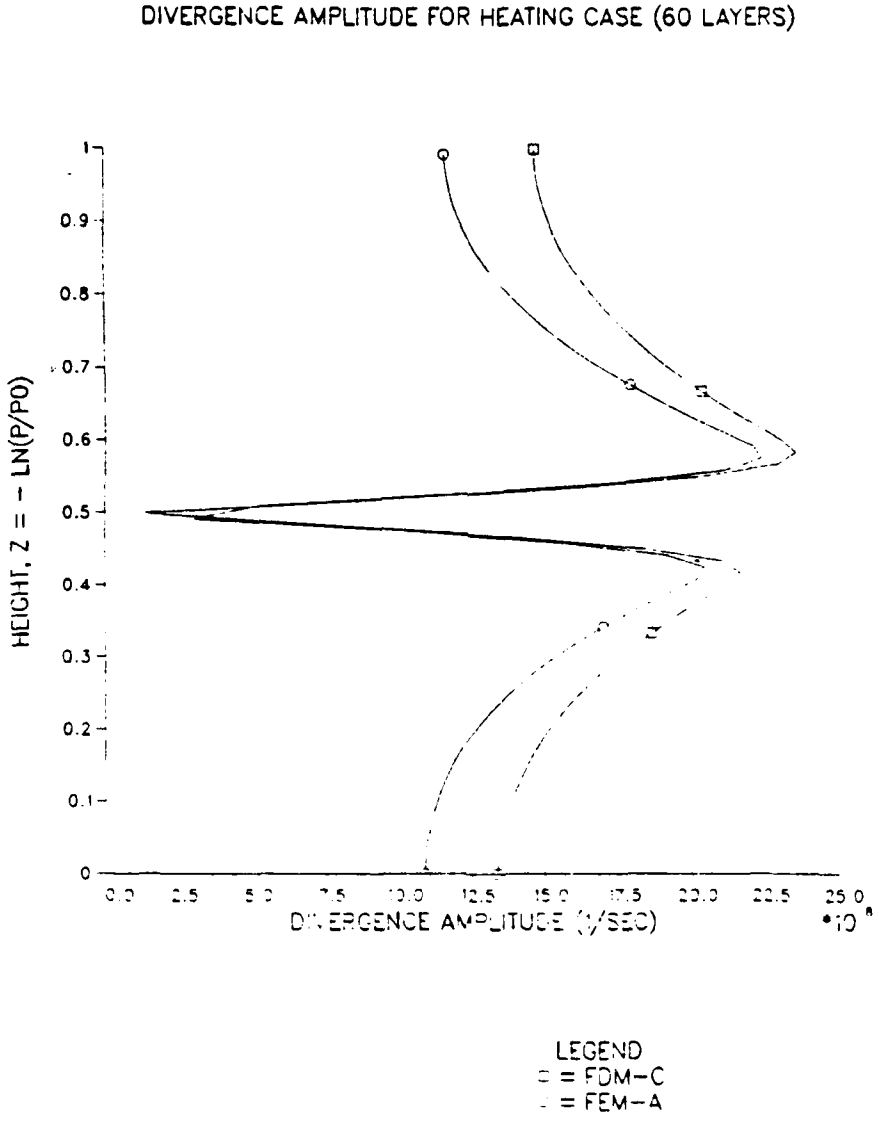

Figure 57. As in Fig. 55 but models FEM-A and FDM-C are compared.

except FEM-A (Figure 57). The divergence phase profiles are virtually identical for models FDM-A, FDM-B, FDM-C and FEM-C (Figure 58). The divergence phase passes through zero at a different level for model FEM-B than the consensus, but this difference is not physically significant (Figure 59). The FEM-A profile differs slightly from the consensus outside the heated layer (Figure 60). In conclusion, the six models are converging to the same 60-layer divergence solution inside the heated layer, but model FEM-A does not agree with the solution of the other five models outside this region.

2. Six and Twelve-Layer Models

The difference between grids is more evident in this experiment than in the other experiments. Each model is run with both six and twelve layers and the results are compared with the 60-layer consensus of the six models. The temperature amplitude consensus profile has a small-scale decrease at each boundary of the heated layer that cannot be reproduced using either six- or twelve-layer resolution.

The six-layer grid A model temperature and divergence fields barely respond to the diabatic heating. The grid A models have identical temperature responses for both six and twelve layers. The six-layer perturbation, constant with height in the heated layer, is an order of magnitude smaller than maximum consensus perturbation (Figures 61-62). The grid A models have a stronger response to the heating with twelve layers than with six layers, but the maximum amplitude

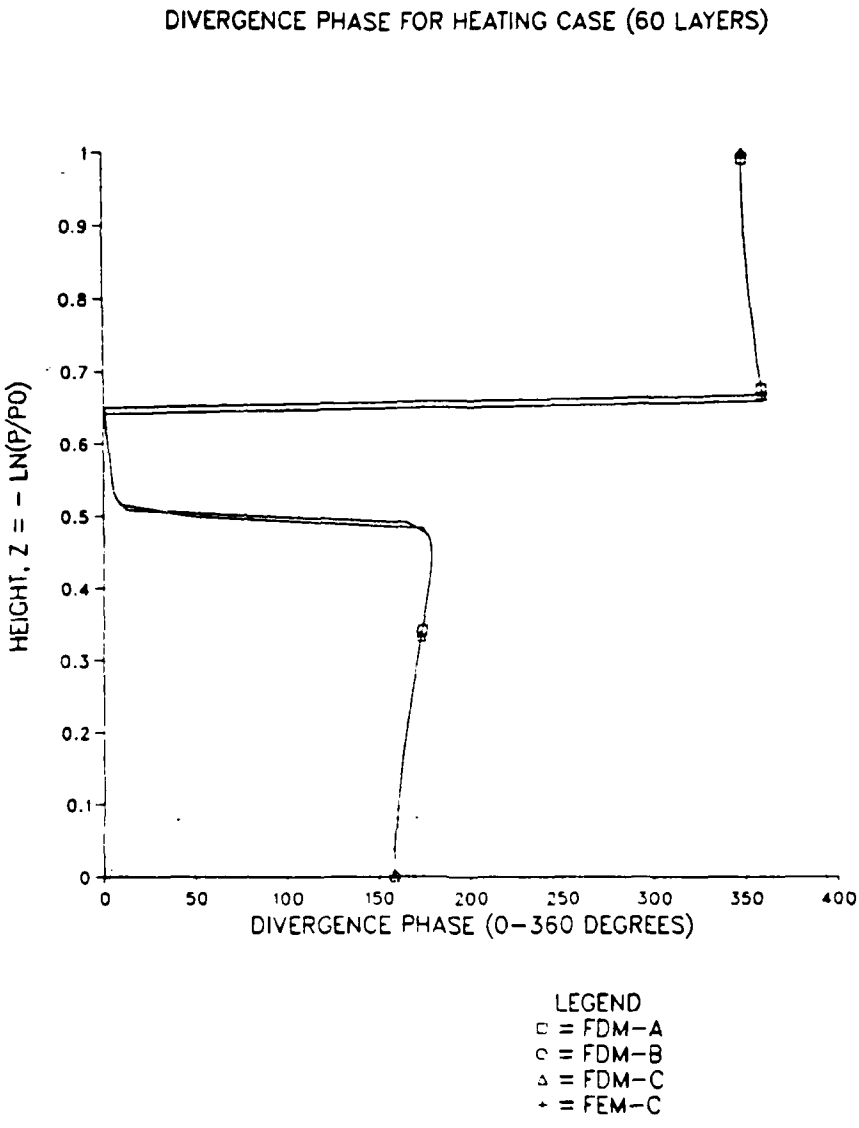

Figure 58. As in Fig. 48 but for divergence phase.

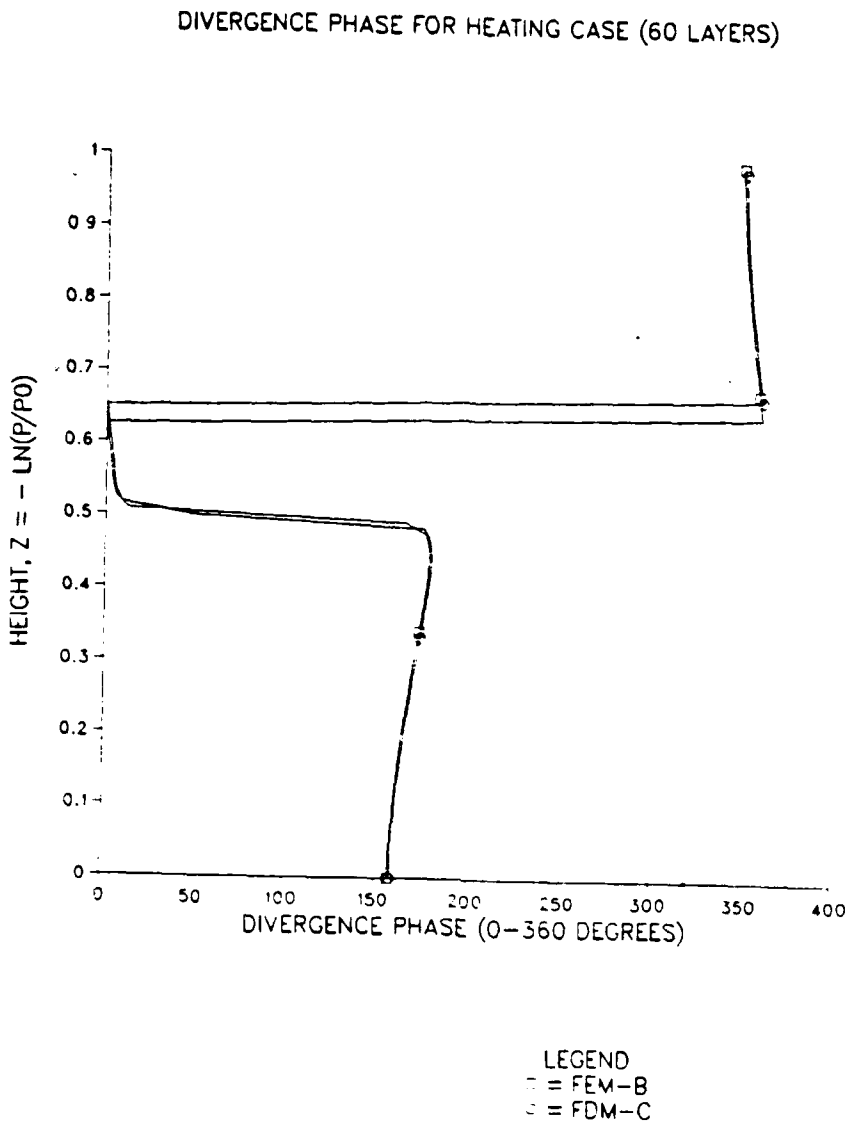

Figure 59. As in Fig. 56 but for divergence phase.

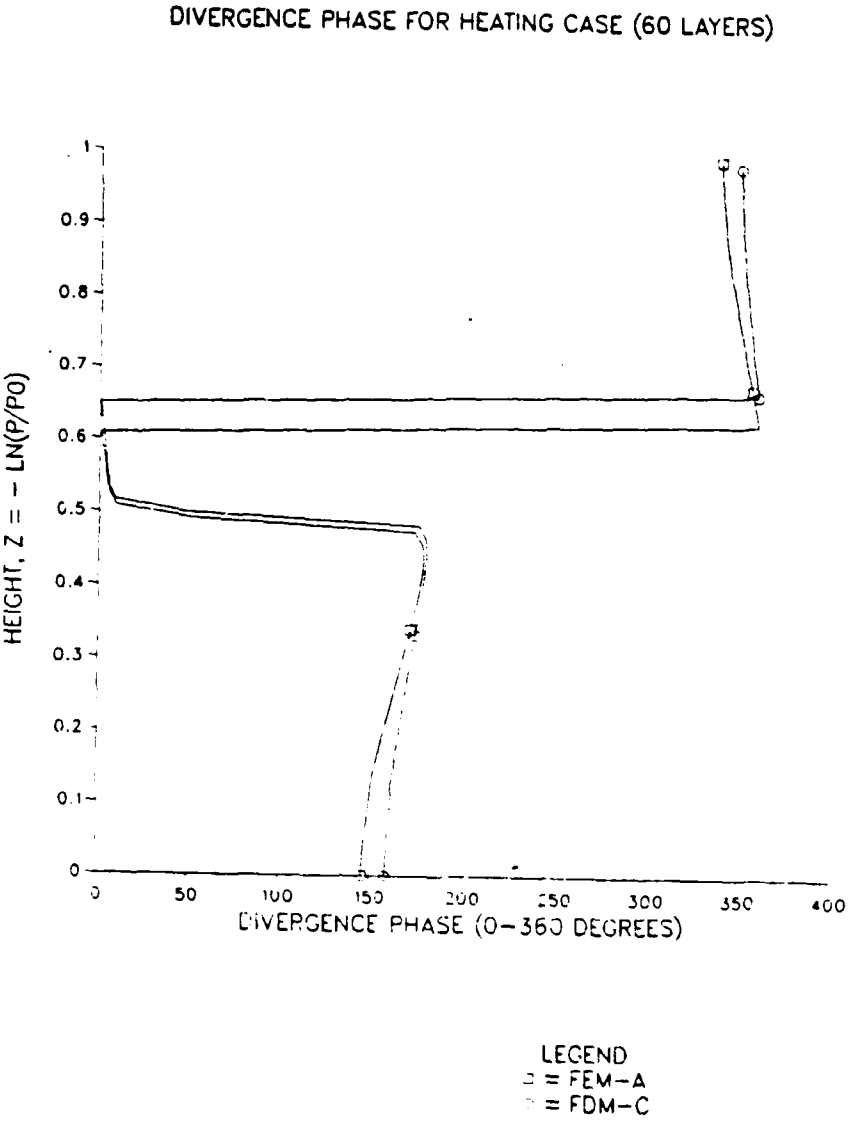

Figure 60. As in Fig. 57 but for divergence phase.

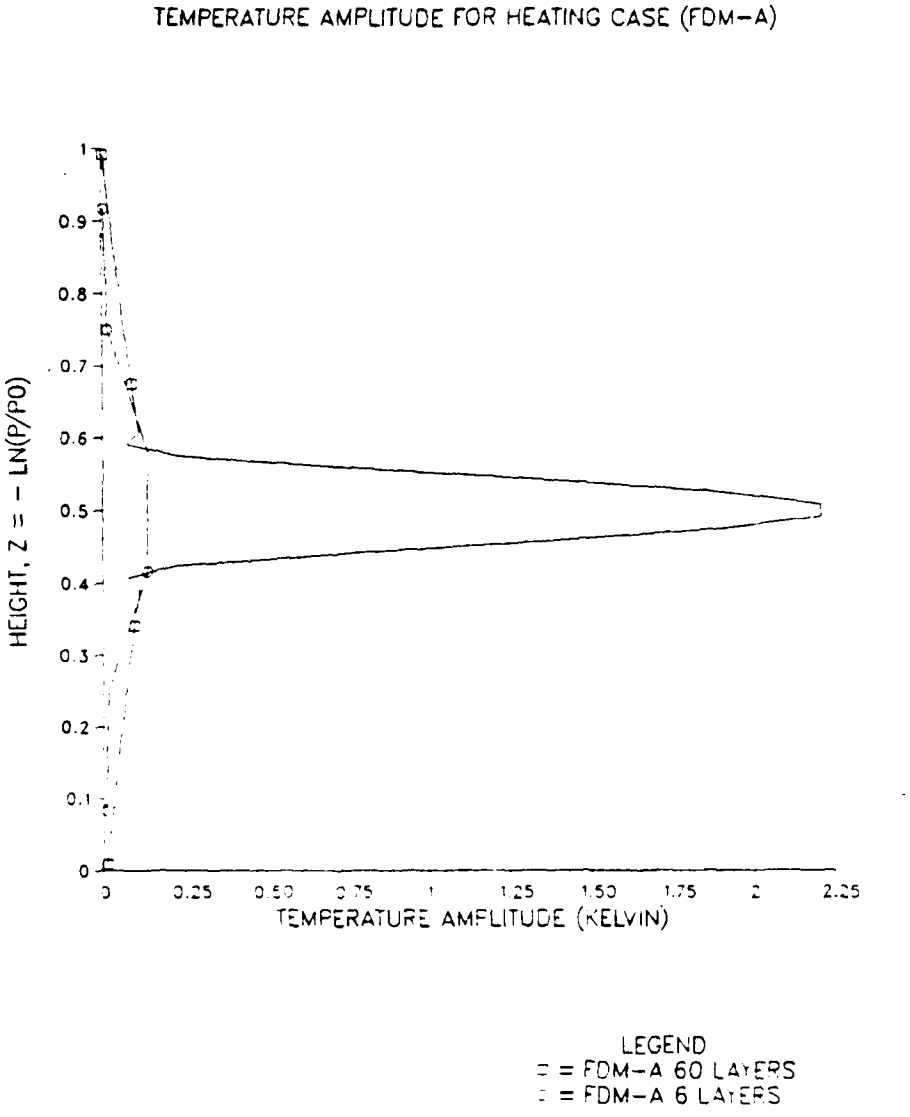

Figure 61. Six-layer diabatic heating experiment at 12 hours. Temperature amplitude profiles are compared for the six-layer and 60-layer FDM-A models.

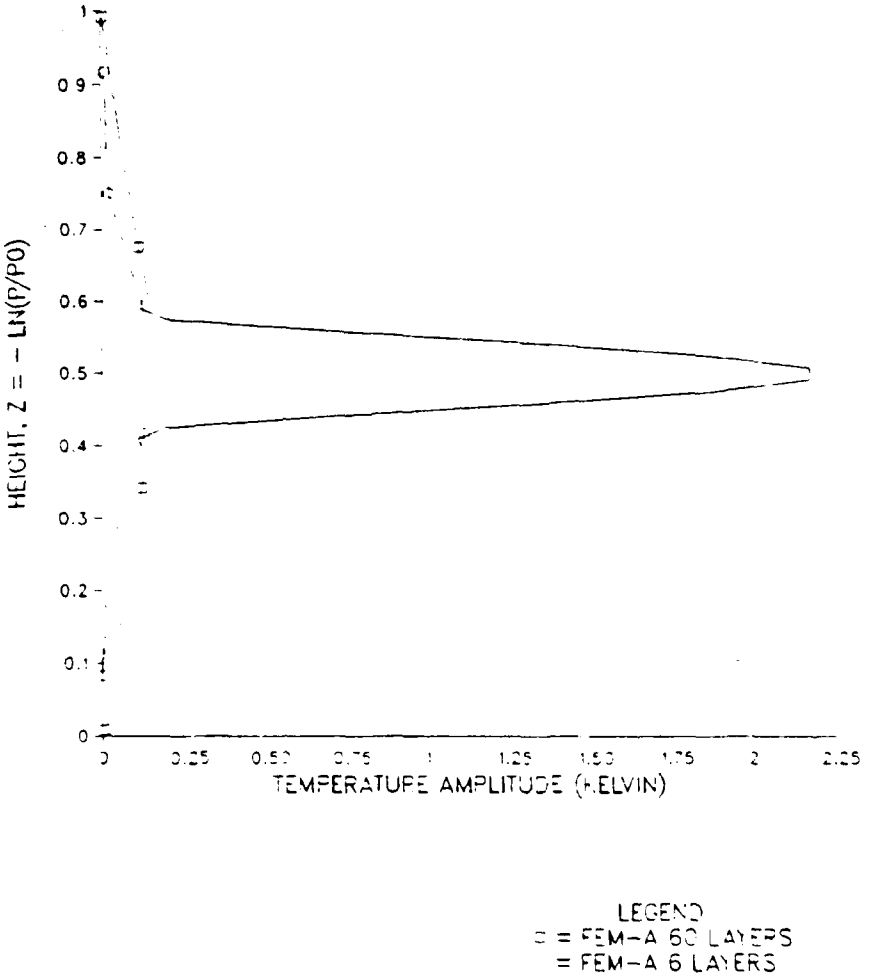

Figure 62. As in Fig. 61 but for model FEM-A.

is only 60% of the 60-layer consensus response (Figures 63-64). For both the six- and twelve-layer profiles, the temperature amplitude at the two staggered nodal points defined closest to the heated layer lie directly on the 60-layer profile. This may indicate that for much less than 60-layer resolution the amplitude of the spike will not equal the maximum amplitude in the 60-layer experiment. The divergence fields of the six-layer grid A models is also an order of magnitude lower than their corresponding 60-layer solutions (Figures 65-66). The characteristic sharp divergence decrease in the heated layer is roughly approximated by the 12-layer models (Figures 67-68). The minimum divergence is much larger than in the consensus profile and the base of the spike decrease is much broader than in the 60-layer solutions. Outside the heated layer, the shape of the 12-layer profile is similar to the consensus, but the amplitude is lower.

The six-layer temperature amplitude response of the B and C grid models are virtually identical (Figures 69-72). The base of the profile spike is broader in the six-layer models than in the consensus, but the four models closely approximate the magnitude and width of the tip of the spike. The 12-layer temperature profiles for grids B and C are also identical (Figures 73-76). The profiles slightly underestimate the magnitude of the perturbation in the top half of the spikes, but the width at the base of the spikes are the same as in the 60-layer consensus. The small scale dip at the

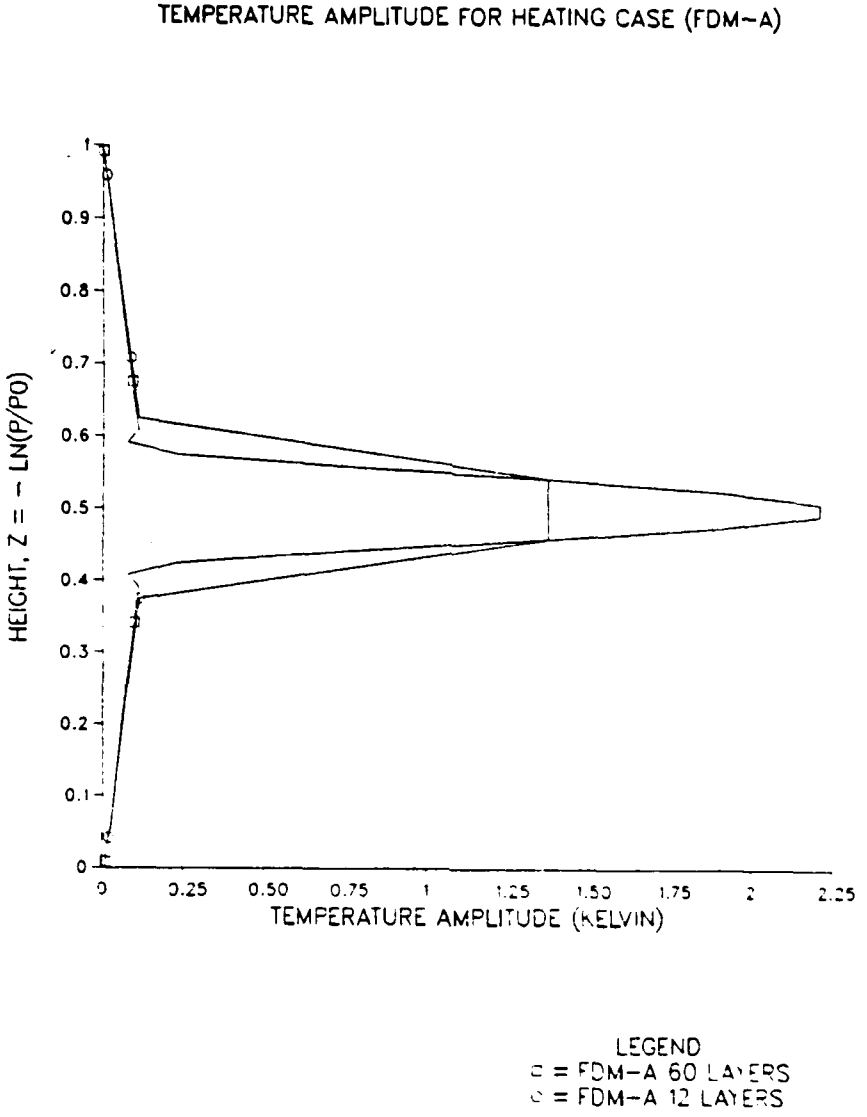

Figure 63. Twelve-layer diabatic heating experiment at 12 hours. Temperature amplitude profiles are compared for the 12-layer and 60-layer FDM-A models.

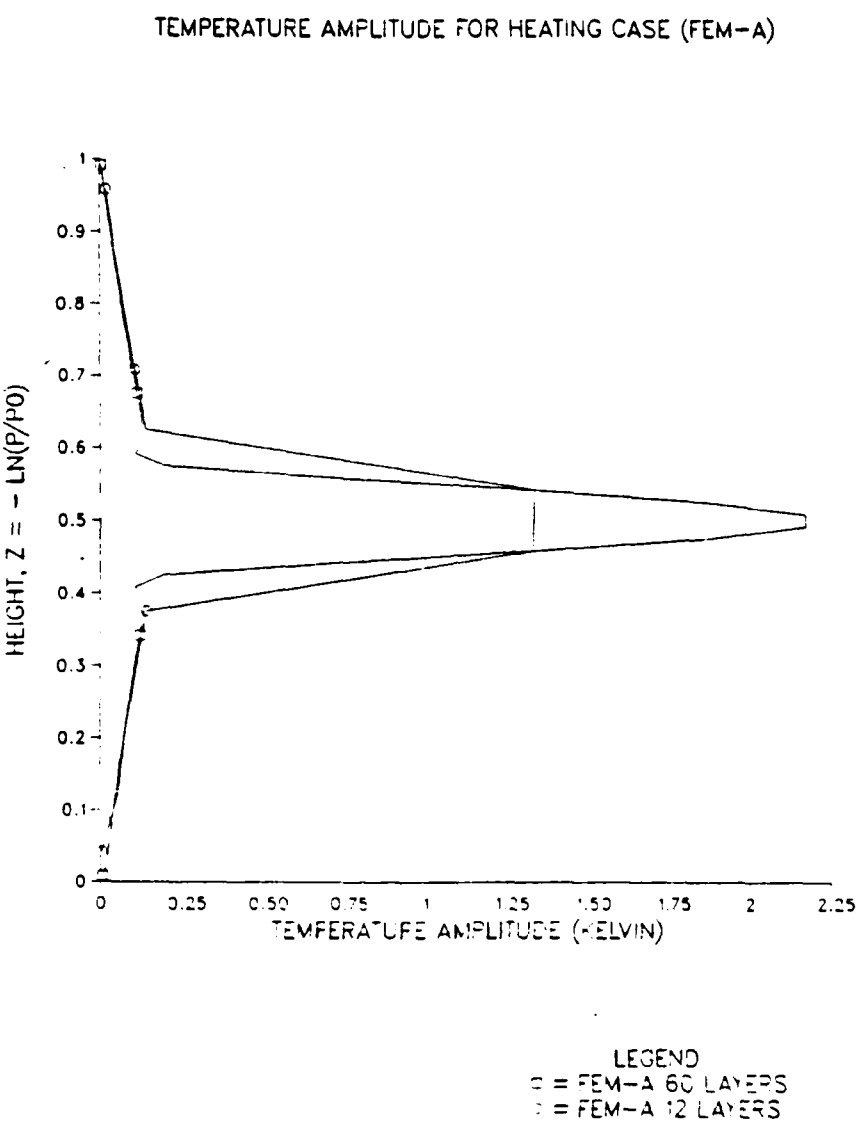

Figure 64. As in Fig. 63 but for model FEM-A.

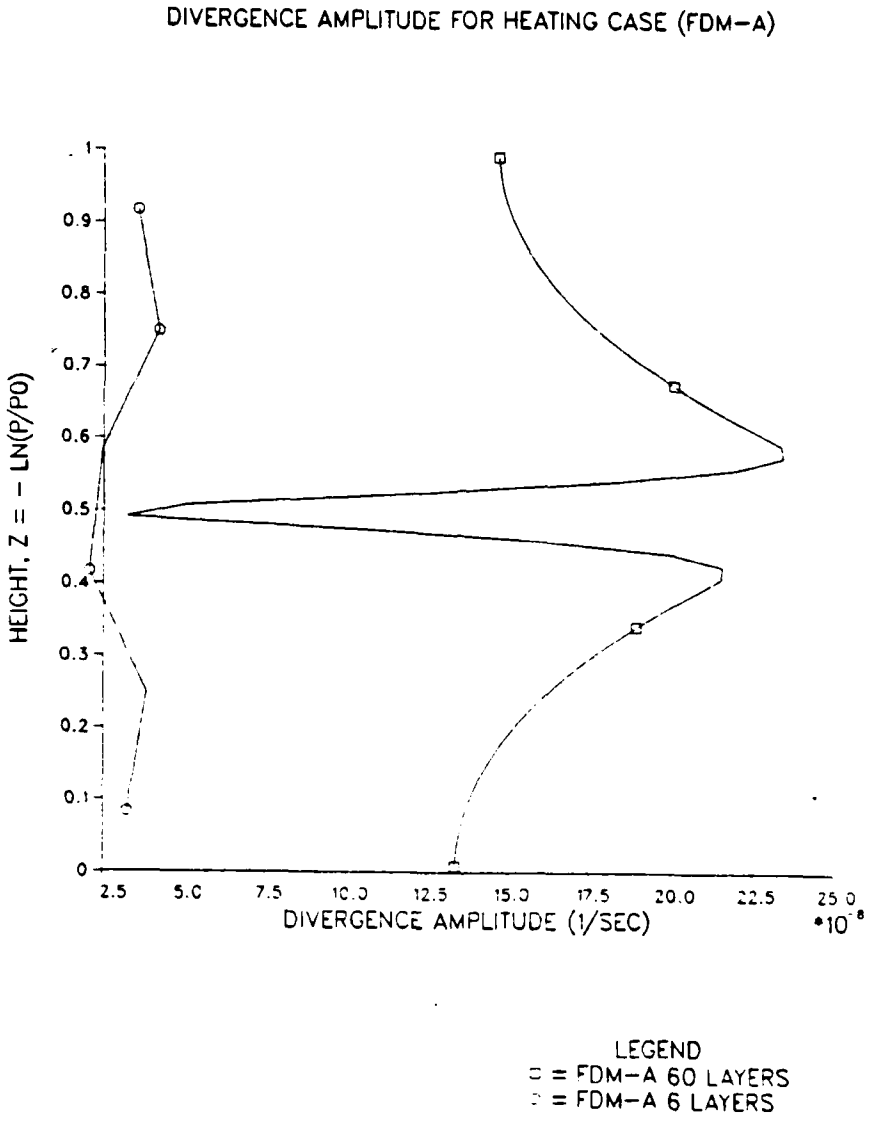

Figure 65. As in Fig. 61 but for divergence amplitude.

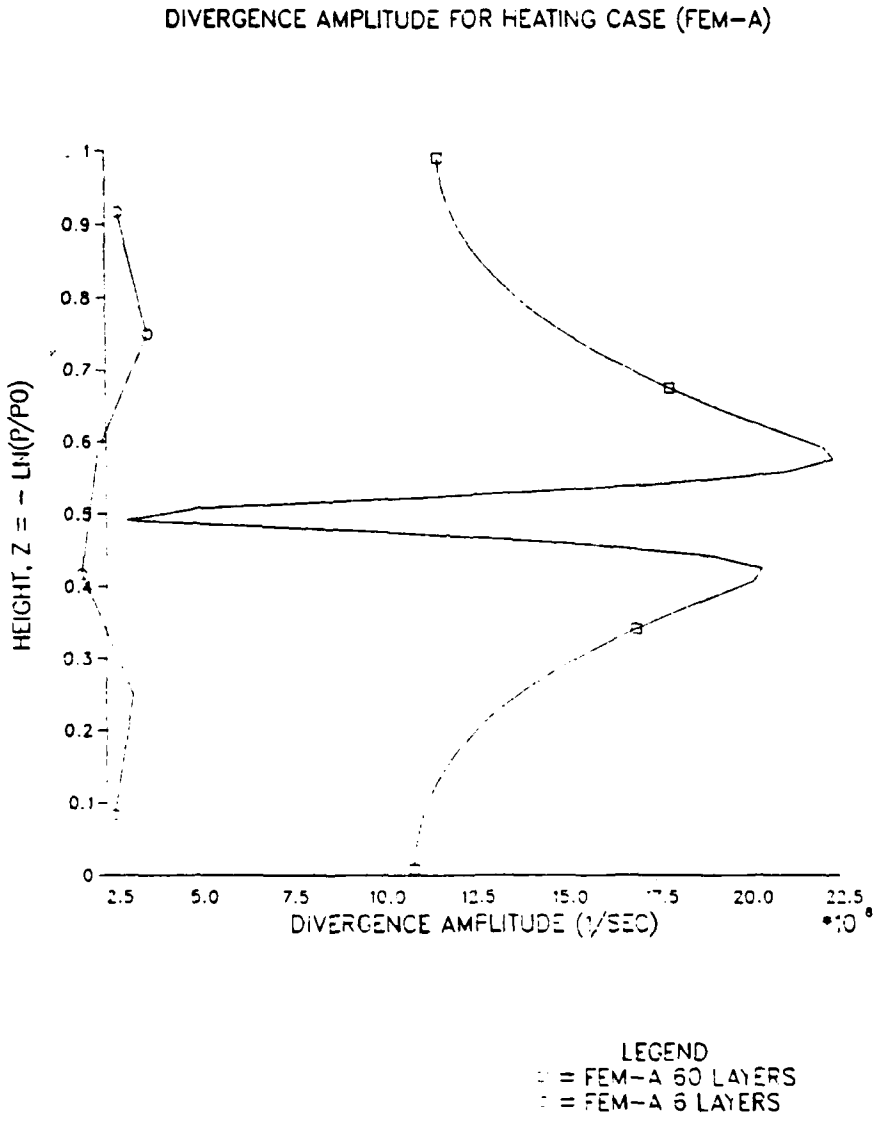

Figure 66. As in Fig. 62 but for divergence amplitude.

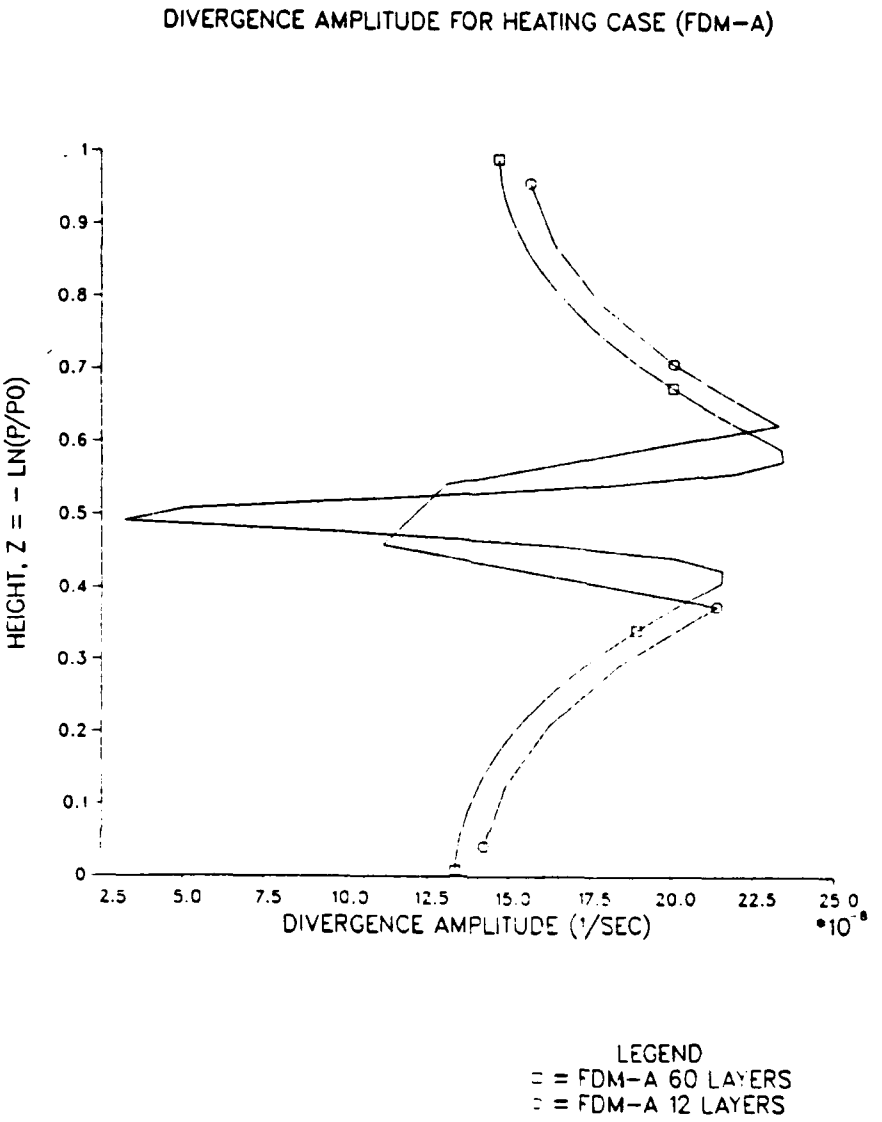

Figure 67. As in Fig. 63 but for divergence amplitude.

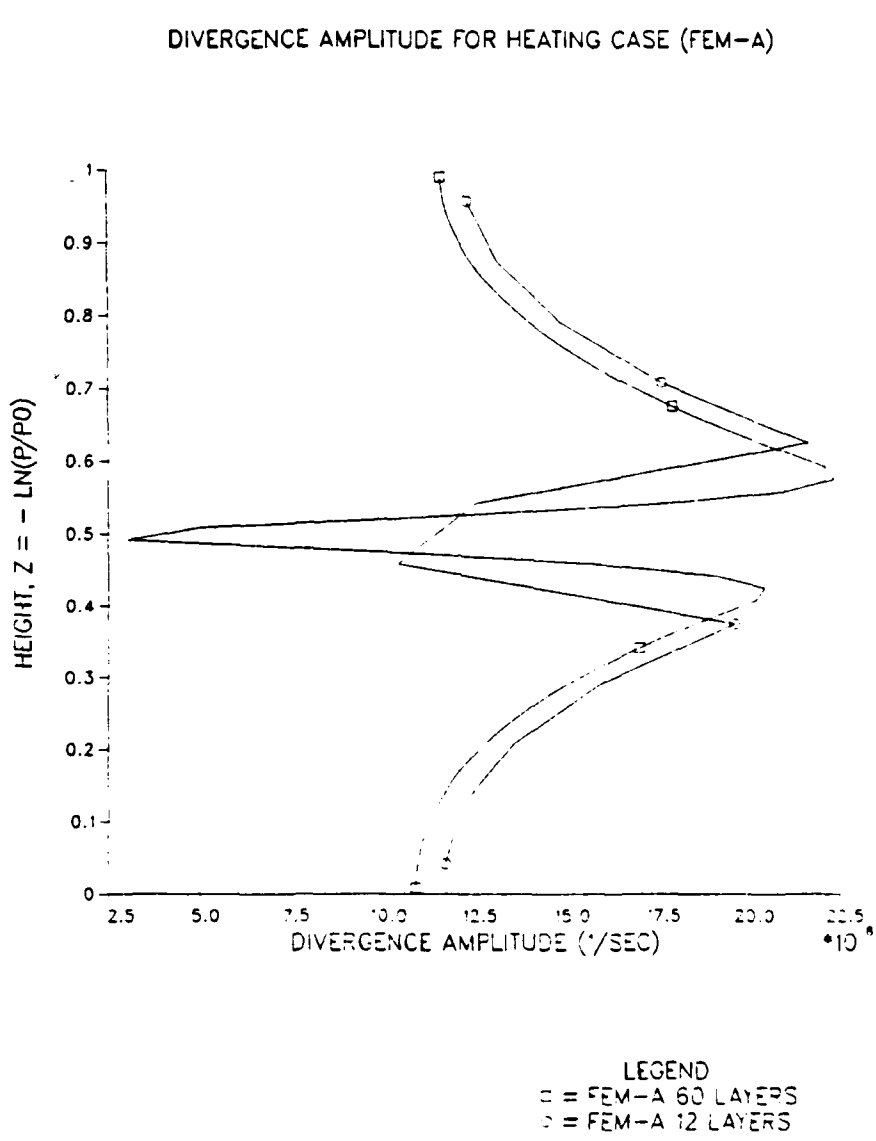

Figure 68. As in Fig. 64 but for divergence amplitude.

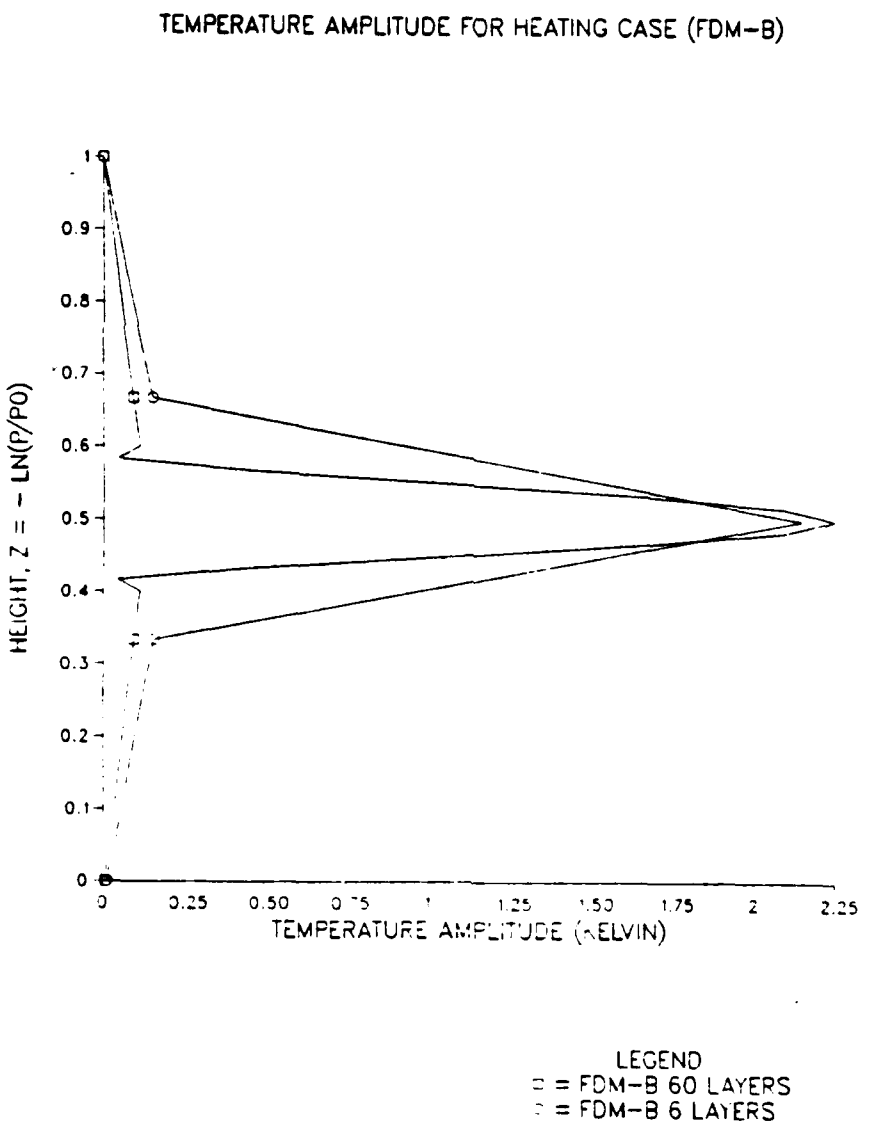

Figure 69. As in Fig. 61 but for model FDM-B.

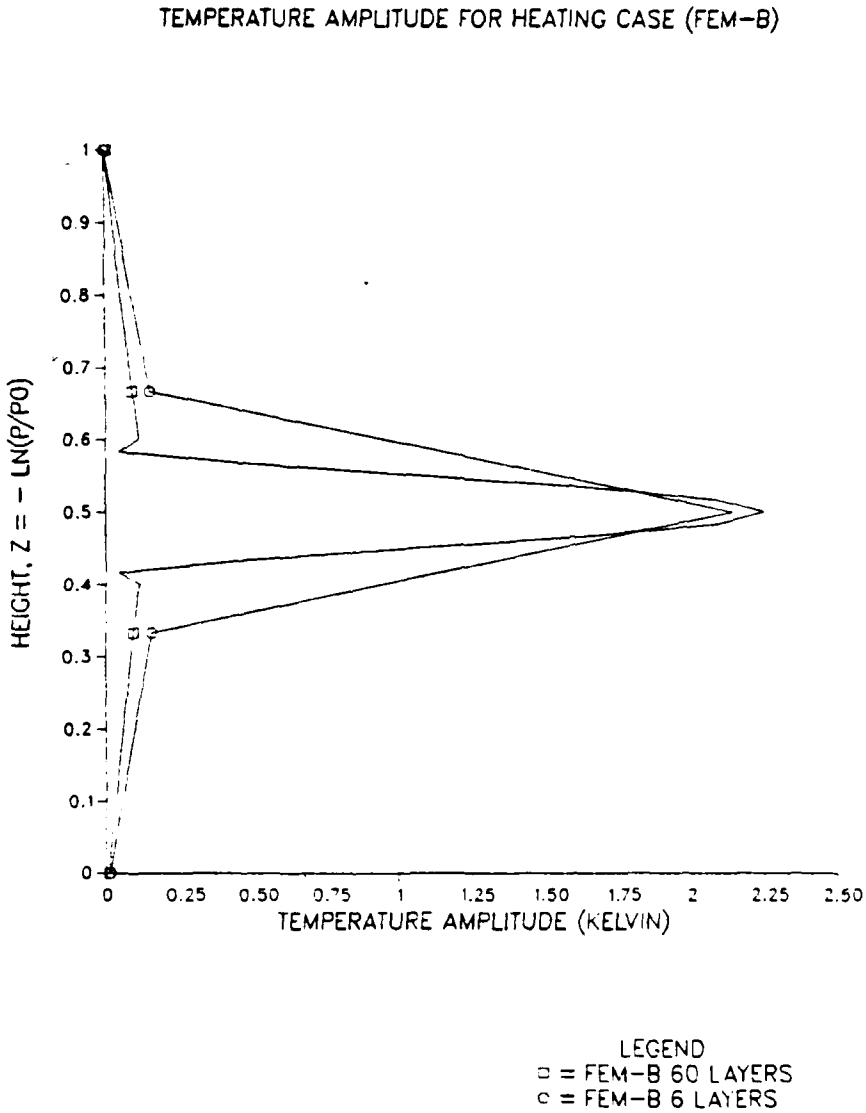

Figure 70. As in Fig. 61 but for model FEM-B.

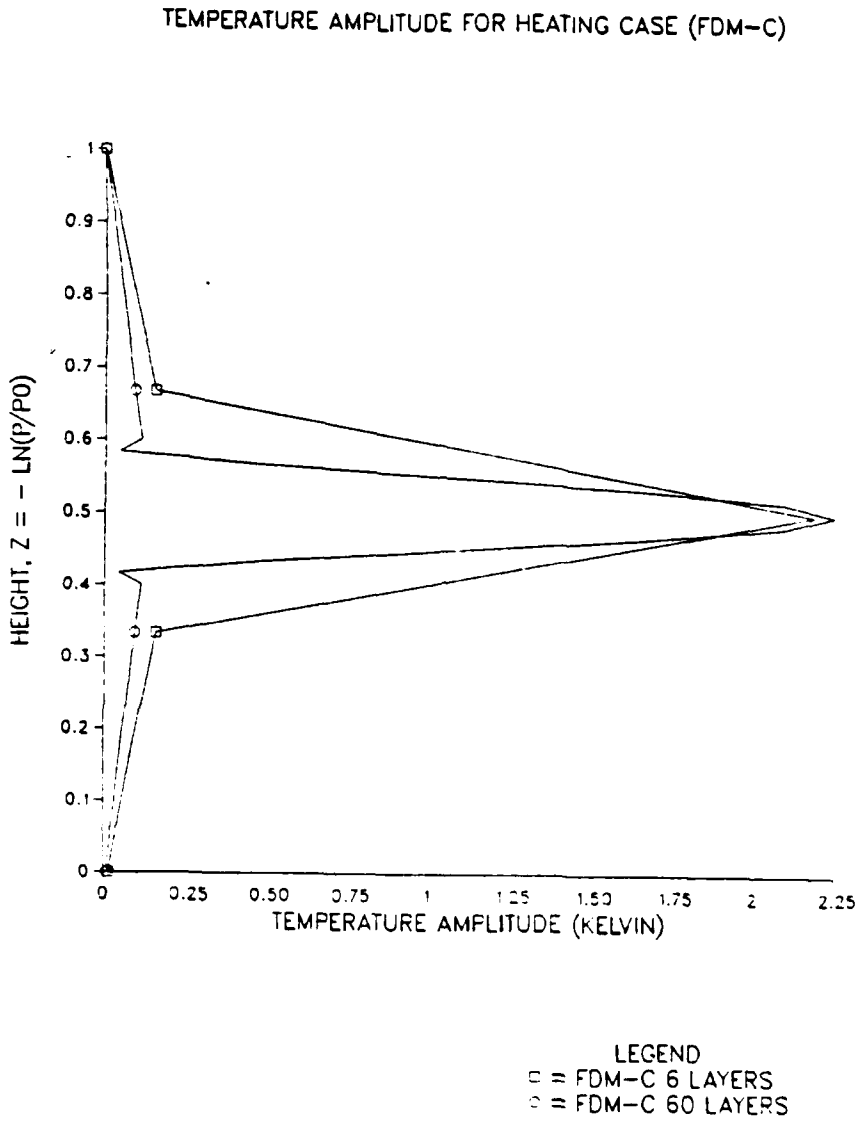

Figure 71. As in Fig. 61 but for model FDM-C.

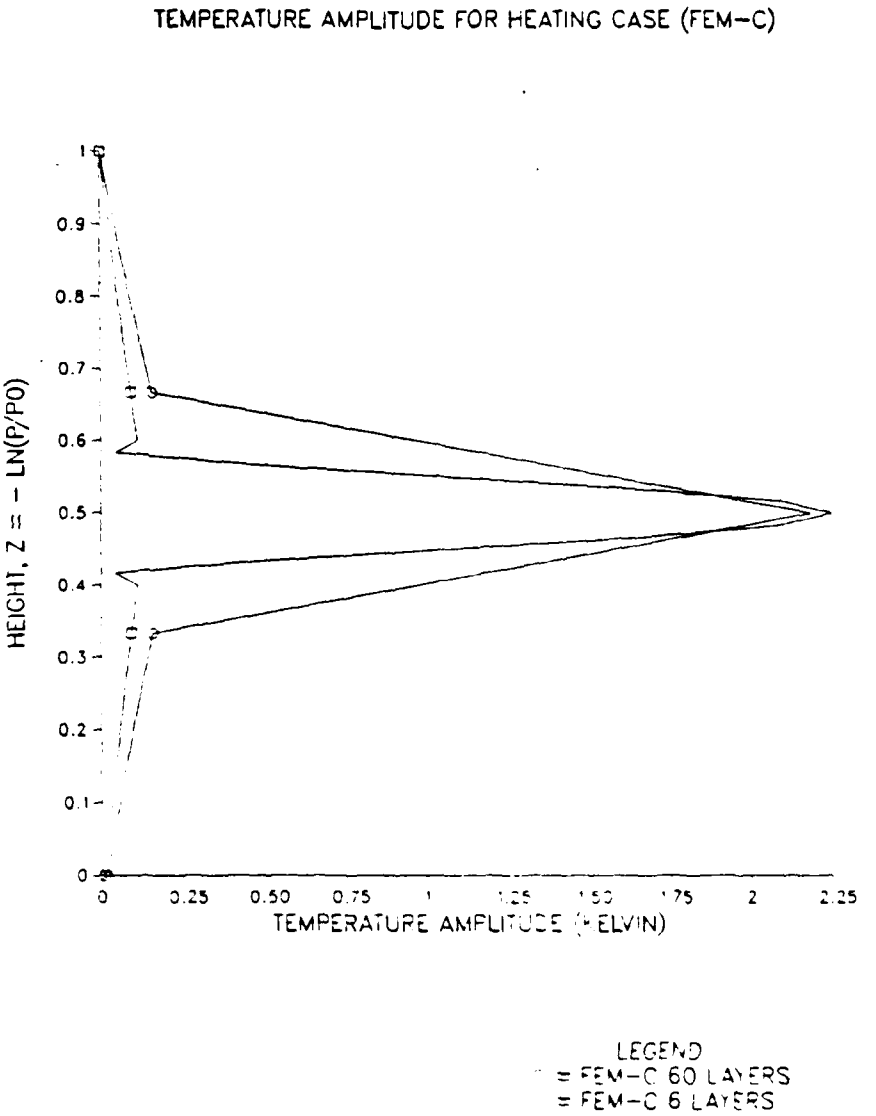

Figure 72. As in Fig. 61 but for model FEM-C.

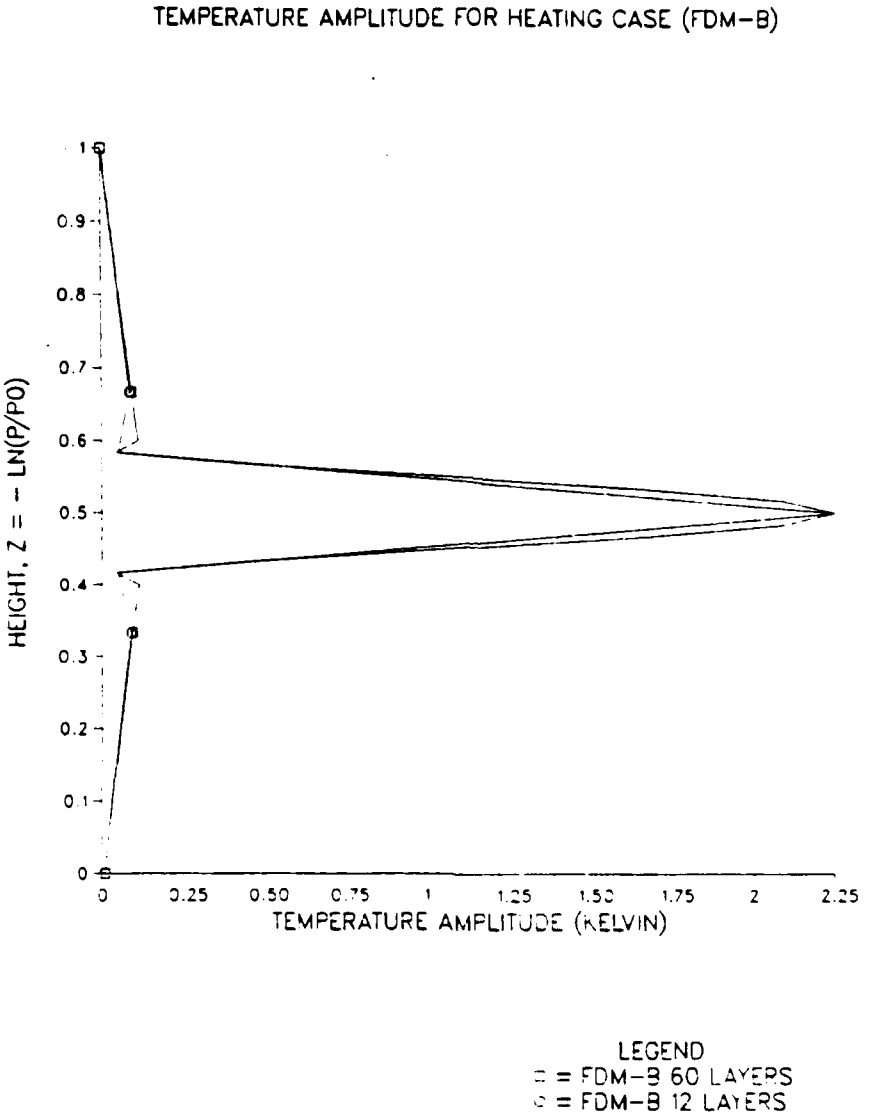

Figure 73. As in Fig. 63 but for model FDM-B.

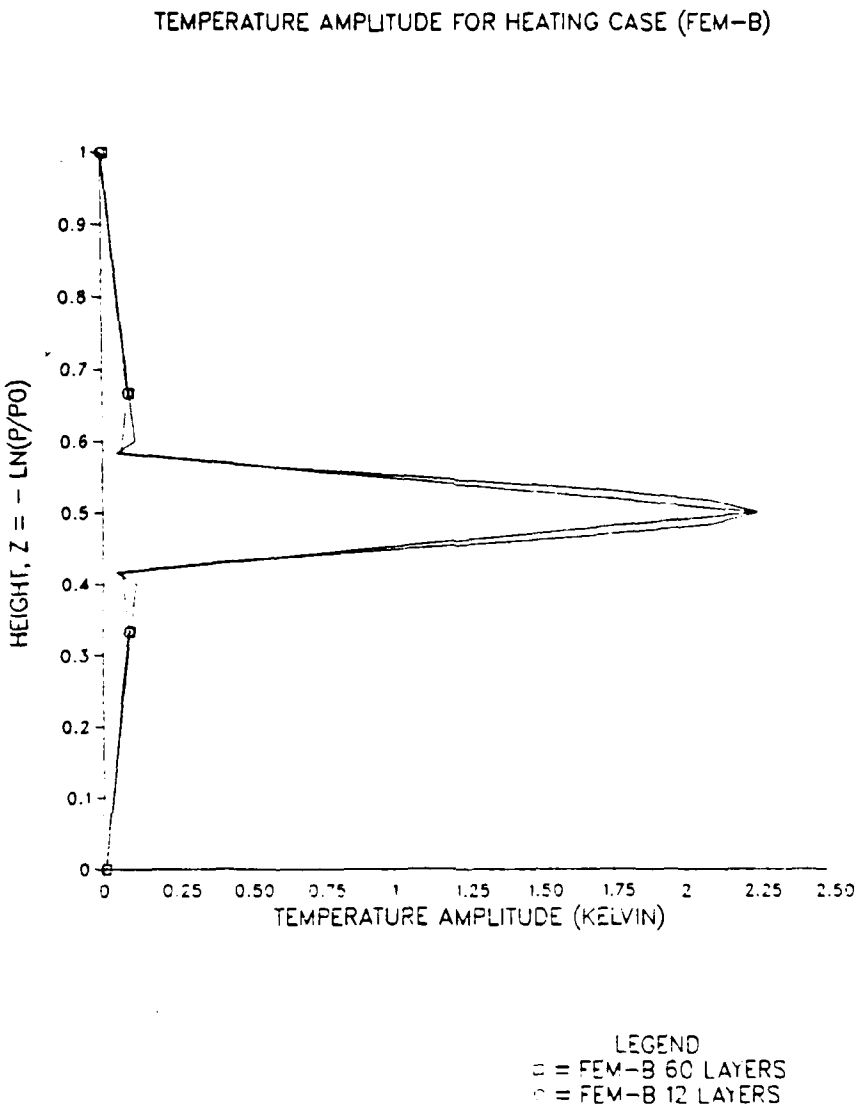

Figure 74. As in Fig. 63 but for model FEM-B.

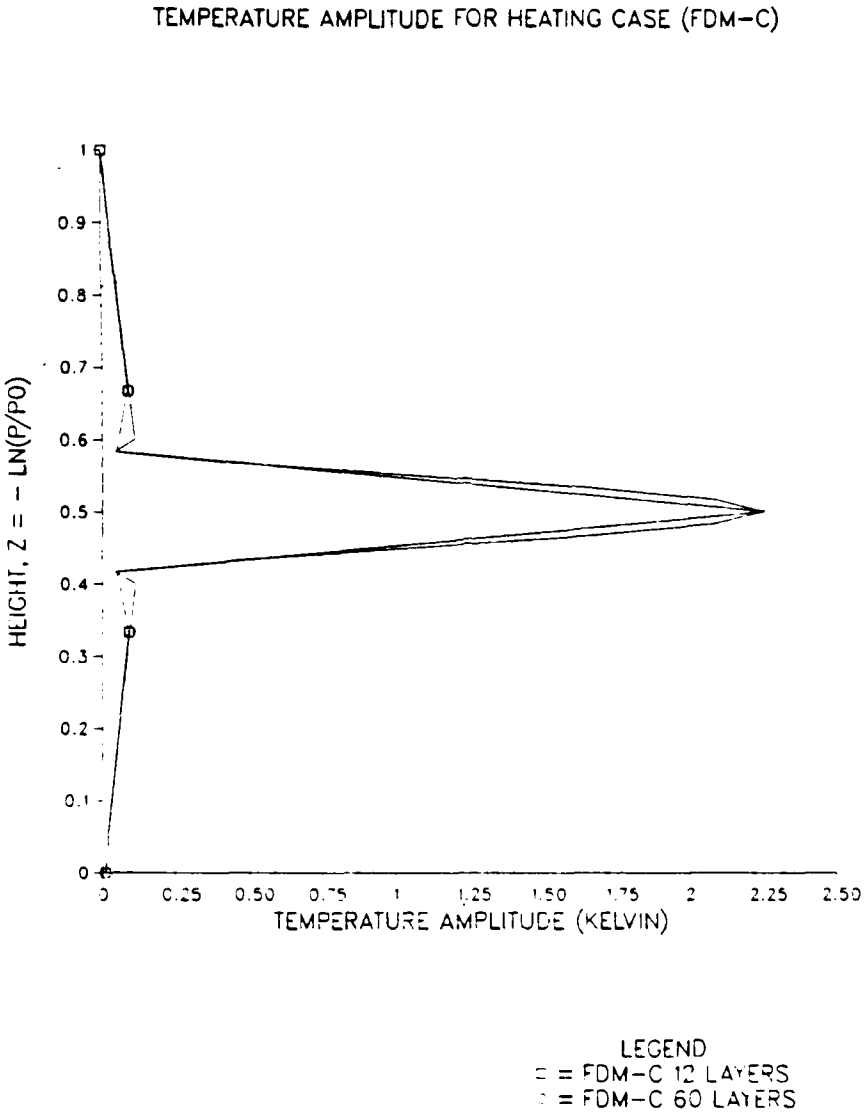

Figure 75. As in Fig. 63 but for model FDM-C.

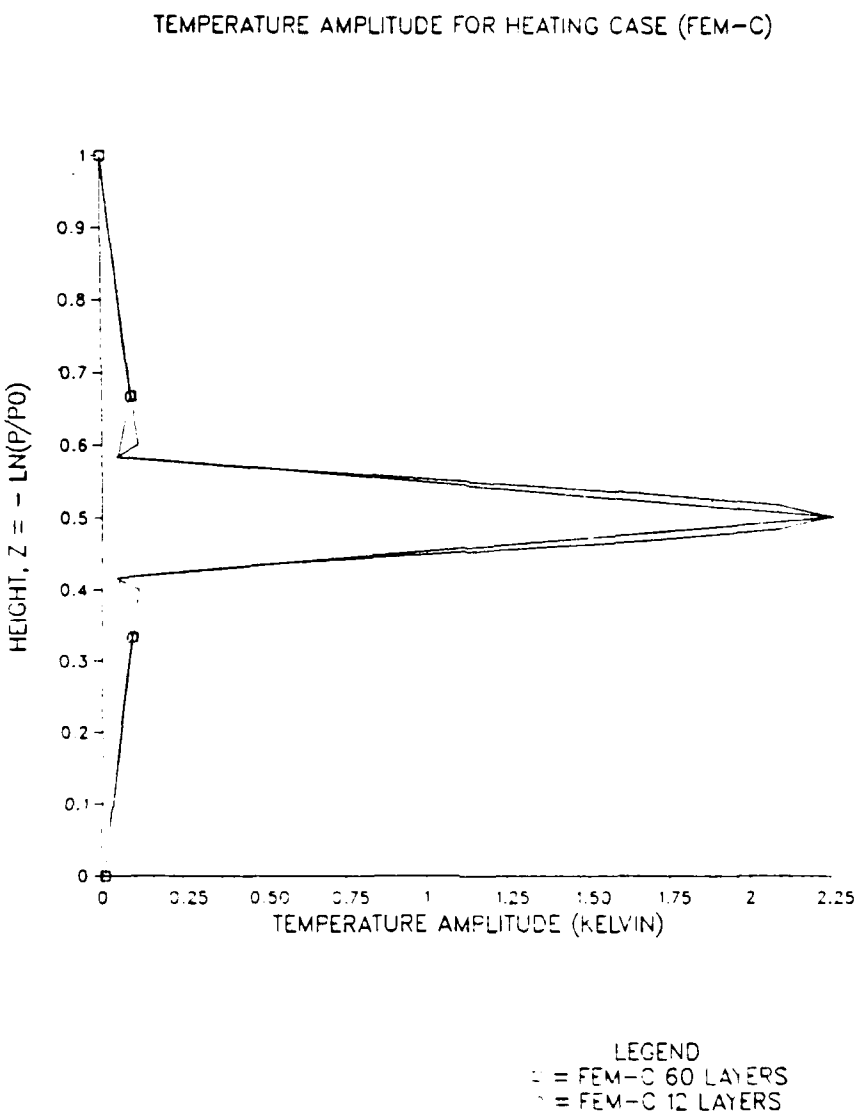

Figure 76. As in Fig. 63 but for model FEM-C.

boundaries of the heated layer in the consensus profile is not reproduced by the 12-layer models, otherwise the profiles agree with the consensus outside the heated layer.

The diabatic heating causes different divergence amplitude responses for the B and C grids. The grid C models have similar six-level profiles (Figures 77-78). The minimum divergence, which occurs at the center of the heated layer, is nearly the same in the six and sixty-layer models. There are differences between the two grid C models away from the divergence minimum. Outside the heated layer the six-layer divergence amplitude of the FEM-C model provides the closer approximation of the 60-layer consensus profile. Similarly, the 12-layer FEM-C profile (Figure 79) is a better approximation of the consensus than the 12-layer FDM-C model (Figure 80).

For both six and twelve layers, the grid B models very poorly approximate the 60-layer divergence amplitude within the heated layer. The 12-layer profiles (Figures 81-82) are identical for the grid B models and are closer approximations of the consensus 60-layer profile than the six-layer results. The 12-layer model is asymmetric within the heated layer and does not have the dramatic decrease in divergence that exists in the consensus. The twelve and sixty-layer profiles are similar outside the heated layer.

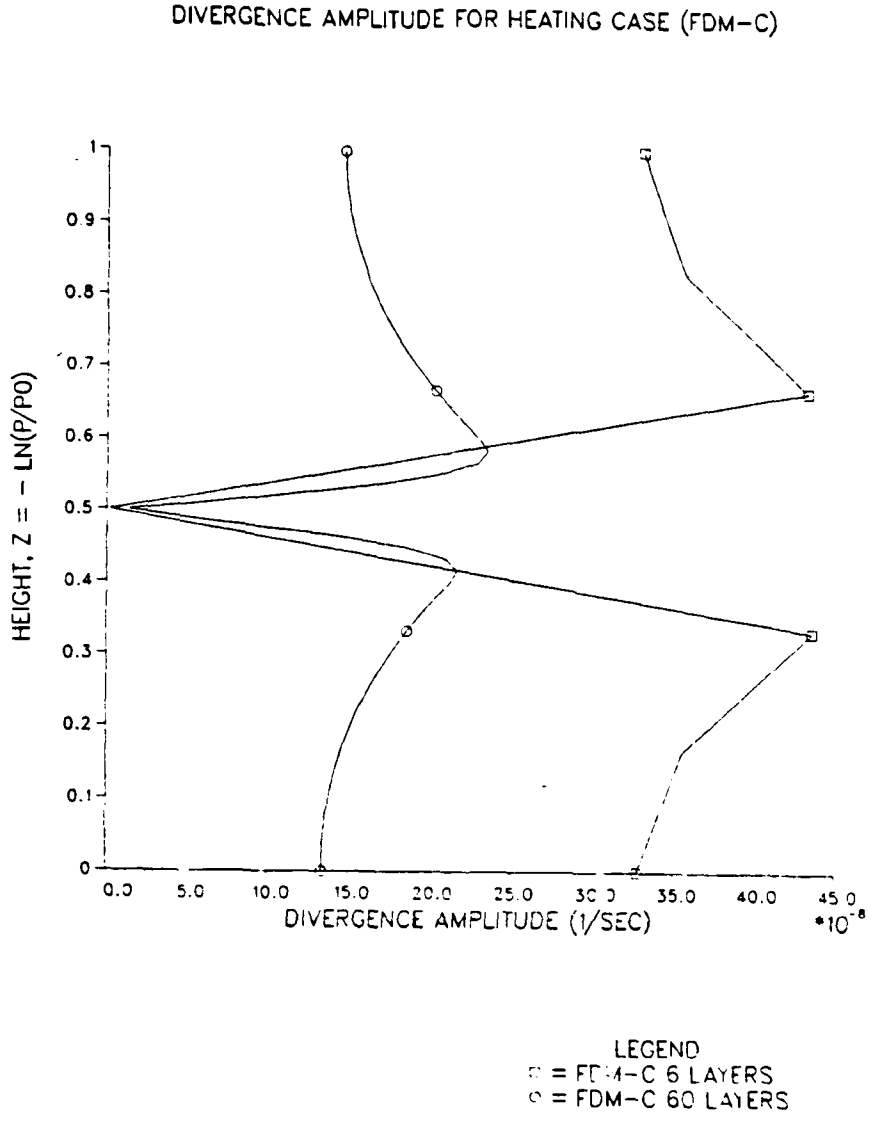

Figure 77. As in Fig. 61 but divergence amplitude for model FDM-C.

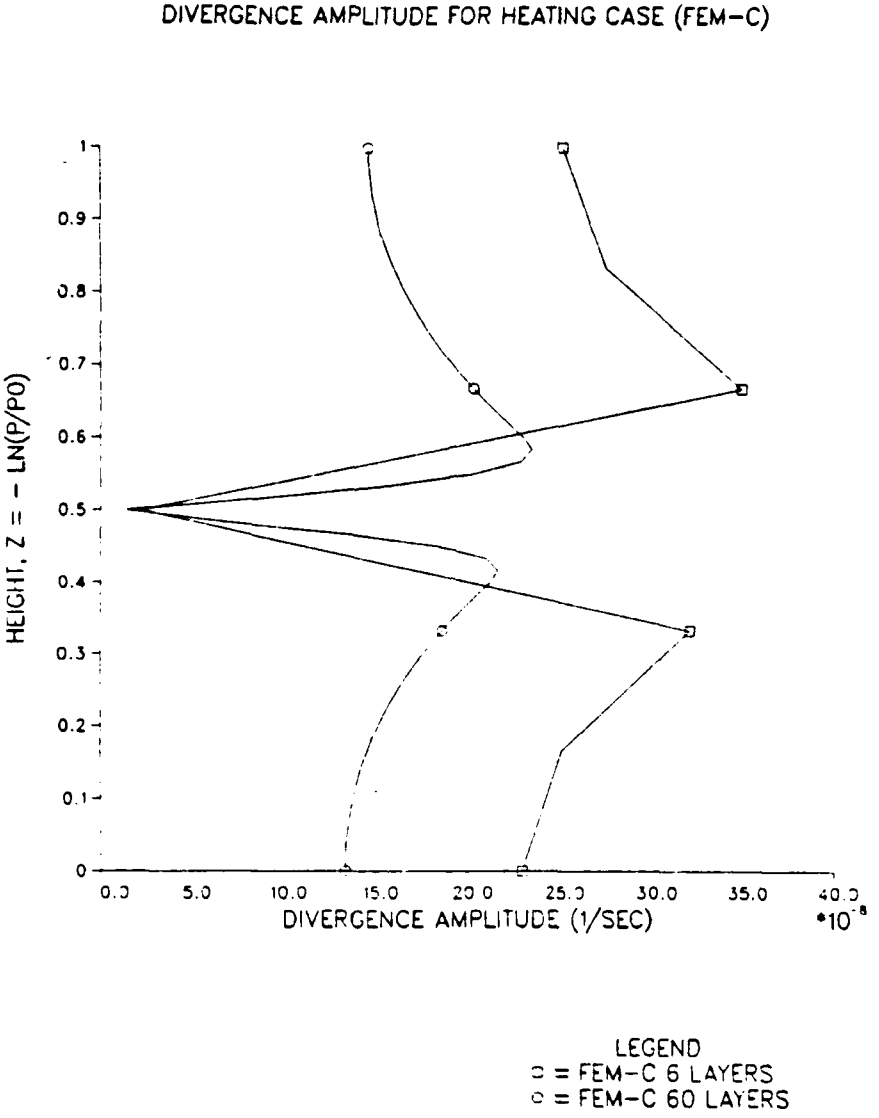

Figure 78. As in Fig. 61 but divergence amplitude for model FEM-C.

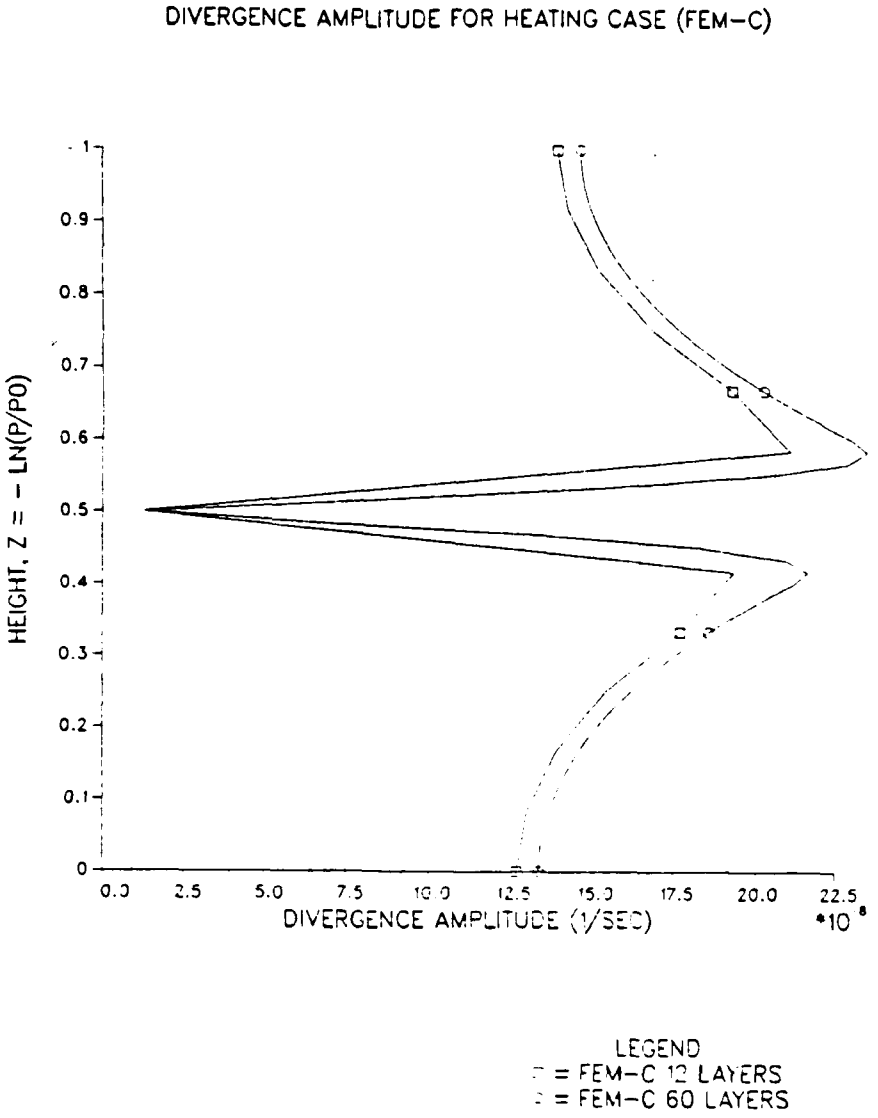

Figure 79. As in Fig. 63 but divergence amplitude for model FEM-C.

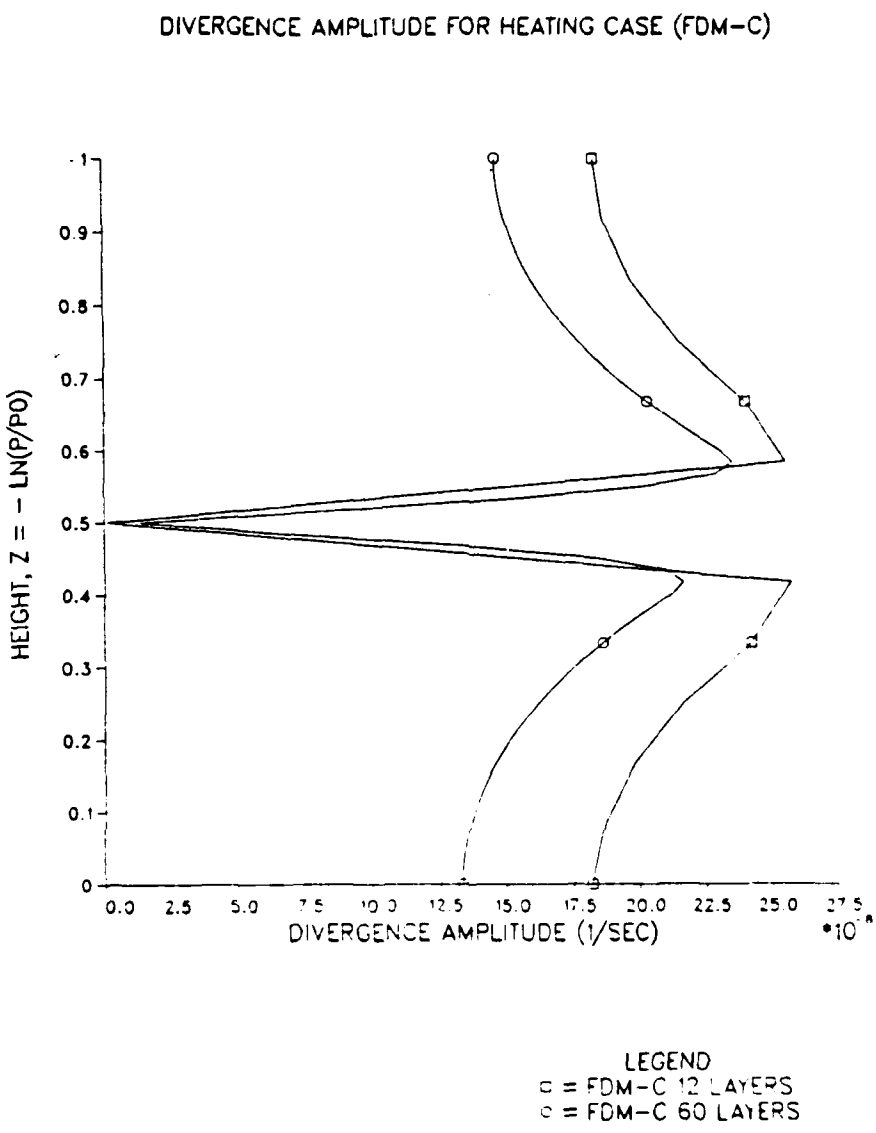

Figure 80. As in Fig. 63 but divergence amplitude for model FDM-C.

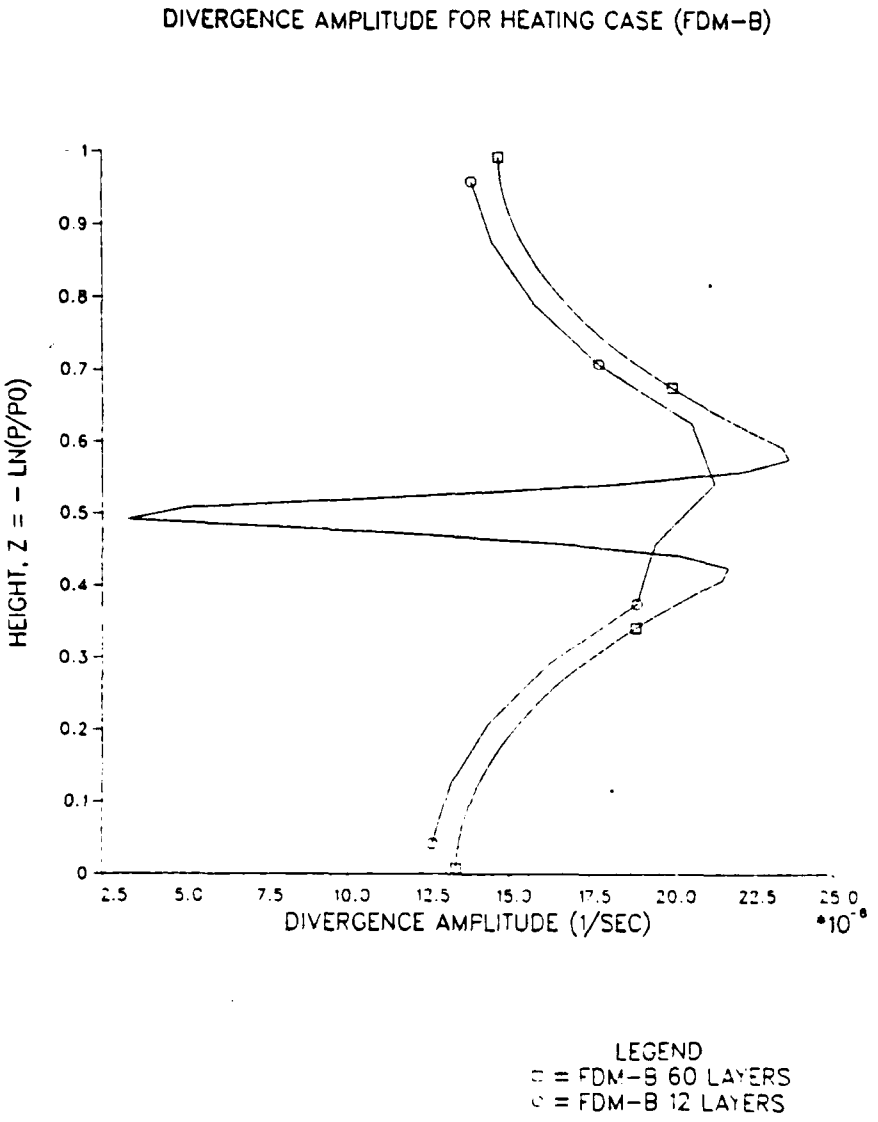

Figure 81. As in Fig. 63 but divergence amplitude for model FDM-B.

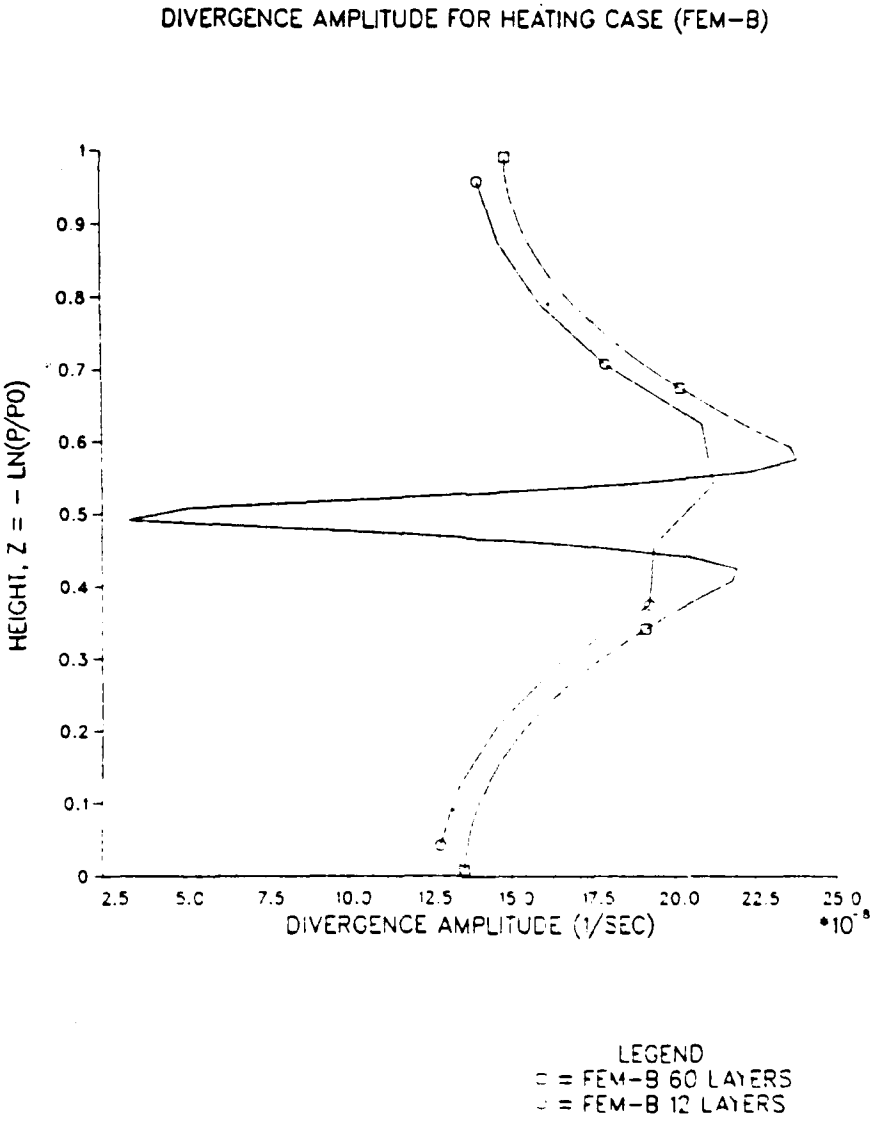

Figure 82. As in Fig. 63 but divergence amplitude for model FEM-B.

IV. CONCLUSIONS

Although the analytic solutions of each experiment have not been derived, some conclusions about the characteristics of each model can be drawn. During the Rossby wave and mountain topography experiments the staggered finite element models, FEM-A and FEM-B, display unusual temperature amplitude behavior in the lowest two layers of the model. The oscillation in the temperature profiles of both models may be generated by the matrix elements which represent the contributions from the eigenfunctions near the surface. It is possible that better representations of the staggered eigenfunctions near the lower boundary may reduce or eliminate this problem. Jagged temperature profiles were not observed in the diabatic heating experiment. The 12-hour forecast period in the heating experiment may be too short for the profile discontinuities to grow to substantial amplitudes.

The differences between the grids is most apparent in the diabatic heating experiment. The 60-layer temperature profiles of all six models represent the same physical solution. The FEM-A model has a slightly different 60-layer divergence response outside the heated layer than the other five models. The grid B and C models have identical temperature amplitude profiles for both six and twelve layers. However, the divergence amplitude profiles are quite different and the grid C

models provide the better approximation for both resolutions. The grid A models barely respond to the diabatic heating with six layers, and poorly approximate their consensus profiles with twelve layers. There are indications that both grid A models may not converge to their 60-layer temperature and divergence solutions with much less than 60-layer resolution.

In all experiments, the grid B model produces virtually identical results, aside from the small amplitude oscillation in the FEM-B temperature profiles. Based on these experiments, no accuracy is gained by using the finite element approximations with grid B. In two of the three experiments the grid C results are identical. The FEM-C model provides a closer approximation of the consensus 60-layer divergence profile than the FDM-C model in the diabatic heating experiment. Generally, the lower resolution FEM-A model does not approximate its 60-layer solution as well as the FDM-A model. It is not known if the different approximation characteristics of the FEM-A model are due solely to its profile problems at the bottom of the atmosphere.

The importance of the $\phi_1(Z)$ and $\phi_{N+2}(Z)$ eigenfunctions in the staggered finite element models is not clear. They are prominent terms in the mathematical derivations, but their physical significance is not apparent.

APPENDIX A

FINITE DIFFERENCE APPROXIMATIONS

1. For terms of the form $\frac{d\bar{u}}{dZ} W$:

   a. FDM-A and FDM-B, at level $Z = Z_i$:

$$\frac{d\bar{u}}{dZ} \cdot W = \frac{1}{2}\left[W_i \cdot \left(\frac{\bar{u}_{i+1} - \bar{u}_i}{Z_{i+1} - Z_i}\right) + W_{i-1} \cdot \left(\frac{\bar{u}_i - \bar{u}_{i-1}}{Z_i - Z_{i-1}}\right)\right]$$

   b. FDM-C, at level $Z = Z'_i$:

$$\frac{d\bar{u}}{dZ} \cdot W = \frac{1}{2} \cdot W_i \cdot \left[\left(\frac{\bar{u}_{i+1} - \bar{u}_i}{Z'_{i+1} - Z'_i}\right) + \left(\frac{\bar{u}_i - \bar{u}_{i-1}}{Z'_i - Z'_{i-1}}\right)\right]$$

2. For terms of the form $\frac{\partial \bar{T}}{\partial Z} W$:

   a. FDM-A, at level $Z = Z_i$:

$$\frac{\partial \bar{T}}{\partial Z} \cdot W = \frac{1}{2}\left[W_i \cdot \left(\frac{\bar{T}_{i+1} - \bar{T}_i}{Z_{i+1} - Z_i}\right) + W_{i-1} \cdot \left(\frac{\bar{T}_i - \bar{T}_{i-1}}{Z_i - Z_{i-1}}\right)\right]$$

   b. FDM-B and FDM-C, at level $Z = Z_i$:

$$\frac{\partial \bar{T}}{\partial Z} \cdot W = \frac{1}{2} \cdot W_i \cdot \left[\left(\frac{\bar{T}_{i+1} - \bar{T}_{i-1}}{Z'_{i+1} - Z'_i}\right) + \left(\frac{\bar{T}_i - \bar{T}_{i-1}}{Z'_i - Z'_{i-1}}\right)\right]$$

3. For terms of the form $\frac{d\bar{u}}{dZ} V$:

   a. FDM-A, at level $Z = Z_i$:

$$\frac{d\bar{u}}{dZ} \cdot V = \frac{1}{2} \cdot V \cdot \left[\left(\frac{\bar{u}_{i+1} - \bar{u}_i}{Z_{i+1} - Z_i}\right) + \left(\frac{\bar{u}_i - \bar{u}_{i-1}}{Z_i - Z_{i-1}}\right)\right]$$

b. FDM-B, at level $Z = Z'_i$:

$$\frac{d\bar{u}}{dZ} \cdot V = \frac{1}{2}(V_{i+1} + V_i) \cdot \left(\frac{\bar{u}_{i+1} - \bar{u}_i}{Z_{i+1} - Z_i}\right)$$

c. FDM-C, at level $Z = Z'_i$:

$$\frac{d\bar{u}}{dZ} \cdot V = \frac{1}{2} \cdot V \cdot \left[\left(\frac{\bar{u}_{i+1} - \bar{u}_i}{Z'_{i+1} - Z'_i}\right) + \left(\frac{\bar{u}_i - \bar{u}_{i-1}}{Z'_i - Z'_{i-1}}\right)\right]$$

APPENDIX B

GALERKIN FORM OF FEM-C PROGNOSTIC EQUATIONS

1. Vorticity Equations (2-35)-(2-36):

$$\sum_{j=i-1}^{i+1} \frac{dA_1^j}{dt} \int_{Z_0}^{Z_T} \phi_j(Z)\phi_i(Z)dZ = -f \sum_{j=i-1}^{i+1} D_1^j(t) \int_{Z_0}^{Z_T} \phi_j(Z)\phi_i(Z)dZ$$

$$- \mu \sum_{j=i-1}^{i+1} \sum_{k=i-1}^{i+1} \bar{u}_j A_2^k(t) \int_{Z_0}^{Z_T} \phi_j(Z)\phi_k(Z)\phi_i(Z)dZ$$

$$- \beta \sum_{j=i-1}^{i+1} V_1^j(t) \int_{Z_0}^{Z_T} \phi_j(Z)\phi_i(Z)dZ \qquad \text{(B-1)}$$

$$\sum_{j=i-1}^{i+1} \frac{dA_2^j}{dt} \int_{Z_0}^{Z_T} \phi_j(Z)\phi_i(Z)dZ = -f \sum_{j=i-1}^{i+1} D_2^j(t) \int_{Z_0}^{Z_T} \phi_j(Z)\phi_i(Z)dZ$$

$$+ \mu \sum_{j=i-1}^{i+1} \sum_{k=i-1}^{i+1} \bar{u}_j A_1^k(t) \int_{Z_0}^{Z_T} \phi_j(Z)\phi_k(Z)\phi_i(Z)dZ$$

$$- \beta \sum_{j=i-1}^{i+1} V_2^j(t) \int_{Z_0}^{Z_T} \phi_j(Z)\phi_i(Z)dZ \qquad \text{(B-2)}$$

a. Divergence Equations (2-37)-(2-38):

$$\sum_{j=i-1}^{i+1} \frac{dD_1^j}{dt} \int_{Z_0}^{Z_T} \phi_j(Z)\phi_i(Z)dZ = f \sum_{j=i-1}^{i+1} A_1^j(t) \int_{Z_0}^{Z_T} \phi_j(Z)\phi_i(Z)dZ$$

$$- \mu \sum_{j=i-1}^{i+1} \sum_{k=i-1}^{i+1} \bar{u}_j D_2^k(t) \int_{Z_0}^{Z_T} \phi_j(Z)\phi_k(Z)\phi_i(Z)dZ$$

$$- \beta \sum_{j=i-1}^{i+1} U_1^j(t) \int_{Z_0}^{Z_T} \phi_j(Z)\phi_i(Z)dZ$$

$$- \mu \sum_{j=i-1}^{i+1} \sum_{k=i-1}^{i+1} \bar{u}_j W_2^k(t) \int_{Z_0}^{Z_T} \frac{d\phi_j}{dZ} \phi_k(Z)\phi_i(Z)dZ$$

$$+ \mu^2 \sum_{j=i-1}^{i+1} H_1^j(t) \int_{Z_0}^{Z_T} \phi_j(Z)\phi_i(Z)dZ \qquad \text{(B-3)}$$

$$\sum_{j=i-1}^{i+1} \frac{dD_2^j}{dt} \int_{Z_0}^{Z_T} \phi_j(Z)\phi_i(Z)dZ = f \sum_{j=i-1}^{i+1} A_2^j(t) \int_{Z_0}^{Z_T} \phi_j(Z)\phi_i(Z)dZ$$

$$+ \mu \sum_{j=i-1}^{i+1} \sum_{k=i-1}^{i+1} \bar{u}_j D_1^k(t) \int_{Z_0}^{Z_T} \phi_j(Z)\phi_k(Z)\phi_i(Z)dZ$$

$$- \beta \sum_{j=i-1}^{i+1} U_2^j(t) \int_{Z_0}^{Z_T} \phi_j(Z)\phi_i(Z)dZ$$

$$+ \mu \sum_{j=i-1}^{i+1} \sum_{k=i-1}^{i+1} \bar{u}_j W_1^k(t) \int_{Z_0}^{Z_T} \frac{d\phi_j}{dZ} \phi_k(Z)\phi_i(Z)dZ$$

$$+ \mu^2 \sum_{j=i-1}^{i+1} H_2^j(t) \int_{Z_0}^{Z_T} \phi_j(Z)\phi_i(Z)dZ \qquad \text{(B-4)}$$

3. Thermodynamic Equations (2-39)-(2-40):

$$\sum_{j=i-1}^{i+1} \frac{dT_1^j}{dt} \int_{Z_0}^{Z_T} \phi_j(Z)\phi_i(Z)dZ$$

$$= -\mu \sum_{j=i-1}^{i+1} \sum_{k=i-1}^{i+1} \bar{u}_j T_2^k(t) \int_{Z_0}^{Z_T} \phi_j(Z)\phi_k(Z)\phi_i(Z)dZ$$

$$+ \left(\frac{f}{R}\right) \sum_{j=i-1}^{i+1} \sum_{k=i-1}^{i+1} \bar{u}_j V_1^k(t) \int_{Z_0}^{Z_T} \frac{d\phi_j}{dZ} \phi_k(Z)\phi_i(Z)dZ$$

$$- \sum_{j=i-1}^{i+1} \sum_{k=i-1}^{i+1} \bar{T}_j W_1^k(t) \int_{Z_0}^{Z_T} \frac{d\phi_j}{dZ} \phi_k(Z)\phi_i(Z)dZ$$

$$+ \sum_{j=i-1}^{i+1} Q_1^j(t) \int_{Z_0}^{Z_T} \phi_j(Z)\phi_i(Z)dZ \qquad \text{(B-5)}$$

$$\sum_{j=i-1}^{i+1} \frac{dT_2^j}{dt} \int_{Z_0}^{Z_T} \phi_j(Z)\phi_i(Z)dZ$$

$$= \mu \sum_{j=i-1}^{i+1} \sum_{k=i-1}^{i+1} \bar{u}_j T_1^k(t) \int_{Z_0}^{Z_T} \phi_j(Z)\phi_k(Z)\phi_i(Z)dZ$$

$$+ \left(\frac{f}{R}\right) \sum_{j=i-1}^{i+1} \sum_{k=i-1}^{i+1} \bar{u}_j V_2^k(t) \int_{Z_0}^{Z_T} \frac{d\phi_j}{dZ} \phi_k(Z)\phi_i(Z)dZ$$

$$- \sum_{j=i-1}^{i+1} \sum_{k=i-1}^{i+1} \bar{T}_j W_2^k(t) \int_{Z_0}^{Z_T} \frac{d\phi_j}{dZ} \phi_k(Z)\phi_i(Z)dZ$$

$$+ \sum_{j=i-1}^{i+1} Q_2^j(t) \int_{Z_0}^{Z_T} \phi_j(Z)\phi_i(Z)dZ \qquad \text{(B-6)}$$

APPENDIX C

MATRIX ELEMENTS FOR FEM-C

1. Notation: $\Delta_i = Z_i - Z_{i-1}$, but $\Delta_2 = Z_2 - Z_i'$

$\Delta_i' = Z_i' - Z_{i-1}'$

$\bar{u}_i, \bar{T}_i = \bar{u}_1 \bar{T}$ at i^{th} vertical level

2. Matrix definition: M (row, column)

The i^{th} row of a matrix contains the weighting factors of the terms that affect the value of the forecast variable at the i^{th} vertical level. The weighting factor in the j^{th} column of the i^{th} row is the influence on the forecast variable at the i^{th} level from the variable at the j^{th} vertical level. Level i = 1 is the surface, level i = N+1 is the top of the atmosphere.

3. To calculate the terms of each matrix, substitute in the matrix formula for $\phi_{i+1}(Z)$, $\phi_i(Z)$, $\phi_{i-1}(Z)$ using functions defined in local coordinates with respect to $\phi_i(Z)$. Define $\xi = Z - Z_i'$.

The eigenfunctions in local coordinates are

$$\phi_1(\xi) = \begin{cases} \dfrac{\xi + \Delta_i'}{\Delta_i'} & -\Delta_i' \leq \xi \leq 0 \\ \dfrac{-\xi + \Delta_{i+1}'}{\Delta_{i+1}'} & 0 \leq \xi \leq \Delta_{i+1}' \end{cases}, \qquad \text{(C-1)}$$

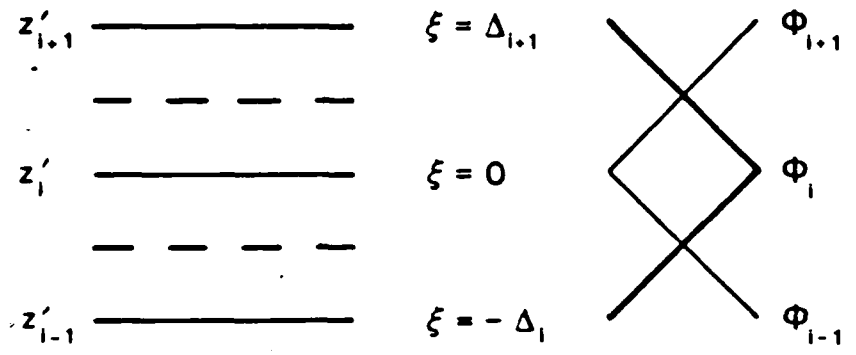

$$\Phi_{i+1}(\xi) = \frac{\xi}{\Delta'_{i+1}} \qquad 0 \le \xi \le \Delta'_{i+1} , \tag{C-2}$$

$$\Phi_{i-1}(\xi) = \frac{-\xi}{\Delta'_i} \qquad -\Delta'_i \le \xi \le 0 . \tag{C-3}$$

To calculate the matrix elements corresponding to the surface and the top of the atmosphere, use the above formulas for $i = 1$ and $i = N+1$, respectively.

4. Mass matrix, $\underline{\underline{M}}$:

   a. General formulas, $i = 2,\ldots,N$:

$$M(i,i-1) = \frac{1}{6}\Delta_i \tag{C-4}$$

$$M(i,i) = \frac{1}{3}(\Delta_{i+1} + \Delta_i) \tag{C-5}$$

$$M(i,i+1) = \frac{1}{6}\Delta_{i+1} \tag{C-6}$$

   b. At level $i = 1$:

$$M(1,1) = \frac{1}{3}\Delta_2 \tag{C-7}$$

$$M(1,2) = \frac{1}{6}\Delta_2 \qquad \text{(C-8)}$$

c. At level i = N+1:

$$M(N+1,N) = \frac{1}{6}\Delta_{N+1} \qquad \text{(C-9)}$$

$$M(N+1,N+1) = \frac{1}{3}\Delta_{N+1} \qquad \text{(C-10)}$$

5. Matrix $\underline{\underline{N}}$:

a. General formulas, i = 2,...,N

$$N(i,i-1) = \frac{1}{12}\Delta_i \cdot (\bar{u}_i + \bar{u}_{i-1}) \qquad \text{(C-11)}$$

$$N(i,i) = \frac{1}{4}\bar{u}_i \cdot (\Delta_{i+1} + \Delta_i) + \frac{1}{12} \cdot (\bar{u}_{i+1} \cdot \Delta_{i+1} + \bar{u}_{i-1} \cdot \Delta_i) \qquad \text{(C-12)}$$

$$N(i,i+1) = \frac{1}{12}\Delta_{i+1} \cdot (\bar{u}_{i+1} + \bar{u}_i) \qquad \text{(C-13)}$$

b. At level i = 1:

$$N(1,1) = \frac{1}{4}\,\bar{u}_1 \cdot \Delta_2 + \frac{1}{12}\,\bar{u}_2 \cdot \Delta_2 \qquad \text{(C-14)}$$

$$N(1,2) = \frac{1}{12} \cdot \Delta_2 \cdot (\bar{u}_2 + \bar{u}_1) \qquad \text{(C-15)}$$

c. At level i = N+1:

$$N(i,i-1) = \frac{1}{12} \cdot \Delta_i (\bar{u}_i + \bar{u}_{i-1}) \qquad \text{(C-16)}$$

$$N(i,i) = \frac{1}{4} \cdot \Delta_i \cdot \bar{u}_i + \frac{1}{12} \cdot \Delta_i \cdot \bar{u}_{i-1} \qquad \text{(C-17)}$$

6. Matrix $\underline{\underline{P}}$:

a. General Formulas, i = 2,...,N

$$P(i,i-1) = \frac{1}{6}(\bar{u}_i - \bar{u}_{i-1}) \quad \text{(C-18)}$$

$$P(i,i) = \frac{1}{3}(\bar{u}_{i+1} - \bar{u}_{i-1}) \quad \text{(C-19)}$$

$$P(i,i+1) = \frac{1}{6}(\bar{u}_{i+1} - \bar{u}_i) \quad \text{(C-20)}$$

b. At level i = 1:

$$P(1,1) = \frac{1}{3}(\bar{u}_2 - \bar{u}_1) \quad \text{(C-21)}$$

$$P(1,2) = \frac{1}{6}(\bar{u}_2 - \bar{u}_1) \quad \text{(C-22)}$$

c. At level i = N+1:

$$P(N+1,N) = \frac{1}{6}(\bar{u}_{N+1} - \bar{u}_N) \quad \text{(C-23)}$$

$$P(N+1,N+1) = \frac{1}{3}(\bar{u}_{N+1} - \bar{u}_N) \quad \text{(C-24)}$$

7. Matrix $\underline{\underline{R}}$:

a. General formulas, i = 2,...,N

$$R(i,i-1) = \frac{1}{6}(\bar{T}_i - \bar{T}_{i-1}) \quad \text{(C-25)}$$

$$R(i,i) = \frac{1}{3}(\bar{T}_{i+1} - \bar{T}_{i-1}) \quad \text{(C-26)}$$

$$R(i,i+1) = \frac{1}{6}(\bar{T}_{i+1} - \bar{T}_i) \quad \text{(C-27)}$$

b. At level i = 1:

$$R(1,1) = \frac{1}{3}(\bar{T}_2 - \bar{T}_1) \tag{C-28}$$

$$R(1,2) = \frac{1}{6}(\bar{T}_2 - \bar{T}_1) \tag{C-29}$$

c. At level i = N+1:

$$R(N+1,N) = \frac{1}{6}(\bar{T}_{N+1} - \bar{T}_N) \tag{C-30}$$

$$R(N+1,N+1) = \frac{1}{3}(\bar{T}_{N+1} - \bar{T}_N) \tag{C-31}$$

APPENDIX D

GALERKIN FORM OF FEM-A PROGNOSTIC EQUATIONS

1. The vorticity equations, (2-35)-(2-36), have the same form as the vorticity equations in FEM-C. While the FEM-A equations look the same as equations (B-1)-(B-2) in Appendix B, the equations for ϕ_i, ϕ_j and ϕ_k are different because the $\phi(Z)$ eigenfunctions are defined for the staggered levels in model FEM-A.

2. Divergence Equations (2-37)-(2-38):

$$\sum_{j=i-1}^{i+1} \frac{dD_1^j}{dt} \int_{Z_0}^{Z_T} \phi_j(Z)\phi_i(Z)dZ = f \sum_{j=i-1}^{i+1} A_1^j(t) \int_{Z_0}^{Z_T} \phi_j(Z)\phi_i(Z)dZ$$

$$- \mu \sum_{j=i-1}^{i+1} \sum_{k=i-1}^{i+1} \bar{u}_j D_2^k(t) \int_{Z_0}^{Z_T} \phi_j(Z)\phi_k(Z)\phi_i(Z)dZ$$

$$- \beta \sum_{j=i-1}^{i+1} U_1^j(t) \int_{Z_0}^{Z_T} \phi_j(Z)\phi_i(Z)dZ$$

$$- \mu \sum_{j=i-1}^{i+1} \sum_{k=i-1}^{i+1} \bar{u}_j W_2^k(t) \int_{Z_0}^{Z_T} \frac{d\phi_j}{dZ} \psi_k(Z)\phi_i(Z)dZ$$

$$+ \mu^2 \sum_{j=i-1}^{i+1} H_1^j(t) \int_{Z_0}^{Z_T} \phi_j(Z)\phi_i(Z)dZ \qquad \text{(D-1)}$$

$$\sum_{j=i-1}^{i+1} \frac{dD_2^j}{dt} \int_{Z_0}^{Z_T} \phi_j(Z)\phi_i(Z)dZ = f \sum_{j=i-1}^{i+1} A_2^j(t) \int_{Z_0}^{Z_T} \phi_j(Z)\phi_i(Z)dZ$$

$$+ \mu \sum_{j=i-1}^{i+1} \sum_{k=i-1}^{i+1} \bar{u}_j D_1^k(t) \int_{Z_0}^{Z_T} \phi_j(Z)\phi_k(Z)\phi_i(Z)dZ$$

$$- \beta \sum_{j=i-1}^{i+1} U_2^j(t) \int_{Z_0}^{Z_T} \phi_j(Z)\phi_i(Z)dZ$$

$$+ \mu \sum_{j=i-1}^{i+1} \sum_{k=i-1}^{i+1} \bar{u}_j W_1^k(t) \int_{Z_0}^{Z_T} \frac{d\phi_j}{dZ} \psi_k(Z)\phi_i(Z)dZ$$

$$+ \mu^2 \sum_{j=i-1}^{i+1} H_2^j(t) \int_{Z_0}^{Z_T} \phi_j(Z)\phi_i(Z)dZ \qquad \text{(D-2)}$$

3. Thermodynamic Equations (2-39)-(2-40):

$$\sum_{j=i-1}^{i+1} \frac{dT_1^j}{dt} \int_{Z_0}^{Z_T} \phi_j(Z)\phi_i(Z)dZ$$

$$= - \mu \sum_{j=i-1}^{i+1} \sum_{k=i-1}^{i+1} \bar{u}_j T_2^k(t) \int_{Z_0}^{Z_T} \phi_j(Z)\phi_k(Z)\phi_i(Z)dZ$$

$$+ \left(\frac{f}{R}\right) \sum_{j=i-1}^{i+1} \sum_{k=i-1}^{i+1} \bar{u}_j V_1^k(t) \int_{Z_0}^{Z_T} \frac{d\phi_j}{dZ} \phi_k(Z)\phi_i(Z)dZ$$

$$- \sum_{j=i-1}^{i+1} \sum_{k=i-1}^{i+1} \bar{T}_j W_1^k(t) \int_{Z_0}^{Z_T} \frac{d\phi_j}{dZ} \psi_k(Z)\phi_i(Z)dZ$$

$$+ \sum_{j=i-1}^{i+1} Q_1^j(t) \int_{Z_0}^{Z_T} \phi_j(Z)\phi_i(Z)dZ \qquad \text{(D-3)}$$

$$\sum_{j=i-1}^{i+1} \frac{dT_2^j}{dt} \int_{z_0}^{z_T} \phi_j(Z)\phi_i(Z)dZ$$

$$= \mu \sum_{j=i-1}^{i+1} \sum_{k=i-1}^{i+1} \bar{u}_j T_1^k(t) \int_{z_0}^{z_T} \phi_j(Z)\phi_k(Z)\phi_i(Z)dZ$$

$$+ \left(\frac{f}{R}\right) \sum_{j=i-1}^{i+1} \sum_{k=i-1}^{i+1} \bar{u}_j V_2^k(t) \int_{z_0}^{z_T} \frac{d\phi_j}{dZ} \phi_k(Z)\phi_i(Z)dZ$$

$$- \sum_{j=i-1}^{i+1} \sum_{k=i-1}^{i+1} \bar{T}_j W_2^k(t) \int_{z_0}^{z_T} \frac{d\phi_j}{dZ} \psi_k(Z)\phi_i(Z)dZ$$

$$+ \sum_{j=i-1}^{i+1} Q_2^j(t) \int_{z_0}^{z_T} \phi_j(Z)\phi_i(Z)dZ \qquad \text{(D-4)}$$

APPENDIX E

LOCAL COORDINATES FOR STAGGERED $\phi_i(Z)$

1. To evaluate the integrals in the finite element approximations of the vorticity and divergence equations in models FEM-A and FEM-B, express Φ_{i+1}, Φ_i, Φ_{i-1}, Ψ_{i+1}, Ψ_i, Ψ_{i-1} and Ψ_{i-2} in terms of the local coordinate $\xi = Z - Z_i$. The general form of the local coordinate system is shown below.

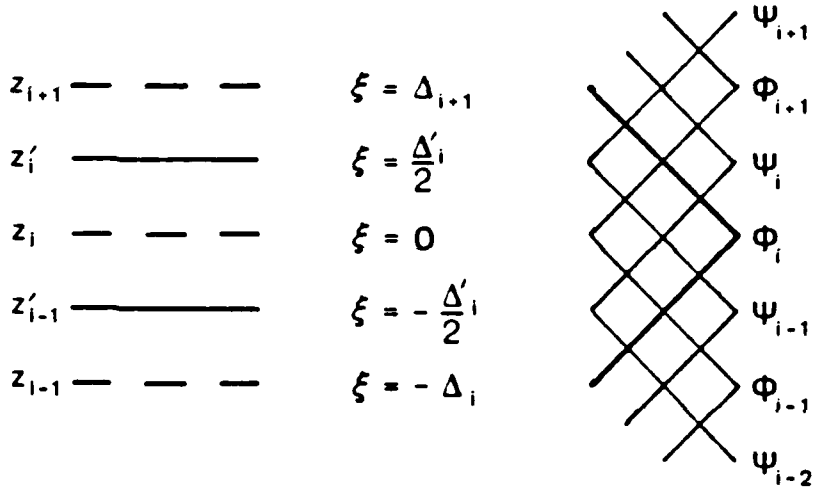

2. In terms of local coordinates for $\phi_i(\xi)$, the equations for ϕ_{i+1}, ϕ_i, ϕ_{i-1}, ψ_{i+1}, ψ_i, ψ_{i-1} and ψ_{i-2} are listed below. The notation used is defined in Appendix C.

$$\phi_i(\xi) = \begin{cases} \dfrac{\xi + \Delta_i}{\Delta_i} & -\Delta_i \le \xi \le 0 \\ \dfrac{-\xi + \Delta_{i+1}}{\Delta_{i+1}} & 0 \le \xi \le \Delta_{i+1} \end{cases}$$

$$\phi_{i+1}(\xi) = \frac{\xi}{\Delta_{i+1}} \qquad 0 \le \xi \le \Delta_{i+1}$$

$$\phi_{i-1}(\xi) = \frac{-\xi}{\Delta_i} \qquad -\Delta_i \le \xi \le 0$$

$$\psi_i(\xi) = \begin{cases} \dfrac{\xi + \frac{1}{2}\Delta_i'}{\Delta_i'} & \dfrac{-\Delta_i'}{2} \le \xi \le \dfrac{\Delta_i'}{2} \\ \dfrac{-\xi + \frac{1}{2}\Delta_i' + \Delta_{i+1}'}{\Delta_{i+1}'} & \dfrac{\Delta_i'}{2} \le \xi \le \Delta_{i+1} \end{cases}$$

$$\psi_{i+1}(\xi) = \frac{\xi - \frac{1}{2}\Delta_i'}{\Delta_{i+1}'} \qquad \frac{\Delta_i'}{2} \le \xi \le \Delta_{i+1}$$

$$\psi_{i-1}(\xi) = \begin{cases} \dfrac{\xi + \frac{1}{2}\Delta_i' + \Delta_{i-1}'}{\Delta_{i-1}'} & -\Delta_i \le \xi \le \dfrac{-\Delta_i'}{2} \\ \dfrac{-\xi + \frac{1}{2}\Delta_i'}{\Delta_i'} & \dfrac{-\Delta_i'}{2} \le \xi \le \dfrac{\Delta_i'}{2} \end{cases}$$

$$\psi_{i-2}(\xi) = \frac{-\xi - \frac{1}{2}\Delta_i'}{\Delta_{i-1}'} \qquad -\Delta_i \le \xi \le \frac{-\Delta_i'}{2}$$

3. With respect to the function $\phi_1(\xi)$, the layer of interest is $z_0 \le z \le z_2$ or $\frac{1}{2}\Delta_2' \le \xi \le \Delta_2'$. Eigenfunctions $\phi_1(\xi)$, $\phi_2(\xi)$, $\psi_1(\xi)$ and $\psi_2(\xi)$ are defined in this layer.

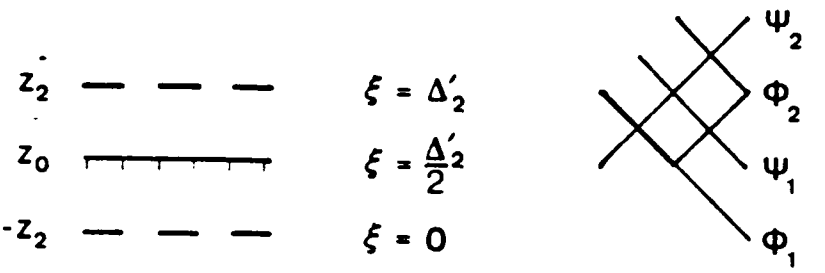

$$\phi_1(\xi) = \frac{-\xi + \Delta'_2}{\Delta'_2} \qquad \psi_1(\xi) = \frac{-\xi + \frac{3}{2}\Delta'_2}{\Delta'_2}$$

$$\phi_2(\xi) = \frac{\xi}{\Delta'_2} \qquad \psi_2(\xi) = \frac{\xi - \frac{1}{2}\Delta'_2}{\Delta'_2}$$

4. With respect to the function $\phi_2(\xi)$, the layer of interest is $Z_0 \leq Z \leq Z_3$ or $\frac{-\Delta'_2}{2} \leq \xi \leq \Delta_3$. Eigenfunctions ϕ_1, ϕ_2, ϕ_3, ψ_1, ψ_2 and ψ_3 are defined in this layer.

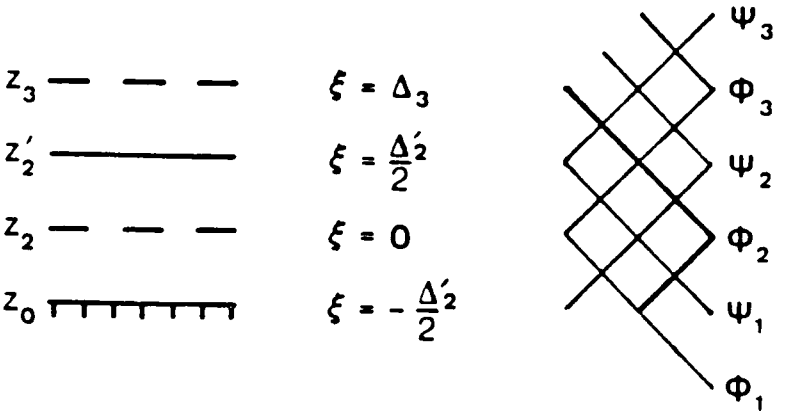

$$\phi_1(\xi) = \frac{-\xi}{\Delta_2'} \qquad -\frac{1}{2}\Delta_2' \le \xi \le 0$$

$$\phi_2(\xi) = \begin{cases} \dfrac{\xi + \Delta_2'}{\Delta_2'} & -\dfrac{\Delta_2'}{2} \le \xi \le 0 \\ \dfrac{-\xi + \Delta_3}{\Delta_3} & 0 \le \xi \le \Delta_3 \end{cases}$$

$$\phi_3(\xi) = \frac{\xi}{\Delta_3} \qquad 0 \le \xi \le \Delta_3$$

$$\psi_1(\xi) = \frac{-\xi + \frac{1}{2}\Delta_2'}{\Delta_2'}$$

$$\psi_2(\xi) = \begin{cases} \dfrac{\xi + \frac{1}{2}\Delta_2'}{\Delta_2'} & \dfrac{-\Delta_2'}{2} \le \xi \le \dfrac{\Delta_2'}{2} \\ \dfrac{-\xi + \frac{1}{2}\Delta_2' + \Delta_3'}{\Delta_3'} & \dfrac{\Delta_2'}{2} \le \xi \le \Delta_3 \end{cases}$$

$$\psi_3(\xi) = \frac{\xi - \frac{1}{2}\Delta_2'}{\Delta_3'} \qquad \frac{\Delta_2'}{2} \le \xi \le \Delta_3$$

5. With respect to the function $\phi_{N+1}(\xi)$, the layer of interest is $Z_N \le Z \le Z'_{N+1}$ or $-\Delta_{N+1} \le \xi \le \frac{1}{2}\Delta'_{N+1}$. Eigenfunctions ϕ_{N+2}, ϕ_{N+1}, ϕ_N, ψ_{N+1}, ψ_N and ψ_{N-1} are defined in this layer.

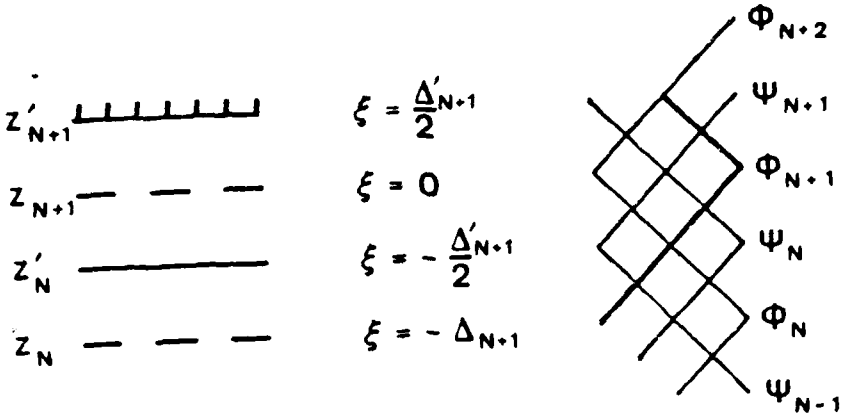

$$\varphi_{N+2}(\xi) = \frac{\xi}{\Delta'_{N+1}} \qquad 0 \le \xi \le \frac{\Delta'_{N+1}}{2}$$

$$\varphi_{N+1}(\xi) = \begin{cases} \dfrac{-\xi + \Delta'_{N+1}}{\Delta'_{N+1}} & 0 \le \xi \le \frac{1}{2}\Delta'_{N+1} \\ \dfrac{\xi + \Delta_{N+1}}{\Delta_{N+1}} & -\Delta_{N+1} \le \xi \le 0 \end{cases}$$

$$\varphi_N(\xi) = \frac{-\xi}{\Delta_{N+1}} \qquad -\Delta_{N+1} \le \xi \le 0$$

$$\psi_{N+1}(\xi) = \frac{\xi + \frac{1}{2}\Delta'_{N+1}}{\Delta'_{N+1}} \qquad 0 \le \xi \le \frac{1}{2}\Delta'_{N+1}$$

$$\psi_N(\xi) = \begin{cases} \dfrac{-\xi + \frac{1}{2}\Delta'_{N+1}}{\Delta'_{N+1}} & 0 \le \xi \le \frac{1}{2}\Delta'_{N+1} \\ \dfrac{\xi + \frac{1}{2}\Delta'_{N+1} + \Delta'_N}{\Delta'_N} & -\Delta_{N+1} \le \xi \le 0 \end{cases}$$

$$\psi_{N-1}(\xi) = \frac{-\xi - \frac{1}{2}\Delta'_{N+1}}{\Delta'_N} \qquad -\Delta_{N+1} \le \xi \le \frac{-\Delta'_{N+1}}{2}$$

APPENDIX F

MATRIX ELEMENTS FOR FEM-A

1. Mass matrix, $\underline{\underline{M}}$, using the notation defined in Appendix C:

   a. General formulas, i = 2,...,N:

$$M(i,i-1) = \frac{1}{6}\Delta_i \tag{F-1}$$

$$M(i,i) = \frac{1}{3}(\Delta_{i+1} + \Delta_i) \tag{F-2}$$

$$M(i,i+1) = \frac{1}{6}\Delta_{i+1} \tag{F-3}$$

   b. At level i = 1:

$$M(1,1) = \frac{1}{3}\Delta_2 \tag{F-4}$$

$$M(1,2) = \frac{1}{6}\Delta_2 \tag{F-5}$$

   c. At level i = N+1

$$M(N+1,N) = \frac{1}{6}\Delta_{N+1} \tag{F-6}$$

$$M(N+1,N+1) = \frac{1}{3}(\Delta_{N+1} + \frac{1}{2}\Delta'_{N+1}) \tag{F-7}$$

2. Matrix $\underline{\underline{N}}$:

   a. General formulas, i = 2,...,N

$$N(i,i-1) = \frac{1}{12}(\bar{u}_i + \bar{u}_{i-1}) \cdot \Delta_i \tag{F-8}$$

$$N(i,i) = \frac{1}{12}(\bar{u}_{i+1}\cdot\Delta_{i+1} + \bar{u}_i\cdot\Delta_i) + \frac{1}{4}\bar{u}_i\cdot(\Delta_{i+1} + \Delta_i) \quad \text{(F-9)}$$

$$N(i,i+1) = \frac{1}{12}(\bar{u}_{i+1} + \bar{u}_i)\cdot\Delta_{i+1} \quad \text{(F-10)}$$

b. At level i = 1:

$$N(1,1) = \frac{1}{12}(\bar{u}_2\cdot\Delta_2) + \frac{1}{4}(\bar{u}_1\cdot\Delta_2) \quad \text{(F-11)}$$

$$N(1,2) = \frac{1}{12}(\bar{u}_2 + \bar{u}_1)\cdot\Delta_2 \quad \text{(F-12)}$$

c. At level i = N+1:

$$N(i,i-1) = \frac{1}{12}(\bar{u}_{N+1} + \bar{u}_N)\cdot\Delta_{N+1} \quad \text{(F-13)}$$

$$N(i,i) = \frac{1}{24}(\bar{u}_{N+2}\cdot\Delta'_{N+1}) + \frac{1}{12}(\bar{u}_{N+1}\cdot\Delta_{N+1}) + \frac{1}{4}\bar{u}_{N+1}\cdot(\Delta_{N+1} + \frac{1}{2}\Delta'_{N+1}) \quad \text{(F-14)}$$

3. Matrix $\underline{\underline{P}}$:

a. General formulas, i = 3,...,N

$$P(i,i-2) = (\bar{u}_i - \bar{u}_{i-1})\cdot\left[\frac{\Delta_i}{6\cdot\Delta'_{i-1}} - \frac{(\Delta'_i)^3}{48\cdot(\Delta_i)^2\cdot(\Delta'_{i-1})}\right] \quad \text{(F-15)}$$

$$P(i,i-1) = \{(\bar{u}_{i+1} - \bar{u}_i)\cdot[\frac{\Delta_i'}{8\cdot\Delta_{i+1}} - \frac{(\Delta_i')^2}{48\cdot(\Delta_{i+1})^2}]$$

$$+ (\bar{u}_i - \bar{u}_{i-1})\cdot[\frac{1}{2} - \frac{\Delta_i}{6\cdot\Delta_{i-1}'} + \frac{\Delta_i'}{4\cdot\Delta_{i-1}'} - \frac{\Delta_i'}{8\cdot\Delta_i}$$

$$+ \frac{(\Delta_i')^2}{48\cdot(\Delta_i)^2} - \frac{(\Delta_i')^2}{8\cdot\Delta_i\cdot\Delta_{i-1}'} + \frac{(\Delta_i')^3}{48\cdot(\Delta_i)^2(\Delta_{i-1}')}]\} \qquad \text{(F-16)}$$

$$P(i,i) = \{(\bar{u}_i - \bar{u}_{i-1})\cdot[\frac{\Delta_i'}{8\cdot\Delta_i} - \frac{(\Delta_i')^2}{48\cdot(\Delta_i)^2}]$$

$$+ (\bar{u}_{i+1} - \bar{u}_i)\cdot[\frac{3\cdot\Delta_i'}{8\cdot\Delta_{i+1}} - \frac{5\cdot(\Delta_i')^2}{48\cdot(\Delta_{i+1})^2}]$$

$$+ (\bar{u}_{i+1} - \bar{u}_i)\cdot[\frac{1}{2} - \frac{\Delta_i'}{2\cdot\Delta_{i+1}} + \frac{\Delta_i'}{2\cdot\Delta_{i+1}'} - \frac{\Delta_{i+1}}{6\cdot\Delta_{i+1}'}$$

$$- \frac{(\Delta_i')^2}{8\cdot(\Delta_{i+1})(\Delta_{i+1}')} + \frac{(\Delta_{i+1}')^2}{8\cdot(\Delta_{i+1})^2} + \frac{(\Delta_i')^3}{48\cdot(\Delta_{i+1})^2(\Delta_{i+1}')}]\}$$

(F-17)

$$P(i,i+1) = (\bar{u}_{i+1} - \bar{u}_i)\cdot[\frac{\Delta_{i+1}}{6\cdot\Delta_{i+1}'} - \frac{\Delta_i'}{4\cdot\Delta_{i+1}'} + \frac{(\Delta_i')^2}{8\cdot\Delta_{i+1}\cdot\Delta_{i+1}'}$$

$$- \frac{(\Delta_i')^3}{48\cdot(\Delta_{i+1})^2(\Delta_{i+1}')}] \qquad \text{(F-18)}$$

b. At level i = 1:

$$P(1,1) = \frac{1}{8}(\bar{u}_2 - \bar{u}_1) \qquad \text{(F-19)}$$

$$P(1,2) = \frac{1}{48}(\bar{u}_2 - \bar{u}_1) \qquad \text{(F-20)}$$

c. At level i = 2:

$$P(2,1) = \frac{13}{48}\cdot(\bar{u}_2 - \bar{u}_1) + (\bar{u}_3 - \bar{u}_2)\cdot\left[\frac{\Delta_2'}{8\cdot\Delta_3} - \frac{(\Delta_2')^2}{48\cdot(\Delta_3)^2}\right] \qquad \text{(F-21)}$$

$$P(2,2) = \frac{5}{48}\cdot(\bar{u}_2 - \bar{u}_1) + (\bar{u}_3 - \bar{u}_2)\cdot\left[\frac{1}{2} - \frac{\Delta_3}{6\Delta_3'} + \frac{\Delta_2'}{4\Delta_3'} - \frac{\Delta_2'}{8\cdot\Delta_3} + \frac{(\Delta_2')^2}{48(\Delta_3)^2} - \frac{(\Delta_2')^2}{8\cdot\Delta_3\cdot\Delta_3'} + \frac{(\Delta_2')^3}{48(\Delta_3)^2(\Delta_3')}\right] \qquad \text{(F-22)}$$

$$P(2,3) = (\bar{u}_3 - \bar{u}_2)\cdot\left[\frac{\Delta_3}{6\cdot\Delta_3'} - \frac{\Delta_2'}{4\cdot\Delta_3'} + \frac{(\Delta_2')^2}{8\cdot\Delta_3\cdot\Delta_3'} - \frac{(\Delta_2')^3}{48(\Delta_3)^2(\Delta_3')}\right] \qquad \text{(F-23)}$$

c. At level i = N+1:

$$P(N+1,N-1) = (\bar{u}_{N+1} - \bar{u}_N)\cdot\left[\frac{\Delta_{N+1}}{6\cdot\Delta_N'} - \frac{(\Delta_{N+1}')^3}{48\cdot(\Delta_{N+1})^2(\Delta_N')}\right] \qquad \text{(F-24)}$$

$$P(N+1,N) = \left\{\frac{5}{48}(\bar{u}_{N+2} - \bar{u}_{N+1}) + (\bar{u}_{N+1} - \bar{u}_N)\cdot\left[\frac{1}{2} - \frac{\Delta_{N+1}}{6\cdot\Delta_N'} + \frac{\Delta_{N+1}'}{4\cdot\Delta_N'} - \frac{\Delta_{N+1}'}{8\cdot\Delta_{N+1}} + \frac{(\Delta_{N+1}')^2}{48\cdot(\Delta_{N+1})^2} - \frac{(\Delta_{N+1}')^2}{8(\Delta_{N+1})^2(\Delta_N')} + \frac{(\Delta_{N+1}')^3}{48(\Delta_{N+1})^2(\Delta_N')}\right]\right\} \qquad \text{(F-25)}$$

$$P(N+1,N+1) = \left\{\frac{13}{48}(\bar{u}_{N+2} - \bar{u}_{N+1}) + (\bar{u}_{N+1} - \bar{u}_N)\cdot\left[\frac{\Delta_{N+1}'}{8\cdot\Delta_{N+1}} - \frac{(\Delta_{N+1}')^2}{48\cdot(\Delta_{N+1})^2}\right]\right\} \qquad \text{(F-26)}$$

4. Matrix $\underline{\underline{Q}}$:

a. General formulas, i = 2,...,N

$$Q(i,i-1) = \frac{1}{6}(\bar{u}_i - \bar{u}_{i-1}) \quad \text{(F-27)}$$

$$Q(i,i) = \frac{1}{3}(\bar{u}_{i+1} - \bar{u}_{i-1}) \quad \text{(F-28)}$$

$$Q(i,i+1) = \frac{1}{6}(\bar{u}_{i+1} - \bar{u}_i) \quad \text{(F-29)}$$

b. At level i = 1:

$$Q(1,1) = \frac{1}{3}(\bar{u}_2 - \bar{u}_1) \quad \text{(F-30)}$$

$$Q(1,2) = \frac{1}{6}(\bar{u}_2 - \bar{u}_1) \quad \text{(F-31)}$$

c. At level i = N+1:

$$Q(N+1,N) = \frac{1}{6}(\bar{u}_{N+1} - \bar{u}_N) \quad \text{(F-32)}$$

$$Q(N+1,N+1) = \frac{1}{3}(\bar{u}_{N+2} - \bar{u}_N) \quad \text{(F-33)}$$

5. Matrix $\underline{\underline{R}}$:

The formulas for the elements of this matrix are the same as those for matrix $\underline{\underline{P}}$, with $\bar{T}$ replacing $\bar{u}$ in equations (F-15)-(F-26).

APPENDIX G

GALERKIN FORM OF FEM-B PROGNOSTIC EQUATIONS

1. The vorticity equations have the same form as the vorticity equations for model FEM-C, equations (B-1)-(B-2). However, the equations for ϕ_1, ϕ_j, and ϕ_k are different because $\phi(Z)$ is defined for the staggered levels in FEM-B.

2. The divergence equations are the same as the divergence equations in model FEM-A, equations (D-1)-(D-2).

3. Thermodynamic Equations (2-39)-(2-40):

$$\sum_{j=i-1}^{i+1} \frac{dT_1^j}{dt} \int_{Z_0}^{Z_T} \psi_j(Z)\psi_i(Z)dZ$$

$$= -\mu \sum_{j=i-1}^{i+2} \sum_{k=i-1}^{i+1} \bar{u}_j T_2^k(t) \int_{Z_0}^{Z_T} \phi_j(Z)\psi_k(Z)\psi_i(Z)dZ$$

$$+ \left(\frac{f}{R}\right) \sum_{j=i-1}^{i+2} \sum_{k=i-1}^{i+2} \bar{u}_j V_1^k(t) \int_{Z_0}^{Z_T} \frac{d\phi_j}{dZ} \phi_k(Z)\psi_i(Z)dZ$$

$$- \sum_{j=i-1}^{i+1} \sum_{k=i-1}^{i+1} \bar{T}_j W_1^k(t) \int_{Z_0}^{Z_T} \frac{d\psi_j}{dZ} \psi_k(Z)\psi_i(Z)dZ$$

$$+ \sum_{j=i-1}^{i+1} Q_1^j(t) \int_{Z_0}^{Z_T} \psi_j(Z)\psi_i(Z)dZ \qquad \text{(G-1)}$$

$$\sum_{j=i-1}^{i+1} \frac{dT_2^j}{dt} \int_{z_0}^{z_T} \psi_j(Z)\psi_i(Z)dZ$$

$$= \mu \sum_{j=i-1}^{i+2} \sum_{k=i-1}^{i+1} \bar{u}_j T_1^k(t) \int_{z_0}^{z_T} \phi_j(Z)\psi_k(Z)\psi_i(Z)dZ$$

$$+ \left(\frac{f}{R}\right) \sum_{j=i-1}^{i+2} \sum_{k=i-1}^{i+2} \bar{u}_j v_2^k(t) \int_{z_0}^{z_T} \frac{d\phi_j}{dZ} \phi_k(Z)\psi_i(Z)dZ$$

$$- \sum_{j=i-1}^{i+1} \sum_{k=i-1}^{i+1} \bar{T}_j W_2^k(t) \int_{z_0}^{z_T} \frac{d\psi_j}{dZ} \psi_k(Z)\psi_i(Z)dZ$$

$$+ \sum_{j=i-1}^{i+1} Q_2^j(t) \int_{z_0}^{z_T} \psi_j(Z)\psi_i(Z)dZ \qquad \text{(G-2)}$$

APPENDIX H

LOCAL COORDINATES FOR UNSTAGGERED $\psi_i(Z)$

1. To evaluate the integrals in finite element approximations of the thermodynamic equations in model FEM-B, express ϕ_{i+2}, ϕ_{i+1}, ϕ_i, ϕ_{i-1}, ψ_{i+1}, ψ_i and ψ_{i-1} in terms of the local coordiante $\eta = Z - Z'_i$. The general form of the local coordinate system is shown below.

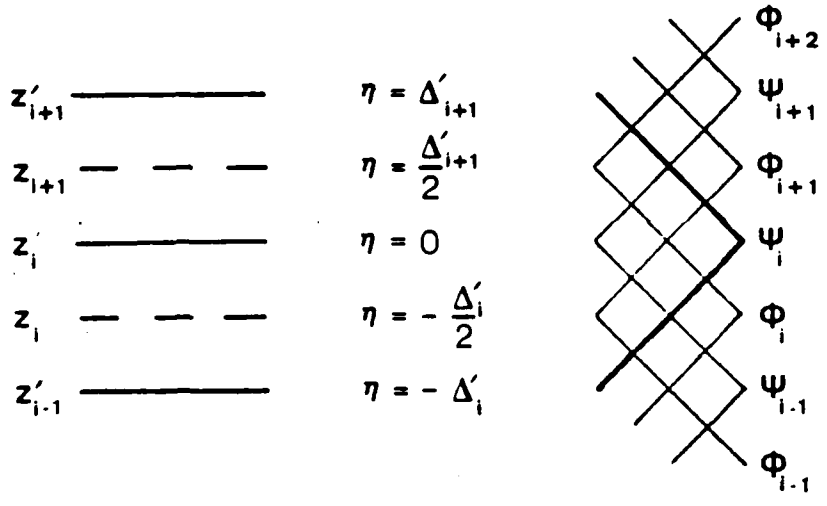

2. In terms of the local coordinates for $\psi_i(\eta)$, the equations for φ_{i+2}, φ_{i+1}, φ_i, φ_{i-1}, ψ_{i+1}, ψ_i and ψ_{i-1} are listed below. The notation used is defined in Appendix C.

$$\phi_i(\eta) = \begin{cases} \dfrac{\eta + \Delta_i' + \frac{1}{2}\Delta_{i-1}'}{\Delta_i} & -\Delta_i' \le \eta \le -\frac{1}{2}\Delta_i' \\ \dfrac{-\eta + \frac{1}{2}\Delta_{i+1}'}{\Delta_{i+1}} & -\frac{1}{2}\Delta_i' \le \eta \le \frac{1}{2}\Delta_{i+1} \end{cases}$$

$$\phi_{i-1}(\eta) = \frac{-\eta - \frac{1}{2}\Delta_i'}{\Delta_i} \qquad \Delta_i' \le \eta \le -\frac{1}{2}\Delta_i'$$

$$\phi_{i+1}(\eta) = \begin{cases} \dfrac{\eta + \frac{1}{2}\Delta_i'}{\Delta_{i+1}} & -\frac{1}{2}\Delta_i' \le \eta \le \frac{1}{2}\Delta_{i+1}' \\ \dfrac{-\eta + \frac{1}{2}\Delta_i' + \Delta_{i+1}'}{\Delta_{i+1}} & \frac{1}{2}\Delta_{i+1}' \le \eta \le \Delta_{i+1}' \end{cases}$$

$$\phi_{i+2}(\eta) = \frac{\eta - \frac{1}{2}\Delta_{i+1}'}{\Delta_{i+1}} \qquad \frac{1}{2}\Delta_{i+1}' \le \eta \le \Delta_{i+1}'$$

$$\psi_i(\eta) = \begin{cases} \dfrac{\eta + \Delta_i'}{\Delta_i'} & -\Delta_i' \le \eta \le 0 \\ \dfrac{-\eta + \Delta_{i+1}'}{\Delta_{i+1}'} & 0 \le \eta \le \Delta_{i+1}' \end{cases}$$

$$\psi_{i-1}(\eta) = \frac{-\eta}{\Delta_i'} \qquad -\Delta_i' \le \eta \le 0$$

$$\psi_{i+1}(\eta) = \frac{\eta}{\Delta_{i+1}'} \qquad 0 \le \eta \le \Delta_{i+1}'$$

3. With respect to the function $\psi_1(\eta)$, the layer of interest is $Z_0 \le Z \le Z_2'$ or $0 \le \eta \le \Delta_2'$. Eigenfunctions ϕ_1, ϕ_2, ϕ_3, ψ_1 and ψ_2 are defined in this layer.

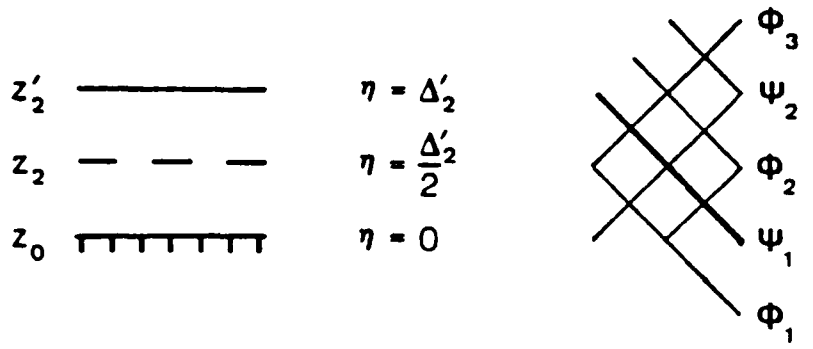

$$\phi_1(\eta) = \frac{-\eta + \frac{1}{2}\Delta_2'}{\Delta_2} \qquad 0 \le \eta \le \frac{1}{2}\Delta_2'$$

$$\phi_2(\eta) = \begin{cases} \dfrac{\eta + \frac{1}{2}\Delta_2'}{\Delta_2'} & 0 \le \eta \le \frac{1}{2}\Delta_2' \\ \dfrac{-\eta + \frac{3}{2}\Delta_2'}{\Delta_2'} & \frac{1}{2}\Delta_2' \le \eta \le \Delta_2' \end{cases}$$

$$\phi_3(\eta) = \frac{\eta - \frac{1}{2}\Delta_2'}{\Delta_3} \qquad \frac{1}{2}\Delta_2' \le \eta \le \Delta_2'$$

$$\psi_1(\eta) = \frac{-\eta + \Delta_2'}{\Delta_2'} \qquad 0 \le \eta \le \Delta_2'$$

$$\psi_2(\eta) = \frac{\eta}{\Delta_2'} \qquad 0 \le \eta \le \Delta_2'$$

4. With respect to the function $\psi_2(\eta)$, the layer of interest is $Z_0 \le Z \le Z_3$. Eigenfunctions ϕ_1, ϕ_2, ϕ_3, ϕ_4, ψ_1, ψ_2 and ψ_3 are defined in this layer. Formulas for ϕ_4, ψ_1, ψ_2 and ψ_3 are obtained from the general formulas with i = 2.

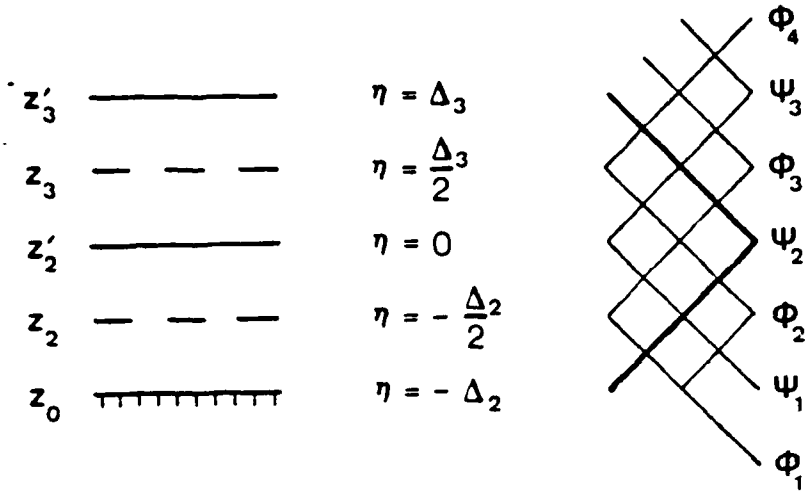

$$\Phi_1(\eta) = \frac{-\eta - \frac{1}{2}\Delta'_2}{\Delta'_2} \qquad -\Delta'_2 \le \eta \le -\frac{1}{2}\Delta'_2$$

$$\Phi_2(\eta) = \begin{cases} \dfrac{\eta + \frac{3}{2}\Delta'_2}{\Delta'_2} & -\Delta'_2 \le \eta \le -\frac{1}{2}\Delta'_2 \\ \dfrac{-\eta + \frac{1}{2}\Delta'_3}{\Delta_3} & -\frac{1}{2}\Delta'_2 \le \eta \le \frac{1}{2}\Delta'_3 \end{cases}$$

$$\Phi_3(\eta) = \begin{cases} \dfrac{\eta + \frac{1}{2}\Delta'_2}{\Delta_2} & -\frac{1}{2}\Delta'_2 \le \eta \le \frac{1}{2}\Delta'_3 \\ \dfrac{-\eta + \frac{1}{2}\Delta'_2 + \Delta'_3}{\Delta_3} & \frac{1}{2}\Delta'_3 \le \eta \le \Delta'_3 \end{cases}$$

5. With respect to the function $\psi_{N+1}(\eta)$, the layer of interest is $Z'_N \le Z \le Z'_{N+1}$ or $-\Delta'_{N+1} \le \eta \le 0$. Eigenfunctions Φ_{N+2}, Φ_{N+1}, Φ_N, ψ_{N+1} and ψ_N are defined in this layer.

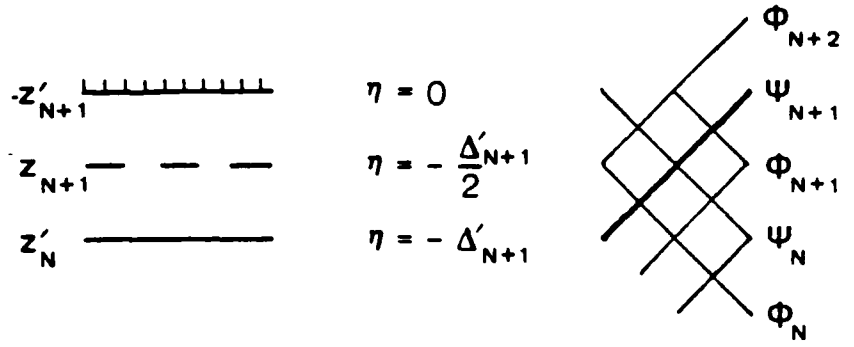

$$\Phi_N(\eta) = \frac{-\eta - \frac{1}{2}\Delta'_{N+1}}{\Delta_{N+1}} \qquad -\Delta'_{N+1} \le \eta \le -\frac{1}{2}\Delta'_{N+1}$$

$$\Phi_{N+1}(\eta) = \begin{cases} \dfrac{-\eta + \frac{1}{2}\Delta'_{N+1}}{\Delta'_{N+1}} & -\frac{1}{2}\Delta'_{N+1} \le \eta \le 0 \\ \dfrac{\eta + \Delta'_{N+1} + \frac{1}{2}\Delta'_N}{\Delta_{N+1}} & -\Delta'_{N+1} \le \eta \le -\frac{1}{2}\Delta'_{N+1} \end{cases}$$

$$\Phi_{N+2}(\eta) = \frac{\eta + \frac{1}{2}\Delta'_{N+1}}{\Delta'_{N+1}} \qquad -\frac{1}{2}\Delta'_{N+1} \le \eta \le 0$$

$$\Psi_N(\eta) = \frac{-\eta}{\Delta'_{N+1}} \qquad -\Delta'_{N+1} \le \eta \le 0$$

$$\Psi_{N+1}(\eta) = \frac{\eta + \Delta'_{N+1}}{\Delta'_{N+1}} \qquad -\Delta'_{N+1} \le \eta \le 0$$

APPENDIX I

MATRIX ELEMENTS FOR FEM-B

1. Matrices $\underline{\underline{M}}$, $\underline{\underline{N}}$, and $\underline{\underline{P}}$ are the same as those defined in model FEM-A. The equations for their elements are listed in Appendix F, equations (F-1)-(F-26).

2. Mass matrix $\underline{\underline{S}}$ is the same as matrix $\underline{\underline{M}}$ in model FEM-C. The equations for the elements of $\underline{\underline{S}}$ are the same as equations (C-4)-(C-10) in Appendix C.

3. Matrix $\underline{\underline{R}}$ is the same as matrix $\underline{\underline{R}}$ in the model FEM-C. Equations (C-25)-(C-31) in Appendix C define the elements of $\underline{\underline{R}}$.

4. Matrix $\underline{\underline{Q}}$, using the notation defined in Appendix C:

   a. General formulas, i = 2,...,N:

$$Q(i,i-1) = (\bar{u}_i - \bar{u}_{i-1}) \cdot \left[\frac{(\Delta_i')^2}{48 \cdot (\Delta_i)^2}\right] \qquad \text{(I-1)}$$

$$Q(i,i) = (\bar{u}_i - \bar{u}_{i-1}) \cdot \left[\frac{(\Delta_i')^2}{24 \cdot (\Delta_i)^2} + \frac{(\Delta_i')(\Delta_{i-1}')}{16 \cdot (\Delta_i)^2}\right]$$

$$+ (\bar{u}_{i+1} - \bar{u}_i) \cdot \left[\frac{(\Delta_i')^2}{12 \cdot (\Delta_{i+1})^2} + \frac{3(\Delta_{i+1}')(\Delta_i')}{16 \cdot (\Delta_{i+1})^2} + \frac{5(\Delta_{i+1}')^2}{48(\Delta_{i+1})^2}\right] \qquad \text{(I-2)}$$

$$Q(i,i+1) = (\bar{u}_{i+1} - \bar{u}_i) \cdot \left[\frac{(\Delta_i')^2}{12 \cdot (\Delta_{i+1})^2} + \frac{3(\Delta_{i+1}')(\Delta_i')}{16 \cdot (\Delta_{i+1})^2}\right.$$

$$\left. + \frac{5(\Delta_i')^2}{48 \cdot (\Delta_{i+1})^2}\right] + (\bar{u}_{i+2} - \bar{u}_{i+1}) \cdot \left[\frac{(\Delta_{i+1}')^2}{24 \cdot (\Delta_{i+1})^2}\right.$$

$$\left. + \frac{(\Delta_{i+1}') \cdot (\Delta_i')}{16 \cdot (\Delta_{i+1})^2}\right] \qquad \text{(I-3)}$$

$$Q(i,i+2) = (\bar{u}_{i+2} - \bar{u}_{i+1}) \cdot \left[\frac{(\Delta_{i+1}')^2}{48 \cdot (\Delta_{i+1})^2}\right] \qquad \text{(I-4)}$$

b. At level i = 1:

$$Q(1,1) = \frac{5 \cdot (\bar{u}_2 - \bar{u}_1)}{48} \qquad \text{(I-5)}$$

$$Q(1,2) = (\bar{u}_2 - \bar{u}_1) \cdot \left[\frac{(\Delta_2')^2}{12 \cdot (\Delta_2)^2}\right] + (\bar{u}_3 - \bar{u}_2) \cdot \left[\frac{(\Delta_2')^2}{24 \cdot (\Delta_2)^2}\right] \qquad \text{(I-6)}$$

$$Q(1,3) = (\bar{u}_3 - \bar{u}_2) \cdot \left[\frac{(\Delta_2')^2}{48 \cdot (\Delta_2)^2}\right] \qquad \text{(I-7)}$$

c. At level i = N+1:

$$Q(N+1,N) = (\bar{u}_{N+1} - \bar{u}_N) \cdot \left[\frac{(\Delta_{N+1}')^2}{48 \cdot (\Delta_{N+1})^2}\right] \qquad \text{(I-8)}$$

$$Q(N+1,N+1) = \frac{13\cdot(\bar{u}_{N+2} - \bar{u}_{N+1})}{48} + (\bar{u}_{N+1} - \bar{u}_N)\cdot\left[\frac{(\Delta_{N+1})^2}{24\cdot(\Delta_{N+1})^2}\right.$$

$$\left. + \frac{(\Delta_{N+1})(\Delta_N)}{16\cdot(\Delta_{N+1})^2}\right] \qquad \text{(I-9)}$$

5. Matrix $\underline{\underline{T}}$:

a. General formulas for i = 3,...,N

$$T(i,i-1) = \frac{\bar{u}_{i-1}\cdot(\Delta'_i)^2}{192\cdot\Delta_i} + \bar{u}_i\cdot\left[\frac{5\cdot(\Delta'_i)^2}{192\cdot\Delta_i} + \frac{(\Delta'_i)(\Delta'_{i-1})}{24\cdot\Delta_i}\right.$$

$$\left. + \frac{(\Delta'_i)^2}{192\cdot\Delta_{i+1}} + \frac{(\Delta'_{i+1})(\Delta'_i)}{192\cdot\Delta_{i+1}}\right] + \frac{\bar{u}_{i+1}\cdot(\Delta'_i)^2}{64\cdot\Delta_{i+1}} \qquad \text{(I-10)}$$

$$T(i,i) = \frac{\bar{u}_{i-1}\cdot(\Delta_i)^2}{192\cdot\Delta_i} + \bar{u}_i\cdot\left[\frac{(\Delta'_i)^2}{64\cdot\Delta_i} + \frac{(\Delta'_i)(\Delta'_{i-1})}{48\cdot\Delta_i}\right.$$

$$\left. + \frac{11\cdot(\Delta'_i)^2}{192\cdot\Delta_{i+1}} + \frac{7(\Delta'_{i+1})(\Delta'_i)}{48\cdot\Delta_{i+1}} + \frac{17\cdot(\Delta'_{i+1})^2}{192\cdot\Delta_{i+1}}\right]$$

$$+ \bar{u}_{i+1}\cdot\left[\frac{17\cdot(\Delta'_i)^2}{192\cdot\Delta_{i+1}} + \frac{11\cdot(\Delta'_{i+1})^2}{192\cdot\Delta_{i+1}} + \frac{7\cdot(\Delta'_{i+1})(\Delta'_i)}{48\cdot\Delta_{i+1}}\right.$$

$$\left. + \frac{(\Delta'_{i+1})^2}{64\cdot\Delta_{i+1}} + \frac{(\Delta'_{i+1})(\Delta'_i)}{48\cdot\Delta_{i+1}}\right] + \frac{\bar{u}_{i+2}\cdot(\Delta'_{i+1})^2}{192\cdot\Delta_{i+1}} \qquad \text{(I-11)}$$

$$T(i,i+1) = \frac{\bar{u}_i \cdot (\Delta'_{i+1})^2}{64 \cdot \Delta_{i+1}} + \bar{u}_{i+1}\left[\frac{(\Delta'_{i+1})^2}{32 \cdot \Delta_{i+1}} + \frac{(\Delta'_{i+1})(\Delta'_i)}{12 \cdot \Delta_{i+1}}\right]$$

$$+ \frac{\bar{u}_{i+2} \cdot (\Delta'_{i+1})^2}{64 \cdot \Delta_{i+1}} \qquad \text{(I-12)}$$

b. At level i = 1:

$$T(1,1) = \frac{17 \cdot \bar{u}_1 \cdot \Delta'_2}{192} + \frac{23 \cdot \bar{u}_2 \cdot \Delta'_2}{96} + \frac{\bar{u}_3 \cdot \Delta'_2}{192}$$

$$T(1,2) = \frac{\bar{u}_1 \cdot \Delta'_2}{64} + \frac{13 \cdot \bar{u}_2 \cdot \Delta'_2}{192} + \frac{\bar{u}_3 (\Delta'_3)^2}{64 \cdot \Delta_3} \qquad \text{(I-13)}$$

c. At level i = 2:

$$T(2,1) = \frac{\bar{u}_1 \cdot \Delta'_2}{64} + \bar{u}_2 \cdot \left[\frac{13 \cdot \Delta'_2}{192} + \frac{(\Delta'_2)^2}{192 \cdot \Delta_3} + \frac{(\Delta'_3)(\Delta'_2)}{24 \cdot \Delta_3}\right]$$

$$+ \frac{\bar{u}_3 \cdot (\Delta'_2)^2}{64 \cdot \Delta_3} \qquad \text{(I-14)}$$

$$T(2,2) = \frac{\bar{u}_1 \cdot \Delta'_2}{192} + \bar{u}_2 \cdot \left[\frac{7 \cdot \Delta'_2}{192} + \frac{11 \cdot (\Delta'_2)^2}{192 \cdot \Delta_3} + \frac{7 \cdot (\Delta'_3)(\Delta'_2)}{48 \cdot \Delta_3}\right.$$

$$\left. + \frac{17 \cdot (\Delta'_3)^2}{192 \cdot \Delta_3}\right] + \bar{u}_3 \cdot \left[\frac{17 \cdot (\Delta'_2)^2}{192 \cdot \Delta_3} + \frac{7 \cdot (\Delta'_3)^2}{96 \cdot \Delta_3}\right.$$

$$\left. + \frac{(\Delta'_3)(\Delta'_2)}{6 \cdot \Delta_3}\right] + \frac{\bar{u}_4 \cdot (\Delta'_3)^2}{192 \cdot \Delta_3} \qquad \text{(I-15)}$$

$$T(2,3) = \frac{\bar{u}_2 \cdot (\Delta'_3)^2}{64 \cdot \Delta_3} + \bar{u}_3 \cdot \left[\frac{(\Delta'_3)^2}{32 \cdot \Delta_3} + \frac{(\Delta'_3)(\Delta'_2)}{12 \cdot \Delta_3}\right] + \frac{\bar{u}_4 \cdot (\Delta'_3)^2}{64 \cdot \Delta_3} \qquad \text{(I-16)}$$

d. At level i = N+1:

$$T(N+1,N) = \frac{\bar{u}_N \cdot (\Delta'_{N+1})^2}{64 \cdot \Delta_{N+1}} + \bar{u}_{N+1} \cdot \left[\frac{5 \cdot (\Delta_{N+1})^2}{192 \cdot \Delta_{N+1}} + \frac{(\Delta'_{N+1})(\Delta'_N)}{24 \cdot \Delta_{N+1}} + \frac{13 \cdot (\Delta'_{N+1})}{192}\right] + \frac{\bar{u}_{N+2} \cdot \Delta'_{N+1}}{64} \qquad \text{(I-17)}$$

$$T(N+1,N+1) = \frac{\bar{u}_N \cdot (\Delta'_{N+1})^2}{192 \cdot \Delta_{N+1}} + \bar{u}_{N+1} \cdot \left[\frac{(\Delta'_{N+1})^2}{64 \cdot \Delta_{N+1}} + \frac{(\Delta'_{N+1})(\Delta'_N)}{48 \cdot \Delta_{N+1}} + \frac{13 \cdot \Delta'_{N+1}}{64}\right] + \frac{17 \cdot \bar{u}_{N+2} \cdot \Delta'_{N+1}}{192} \qquad \text{(I-18)}$$

APPENDIX J

FORCED VERTICAL VELOCITY

1. The contribution to the surface geopotential from the forced vertical velocity is Φ_s,

$$\Phi_s(x,t) = \begin{cases} \phi_M \sin^2(\frac{\pi t}{2T}) \sin(\mu x) & t \leq T \\ \phi_M \sin(\mu x) & t > T \end{cases} , \qquad \text{(J-1)}$$

where ϕ_M is mountain geopotential (m^2/s^2), t is time, and T is the total time to build the mountain. ϕ_M is a constant,

$$\phi_M = gH_M , \qquad \text{(J-2)}$$

where g is gravity and H_M is the height of the mountain. H_M is a parameter specified in each model. H_M = 750 meters in the thesis experiments.

2. The time rate of change of Φ_s is separated into sine and cosine components for use in the surface geopotential forecast equations,

$$\frac{d\Phi_s}{dt} = MTS_1(t) \cdot \cos(\mu x) + MTS_2(t) \cdot \sin(\mu x) , \qquad \text{(J-3)}$$

where $\frac{d}{dt} = \frac{\partial}{\partial t} + \bar{u}_{sfc} \cdot \frac{\partial}{\partial x}$. Equation (J-1) is substituted into equation (J-3) and the resultant expression is separated into sine and cosine equations. The equations to calculate the terms MTS_1 and MTS_2 are

$$MTS_1(t) = \begin{cases} \bar{u}_{sfc} \cdot \phi_M \cdot \mu \cdot \sin^2\left(\frac{\pi t}{2T}\right) & t \leq T \\ \bar{u}_{sfc} \cdot \phi_M \cdot \mu & t > T \end{cases}, \qquad \text{(J-4)}$$

and

$$MTS_2(t) = \begin{cases} \frac{\pi \cdot \phi_M}{T} \cdot \sin\left(\frac{\pi t}{2T}\right) \cdot \cos\left(\frac{\pi t}{2T}\right) & t \leq T \\ 0 & t > T \end{cases}. \qquad \text{(J-5)}$$

These terms are calculated for each time step in the model's forecast subroutine.

APPENDIX K

DIABATIC HEATING TERMS

For the diabatic heating function defined in equation (3-1), the maximum heating occurs at Z = 0.50, the midpoint of the heated layer. Temperature and diabatic heating are defined for grid A at the staggered levels, while they are defined at the unstaggered levels for grids B and C. Consequently, the rate of heating differs between the staggered and unstaggered models. In these experiments, the heated layer is between Z = 0.40 and Z = 0.60, the heating rate is 5.0 K/day, and only the cosine term, Q1, is nonzero in the heated layer. The value of the heating term is listed below for staggered and unstaggered levels for six, twelve and sixty-layer models.

Grid A 60-Layer Models		Grid B and C 60-Layer Models	
Z	Q1	Z	Q1
0.392	0.0	0.400	0.0
0.408	0.986E-06	0.417	0.388E-05
0.425	0.847E-05	0.433	0.145E-04
0.442	0.214E-04	0.450	0.289E-04
0.458	0.364E-04	0.467	0.434E-04
0.475	0.493E-04	0.483	0.540E-04
0.492	0.569E-04	0.500	0.579E-04
0.508	0.569E-04	0.517	0.540E-04
0.525	0.493E-04	0.533	0.434E-04
0.542	0.364E-04	0.550	0.289E-04

0.558	0.214E-04	0.567	0.145E-04
0.575	0.847E-05	0.583	0.388E-05
0.592	0.986E-06	0.600	0.0
0.608	0.0		

Grid A 12-Layer Models

Z	Q1
0.375	0.0
0.458	0.364E-04
0.542	0.364E-04
0.625	0.0

Grid B and C 12-Layer Models

Z	Q1
0.333	0.0
0.417	0.388E-05
0.500	0.579E-04
0.583	0.388E-05
0.667	0.0

Grid A 6-Layer Models

Z	Q1
0.250	0.0
0.417	0.388E-05
0.583	0.388E-05
0.750	0.0

Grid B and C 6-Layer Models

Z	Q1
0.333	0.0
0.500	0.579E-04
0.667	0.0

LIST OF REFERENCES

Arakawa, A., 1984: Vertical Differencing of Filtered Models. Proceedings of European Centre for Medium Range Weather Forecasts: 1983 Seminar on Numerical Methods for Weather Prediction. Vol. 1, pp. 183-206.

_____ and V. Lamb, 1977: Computational design of the basic dynamical processes of the UCLA General Circulation Model. Methods of Computational Physics, Academic Press, 17, 174-266.

Béland, M., J. Coté and A. Staniforth, 1983: The accuracy of a finite-element vertical discretization scheme for primitive equation models: Comparison with a finite-difference scheme. Monthly Weather Review, 111, 2298-2318.

Charney, J.G. and N.A. Phillips, 1953: Numerical integration of the quasi-geostrophic equations for barotropic and simple baroclinic flows. Journal of Meteorology, 10, 71-99.

Haltiner, G.J., and R.T. Williams, 1980: Numerical Prediction and Dynamic Meteorology. John Wiley & Sons, Inc., 477 pp.

Lorenz, E.N., 1960: Energy and numerical weather prediction. Tellus, 12, 364-373.

Schoenstadt, A., 1980: A transfer function analysis of numerical schemes used to simulate geostrophic adjustment. Monthly Weather Review, 108, 1245-1259.

Staniforth, A.N. and H.L. Mitchell, 1977: A semi-implicit finite-element barotropic model. Monthly Weather Review, 105, 154-169.

Tokioka, T., 1978: Some considerations on vertical differencing, Journal of the Meteorological Society of Japan, 44, 25-43.

Williams, R.T., and A.L. Schoenstadt, 1980: Formulation of efficient finite element prediction models. Naval Postgraduate School Report NPS63-80-011, 1-37.

Winninghoff, F., 1968: On the Adjustment Toward a Geostrophic Balance in a Simple Primitive Equation Model with Application to the Problem on Initialization and Objective Analysis. Doctoral Dissertation, UCLA, 161 pp.

INITIAL DISTRIBUTION LIST

		No. Copies
1.	Defense Technical Information Center Cameron Station Alexandria, Virginia 22304-6145	2
2.	Library, Code 0142 Naval Postgraduate School Monterey, California 93943-5100	2
3.	Meteorology Reference Center, Code 63 Department of Meteorology Naval Postgraduate School Monterey, California 93943-5100	1
4.	Chairman (Code 63Rd) Department of Meteorology Naval Postgraduate School Monterey, California 93943-5100	1
5.	Dr. Roger T. Williams, Code 63Wu Department of Meteorology Naval Postgraduate School Monterey, California 93943-5100	5
6.	Director Naval Oceanography Division Naval Observatory 34th and Massachusetts Avenue NW Washington, D.C. 20390	1
7.	Commander Naval Oceanography Command NSTL Station Bay St. Louis, Missouri 39522	1
8.	Commanding Officer Fleet Numerical Oceanography Center Monterey, California 93943	1
9.	Commanding Officer Naval Ocean Research and Development Activity NSTL Station Bay St. Louis, Missouri 39522	1

10. Commanding Officer — 1
Naval Environmental Prediction
Research Facility
Monterey, California 93943

11. Chief of Naval Research — 1
800 N. Quincy Street
Arlington, Virginia 22217

12. Program Manager (CIRF) — 1
Air Force Institute of Technology
Wright-Patterson Air Force Base, Ohio 45433

13. Commander — 1
Air Weather Service
Scott Air Force Base, Illinois 62225

14. Commander — 1
Air Force Global Weather Central
Offutt Air Force Base, Nebraska 68113

15. Captain Mary S. Jordan, USAF — 3
Det 11, 2d Weather Squadron
Patrick Air Force Base, Florida 32925

16. CDR Donald E. Hinsman, USN — 1
Assistant for Environmental Science
Room 5E813 OASN (RE and S)
Pentagon
Washington, D.C. 20350-1000

17. Professor R.L. Elsberry (Code 63Es) — 1
Department of Meteorology
Naval Postgraduate School
Monterey, California 93943-5100

18. Professor R.L. Haney (Code 63Hy) — 1
Department of Meteorology
Naval Postgraduate School
Monterey, California 93943-5100

19. Professor A.L. Schoenstadt — 1
(Code 53Zh)
Department of Mathematics
Naval Postgraduate School
Monterey, California 93943-5100

20. Professor R.E. Newton (Code 69Ne) — 1
Department of Mechanical Engineering
Naval Postgraduate School
Monterey, California 93943-5100

21. Dr. M.A. Rennick, Code 63Rn — 1
Department of Meteorology
Naval Postgraduate School
Monterey, California 93943-5100

22. Dr. Eugene S. Takle — 1
Department of Climatology
and Meteorology
310 Curtiss Hall
Iowa State University
Ames, Iowa 50011

23. Dr. M.J.P. Cullen — 1
Meteorological Office
Bracknell, Berks, United Kingdom

24. Dr. Robert L. Lee — 1
Atmospheric and Geophysical
Science Division
University of California
P.O. Box 808
Livermore, California 94550

25. Professor A.K. MacPherson — 1
Lehigh University
Department of Mechanical Engineering
Bethlehem, Pennsylvania 18015

26. Dr. N.A. Phillips — 1
National Meteorological Center/NOAA
World Weather Building
Washington, D.C. 20233

27. Professor I. Salinas, Code 69Zc — 1
Department of Mechanical Engineering
Naval Postgraduate School
Monterey, California 93943-5100

28. Dr. Y. Sasaki — 1
Department of Meteorology
University of Oklahoma
Norman, Oklahoma 73069

29. Dr. Andrew Staniforth — 1
Recherce-en-Prevision Numerique
West Isle Office Tower, 5 ieme etage
2121 route Trans-Canada
Dorval, Quebec H9P1J3, Canada

30. Professor O.C. Zienkiewicz 1
Head of Civil Engineering Department
Applied Science Building
Singleton Park
Swansea SA2 8PP
United Kingdom

31. Dr. B. Neta (Code 63) 1
Department of Meteorology
Naval Postgraduate School
Monterey, California 93943-5100

END

FILMED

12-85

DTIC